ornl

OAK RIDGE
NATIONAL
LABORATORY

MARTIN MARIETTA

ORNL/TM-10417
ENDF-346

Calculated Neutron-Induced Cross Sections for ^{52}Cr from 1 to 20 MeV and Comparisons with Experiments

D. M. Hetrick
C. Y. Fu
D. C. Larson

OPERATED BY
MARTIN MARIETTA ENERGY SYSTEMS, INC.
FOR THE UNITED STATES
DEPARTMENT OF ENERGY

Printed in the United States of America. Available from
National Technical Information Service
U.S. Department of Commerce
5285 Port Royal Road, Springfield, Virginia 22161
NTIS price codes—Printed Copy: A05 Microfiche A01

ORNL/TM-10417
ENDF-346

Engineering Physics and Mathematics Division

CALCULATED NEUTRON-INDUCED CROSS SECTIONS FOR ^{52}Cr FROM 1 TO 20 MeV AND COMPARISONS WITH EXPERIMENTS

D. M. Hetrick,* C. Y. Fu, and D. C. Larson

*Computer and Telecommunications Division

Manuscript Completed - September 15, 1987

Prepared for the
Office of Basic Energy Sciences

OAK RIDGE NATIONAL LABORATORY
Oak Ridge, Tennessee 37831
operated by
MARTIN MARIETTA ENERGY SYSTEMS, INC.
for the
U.S. DEPARTMENT OF ENERGY
under Contract No. DE-AC05-84OR21400

CONTENTS

ACKNOWLEDGMENTS

This research was sponsored jointly by the Office of Basic Energy Sciences and the Office of Fusion Energy, U.S. Department of Energy, under contract DE-AC05-84OR21400 with Martin Marietta Energy Systems, Inc.

We are grateful to Sue Damewood for preparing this report for publication.

LIST OF FIGURES

LIST OF TABLES

CALCULATED NEUTRON-INDUCED CROSS SECTIONS FOR ^{52}Cr FROM 1 TO 20 MeV AND COMPARISONS WITH EXPERIMENTS

D. M. Hetrick, C. Y. Fu, and D. C. Larson

ABSTRACT

Nuclear model codes were used to compute cross sections for neutron-induced reactions on ^{52}Cr for incident energies from 1 to 20 MeV. The input parameters for the model codes were determined through analysis of experimental data in this energy region. Discussion of the models used, the input data, the resulting calculations, extensive comparisons to measured data, and comparisons to the Evaluated Nuclear Data File (ENDF/B-V) for Cr (MAT 1324) are included in this report.

1. INTRODUCTION

The nuclear data needs specified by the National Nuclear Data Center (NNDC) include evaluated neutron cross sections for chromium, an important material for fusion reactor applications. It has been shown that deficiencies exist for chromium in the Evaluated Nuclear Data File (ENDF/B-V) for the neutron emission spectra from contributing reactions (HE79). Since neutron-emission cross sections (as a function of angle and energy) and charged particle and gamma-ray emission cross sections (as a function of energy) are important for transport calculations for fusion engineering feasibility demonstrations, an extensive effort was made to reproduce the rather sparse experimental data and use realistic models to provide reliable interpolation and extrapolation to other energy and angular regions where no data were available. Guided by experimental data, we have performed a comprehensive set of nuclear model calculations for neutron reactions on ^{52}Cr for incident energies between 1 and 20 MeV in which we have particularly addressed the NNDC requests for chromium as noted in Ref. ND83. This report documents these calculations.

Nuclear model codes were employed in this analysis. Several published optical-model parameter sets (WI64, PE76, AR84) were tried as input for the Hauser-Feshbach code TNG (FU80, FU80a, SH86) in order to determine which gave the best overall fit to measured data. The Distorted Wave Born Approximation (DWBA) program DWUCK (KU72) was used to compute direct-interaction cross sections needed as input for TNG. The applicability of TNG to cross-section evaluations has been extended as TNG is now capable of using variable energy bin widths for outgoing particle energies (SH86). The TNG code provides energy and angular distributions of particles emitted in the compound and precompound reactions, ensures consistency among all reactions, and maintains energy balance.

The optical-model parameter sets, discrete energy levels, and other parameters needed as input for TNG are discussed in Section 2. Section 3 includes a discussion of the computational methods and procedures for the calculations. Figures showing calculated results compared to measured data are given in Section 4, along with some brief discussions. In Section 5, the calculations are compared to cross sections from the ENDF/B-V evaluation for chromium. A short summary is given in Section 6.

2. PARAMETER DETERMINATION

2.1 NEUTRON OPTICAL-MODEL POTENTIAL

Since optical-model parameters are essential input for our nuclear model calculations, effort was spent to find a good documented set of neutron optical-model parameters for $n+^{52}Cr$ so as to reproduce the nonelastic, elastic, and total cross sections. Deficiencies exist for chromium in ENDF/B-V for the neutron emission spectra from contributing reactions (HE79). However, the elastic angular distributions in ENDF/B-V for chromium are in good agreement with measured data (PR79). Thus, we especially emphasized fitting the available nonelastic cross-section data since, for evaluation purposes, measured data are used for the total cross section, and the elastic cross section is obtained by subtracting the nonelastic from the total cross section.

Several published neutron optical-model parameter sets (WI64, PE76, AR84) were tried as input to the Hauser-Feshbach code TNG (FU80, FU80a, SH86). The potential by Wilmore and Hodgson (WI64) resulted in a very good fit to the nonelastic cross-section data and the various reaction cross-section data for incident energies from 1 to 20 MeV, and a satisfactory fit to the total cross section (see Section 4). Other potentials that were tried (PE76, AR84) did not fit the nonelastic, total, and some of the reaction cross sections as well. Therefore, the neutron optical-model potential by Wilmore and Hodgson was chosen and used as input to the TNG code for ^{52}Cr. Values for this potential are given in Table 1.

Table 1. Neutron optical-model parameters

V (MeV)	=	$47.01 - 0.267E_L - 0.0018E_L^2$
W (MeV)	=	0.0
W_D (MeV)	=	$9.52 - 0.053E_L$
U (MeV)	=	7.0
r_v (fm)	=	$1.322 - 7.6A \times 10^{-4} + 4A^2 \times 10^{-6} - 8A^3 \times 10^{-9}$
r_w (fm)	=	$1.266 - 3.7A \times 10^{-4} + 2A^2 \times 10^{-6} - 4A^3 \times 10^{-9}$
r_u (fm)	=	r_v
a_v (fm)	=	0.66
a_w (fm)	=	0.48
a_u (fm)	=	0.66

E_L = incident energy in the laboratory system (MeV),
V = real well depth,
W = imaginary well depth (Wood-Saxon),
W_D = imaginary well depth (Wood-Saxon derivative),
U = spin-orbit potential depth,
A = mass number of the target nucleus,
r_v, r_w, r_u = radii for V, W_D, U potentials,
a_v, a_w, a_u = diffuseness for V, W_D, U potentials.

2.2 CHARGED-PARTICLE OPTICAL-MODEL PARAMETERS

The proton optical-model parameters are taken from the work of Becchetti and Greenlees (BE69). The potential used for the protons is given in Table 2. Originally, the optical-model parameters for the alpha particles were taken from Huizenga and Igo (HU62). However, the calculated total alpha-emission cross section did not agree well with measured data, and, subsequently, the real and imaginary well depths for this potential were increased by 70 percent. This change caused the alpha reaction cross section to increase by 11.2 percent, and the alpha elastic scattering cross section to decrease by 4.7 percent. The resultant parameters are given in Table 3.

2.3 THE DIRECT REACTION MODEL AND PARAMETERS

The Distorted Wave Born Approximation (DWBA) program DWUCK (KU72) was used to calculate the direct-interaction component of the inelastic-scattering cross sections to a number of levels in ^{52}Cr for which information was available. Inputs to this code were the neutron optical-model parameters of Table 1 and the deformation parameters, β_ℓ^2, shown in Table 4. β_ℓ^2 values from numerous references (see table) were averaged to obtain the β_ℓ^2 values shown in Table 4. The resulting calculated direct inelastic excitation cross sections, shown in Fig. 1, were used as input to the TNG code for the purpose of including the direct interaction effects in the gamma-ray cascades calculation. All TNG results were automatically scaled to maintain the same total reaction cross section.

2.4 DISCRETE ENERGY LEVELS AND LEVEL-DENSITY PARAMETERS

The statistical-model calculations with TNG require a complete description of the energy levels of the residual nuclei for the various open channels. The low-energy region of excitation of these nuclei can be adequately described in terms of discrete levels for which we usually know the energy, spin and parity (J^π), and gamma-ray deexcitation branching ratios, hereinafter referred to as branching ratios. As the excitation energy increases, our knowledge of these levels becomes incomplete, and eventually, as their number increases, we prefer to describe them in terms of a level density formula. In this section, we give the discrete levels used in the calculations and discuss the level density formulae and parameters.

The reactions for which we need level information for the residual nuclei are: ^{52}Cr$(n,n')^{52}$Cr, ^{52}Cr$(n,p)^{52}$V, ^{52}Cr$(n,\alpha)^{49}$Ti, ^{52}Cr$(n,np)^{51}$V, ^{52}Cr$(n,n\alpha)^{48}$Ti, ^{52}Cr$(n,2n)^{51}$Cr, and ^{52}Cr$(n,\gamma)^{53}$Cr. The level energies, J^π values and gamma-ray branching ratios adopted for these nuclei are given in Tables 5 to 11. There are a few levels where the energies are known, but J^π values or branching ratios are experimentally undetermined. These J^π values and branching ratios were assigned as indicated by the parentheses in the tables. In most cases, these values are as given in the reference (see below); others were estimated from systematics. Excited states were reported having excitation energies larger than for levels shown in Tables 5 through 11. However, the branching ratios for these higher levels were not known, and thus the levels were not used in the calculations.

The information on the levels and gamma-ray branching ratios of ^{52}Cr in Table 5 was taken from Beene (BE78) and Browne et al. (BR78). We include the 4.563- and 4.64-MeV levels because they are collective and the cross sections for exciting these levels were computed by DWUCK (KU72) and input to TNG. Also, as seen earlier (Table 4), the β_ℓ^2 values for these levels are large, which gives rise to significant contributions to the inelastic-scattering and gamma-ray production cross sections. Although there are many other levels in this energy region (i.e., above 3.7 MeV), the cross section for exciting these levels can be adequately accounted for in the TNG calculation (FU80) with the level density formulae.

Table 2. Proton optical-model parameters[a]

V (MeV)	=	$54.0 - 0.32E_L + \left[\frac{0.4Z}{A^{1/3}} + 24.0\left(\frac{N-Z}{A}\right)\right]$
r_v (fm)	=	1.17
a_v (fm)	=	0.75
W (MeV)	=	$0.22E_L - 2.7$, ($W \geqslant 0.0$)
r_w (fm)	=	1.32
a_w (fm)	=	$0.51 + 0.7\left(\frac{N-Z}{A}\right)$
W_D(MeV)	=	$11.8 - 0.25E_L + 12.0\left(\frac{N-Z}{A}\right)$, ($W_D \geqslant 0.0$)
r_c (fm)	=	1.25

[a]Parameter definitions are as in Table 1; r_c is the Coulomb radius.

Table 3. Alpha Optical-Model Parameters[a]

V (MeV) = 85.0	r_v (fm) = $1.17 + \frac{1.77}{A^{1/3}}$	a_v (fm) = 0.576
W (MeV) = 17.0	r_w (fm) = r_v	a_w (fm) = 0.576
W_D (MeV) = 0.0	r_c (fm) = 1.17	

[a]Parameter definitions are as in Tables 1 and 2.

Table 4. Deformation parameters of ^{52}Cr levels

Level (MeV)	J^{π}	β_{ℓ}^{2}	Ref.
1.434	2^+	0.035	PE69, ST65a, HA68, IS79, PO79, PR70
2.370	4^+	0.0081	PE69, PR70
2.768	4^+	0.0056	PE69, PR70
2.965	2^+	0.001	PE69, PR70
3.114	6^+	0.0058	PE69
3.162	2^+	0.0059	PE69, PR70
3.772	2^+	0.011	PE69, PR70
4.563	3^-	0.023	PE69, PR70
4.640	4^+	0.0137	PE69

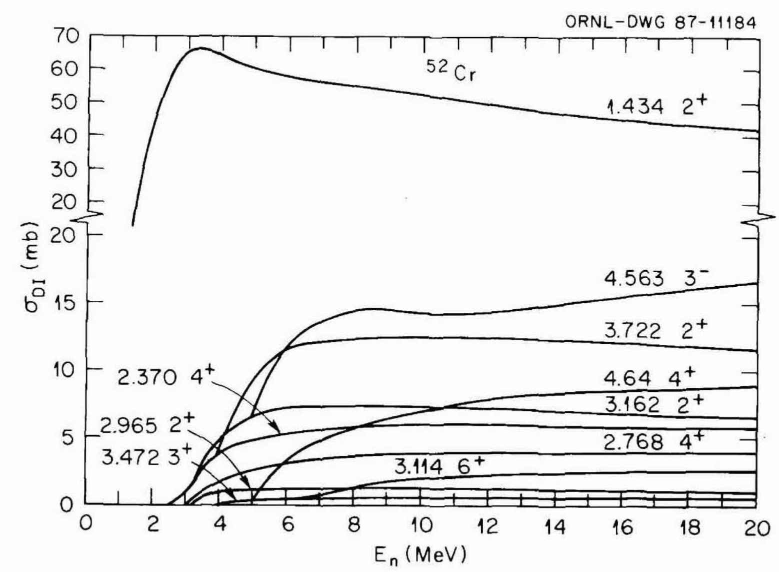

Fig. 1. Calculated direct inelastic excitation cross sections for ^{52}Cr.

Table 5. Energy levels and gamma-ray branching ratios of ^{52}Cr

Initial state			Branching ratios to state N					
N	J^π	E (keV)	1	2	3	5	7	9
1	0^+	0						
2	2^+	1434	100					
3	4^+	2370		100				
4	0^+	2647		100				
5	4^+	2768		99	1			
6	2^+	2965		100				
7	6^+	3114			99	1		
8	2^+	3162	13	87				
9	(4^+)	3415		7	14	79		
10	3^+	3472		22		78		
11	5^+	3616			54	42	3	1
12	2^+	3772	20	80				
13	(3^-)	4563		100				
14	4^+	4640			100			

Table 6. Energy levels and gamma-ray branching ratios of ^{52}V

Initial state			Branching ratios to state N					
N	J^π	E (keV)	1	2	3	4	5	6
1	3^+	0						
2	$(2)^+$	17	100					
3	(5^+)	23	100					
4	1^+	142		100				
5	$(4)^+$	148	15		85			
6	$(2)^+$	437	49	30		21		
7	3^+	794					99	1
8	$(4)^+$	846	83				17	

Table 7. Energy levels and gamma-ray branching ratios of ^{49}Ti

Initial state			Branching ratios to state N	
N	J^{π}	E (keV)	1	2
1	$7/2^-$	0		
2	$3/2^-$	1382	100	
3	$(11/2^-)$	1542	(100)	
4	$3/2^-$	1585	100	
5	$(9/2)^-$	1623	(100)	
6	$1/2^-$	1723		100
7	$5/2^-$	1762	100	

Table 8. Energy levels and gamma-ray branching ratios of ^{51}V

Initial state			Branching ratios to state N			
N	J^{π}	E (keV)	1	2	3	4
1	$7/2^-$	0				
2	$5/2^-$	319	100			
3	$3/2^-$	928	85	15		
4	$11/2^-$	1609	100			
5	$9/2^-$	1813	74	25		1
6	$3/2^-$	2416	20	65	15	
7	$1/2^+$	2547	100			

Table 9. Energy levels and gamma-ray branching ratios of ^{48}Ti

Initial state			Branching ratios to state N			
N	J^π	E (keV)	1	2	3	8
1	0^+	0				
2	2^+	983	100			
3	4^+	2296		100		
4	2^+	2420	4	96		
5	0^+	2997		100		
6	$(3)^+$	3224		74	26	
7	4^+	3240			100	
8	6^+	3333			100	
9	3^-	3359		85	15	
10	2^+	3371	19	81		
11	$(6)^+$	3509			24	76
12	2^+	3618		100		

Table 10. Energy levels and gamma-ray branching ratios of ^{51}Cr

Initial state			Branching ratios to state N									
N	J^π	E (keV)	1	2	3	4	5	6	7	9	11	12
1	$7/2^-$	0										
2	$3/2^-$	749	100									
3	$1/2^-$	777		100								
4	$9/2^-$	1165	100									
5	$5/2^-$	1353	35	56	9							
6	$11/2^-$	1480	52			48						
7	$7/2^-$	1557	16	79			5					
8	$3/2^-$	1899	100									
9	$(5/2)^-$	2002	100									
10	$(15/2)^-$	2256						100				
11	$(7/2)^-$	2313	11			89						
12	$(7/2^-)$	2380	36			12	23	17	12			
13	$(13/2^-)$	2386						100				
14	$(7/2^-)$	2704	11			30		10	49			
15	$1/2^+$	2763		100								
16	$(9/2)^-$	2767	56			20		22			2	
17	$(3/2^-)$	2829		100								
18	$3/2^-$	2890								62		38

Table 11. Energy levels of ^{53}Cr

Initial State			Initial State		
N	J^π	E (keV)	N	J^π	E (keV)
1	$3/2^-$	0	17	$(5/2)^-$	2993
2	$1/2^-$	564	18	$15/2^-$	3084
3	$5/2^-$	1006	19	$(5/2^-)$	3127
4	$7/2^-$	1290	20	$(3/2)^-$	3179
5	$7/2^-$	1537	21	$(5/2^-)$	3244
6	$(5/2)^-$	1974	22	$5/2^+$	3261
7	$11/2^-$	2172	23	$(5/2^-)$	3351
8	$9/2^{(-)}$	2233	24	$(5/2^-)$	3435
9	$3/2^-$	2321	25	$(5/2^-)$	3589
10	$(5/2^-)$	2453	26	$13/2^{(-)}$	3602
11	$5/2^-$	2657	27	$1/2^-$	3617
12	$1/2^-$	2670	28	$(5/2^-)$	3667
13	$(5/2^-)$	2707	29	$9/2^+$	3711
14	$3/2^-$	2708	30	$(5/2^-)$	3781
15	$(5/2^-)$	2772	31	$(5/2^-)$	3838
16	$11/2^{(-)}$	2827			

For ^{52}V, the level energies, the adopted J^π values, and gamma-ray branching ratios are given in Table 6. They were taken from Refs. BE78 and BR78. Table 7 shows the levels, J^π values, and branching ratios for ^{49}Ti. The levels and J^π values were taken from the compilation of Halbert (HA78) and the branching ratios were taken from Ref. BR78. Level information from ^{51}V, given in Table 8, was taken from Ref. BR78 and the branching ratios are from Auble (AU78). For ^{48}Ti (see Table 9), the level energies, adopted J^π values, and branching ratios were compiled from the work of Beene (BE78a) and Browne et al. (BR78). The information on levels, J^π values, and branching ratios of ^{51}Cr, given in Table 10, was taken from Ref. AU78. For ^{53}Cr, the level energies and J^π values were taken from Dickens and Larson (DI87) and are given in Table 11. Although TNG is capable of predicting capture gamma-ray spectra (Shibata and Fu, 1986), the present calculations did not include this option. Thus, branching ratios are not given in Table 11 since they were not needed.

To represent the continuum excitation energy region occurring above the highest-energy discrete level (continuum cutoff E_c), the level-density formulae as described by Fu (FU76 and FU80) were used. The level-density parameters of the residual nuclei of all reactions analyzed are given in Table 12. The formulae of Gilbert and Cameron (GI65) were used in computing most of the parameters. However, it was found that for computing the spin-cutoff parameter, σ^2, a formula due to Facchini and Saetta-Menichella (FA68) produced better results and was used for excitation energies greater than the tangency point (E_x). The spin cutoff parameter at E_c was based on the cumulative sum of the discrete values. In between E_x and E_c, the spin cutoff parameter was assumed to vary linearly with the excitation energy.

Table 12. Level density parameters

Residual Nuclei	T (MeV)	E_o (MeV)	a (MeV^{-1})	Δ (MeV)	σ	E_c (MeV)	E_x (MeV)
^{52}Cr	1.433	0.20	6.154	2.65	12.52	3.7	10.39
^{52}V	1.255	−1.805	6.75	0.0	13.73	0.881	6.309
^{49}Ti	1.336	−0.893	6.85	1.73	13.39	1.80	9.432
^{51}V	1.236	0.069	6.4	1.3	12.85	2.56	6.741
^{48}Ti	1.374	0.161	6.93	3.27	13.36	3.633	11.74
^{51}Cr	1.384	−1.129	6.44	1.35	12.935	2.908	8.961
^{53}Cr	1.332	−0.754	6.5	1.35	13.39	3.84	8.306

T = nuclear temperature
E_o = parameter for matching lower energy level density to the higher one
$a = \pi^2 g/6$ (g = density of uniformly spaced single particle states)
Δ = pairing energy correction
σ^2 = spin cut-off parameter = $2c\sqrt{(E-\Delta)/a}$ where E is the excitation energy,
E_c = continuum cutoff
E_x = tangency point

2.5 GIANT DIPOLE RESONANCE PARAMETERS

The giant dipole resonance parameters used as input to TNG in this analysis are those reported by Fuller et al. (FU73). For ^{52}Cr the resonance has a peak cross section of 97 mb, the width of the resonance is 5.0 MeV, and the energy of the resonance is 18.5 MeV.

2.6 (*n,t*), (*n*, ^{3}He), and (*n,d*) CROSS SECTIONS

The TNG code is not capable of calculating the (*n,d*), (*n,t*), and (*n*,^{3}He) cross sections. TNG can accept them in the input data as correction factors to reduce proportionately the other TNG calculated cross sections. The only measured data found was for the (*n,d*) reaction. Grimes et al. (GR79) reported an (*n,d*) cross section of 8.0 mb at 14.8 MeV incident neutron energy. The ENDF/B-V energy dependent cross-section shape for (*n,d*) was normalized to this measurement and input to TNG. The (*n,t*) cross sections given in ENDF/B-V were too large when compared to systematics and the energy-dependent shape was normalized to a cross section of 0.07 mb at 14.0 MeV incident neutron energy. The (*n*,^{3}He) cross sections included in ENDF/B-V were very small and were ignored in the TNG calculations.

3. COMPUTATIONAL METHODS AND PROCEDURES

Nuclear model calculations play an important role in modern evaluations for the interpolation and extrapolation of cross sections to energy regions where no data exist, and for predictions of reaction cross sections for which there are few or no experimental data. However, in order to ensure internal consistency, the model calculations should simultaneously reproduce as much of the experimental information as possible for as many reaction channels as reliable data are available. As noted earlier, the model code TNG (FU80, FU80a, SH86) was used exclusively for this analysis. The applicability of TNG to cross-section evaluations has been extended as TNG is now capable of using variable energy bin widths for outgoing particle energies (SH86).

Calculations for ^{52}Cr at a number of incident energies from 1.0 to 20.0 MeV were performed. Parameters required as input to TNG are now summarized. The discrete energy levels for each of the residual nuclei and the gamma-ray branching ratios (Tables 5 through 11), the level density parameter (Table 12), the direct inelastic cross sections calculated by DWUCK (KU72) as discussed in Section 2, the optical-model parameters (Tables 1 though 3), the giant dipole resonance parameters, and the (*n,d*) and (*n,t*) cross sections were all used as input to the TNG computer code. Parameters required for the precompound mode of reaction were the same as determined previously in a global analysis (FU80) and were found to be satisfactory for the present calculations.

TNG simultaneously computes cross sections for all energetically possible binary reactions and tertiary reactions, and also computes the resulting gamma-ray production cross sections. Also, TNG computes the compound and precompound cross sections in a consistent fashion and conserves angular momentum in both compound and precompound reactions. Thus, the resulting cross-section sets are consistent and energy balance is ensured. The results from TNG are found to agree reasonably well with available data, and these comparisons are discussed in the next section.

4. COMPARISON OF CALCULATIONS WITH EXPERIMENTS

In this section the TNG calculated cross sections are compared with available data obtained from the National Nuclear Data Center CSISRS file (CS86). When comparisons were made for natural Cr, the calculated cross sections for ^{52}Cr were multiplied by 0.90 and added to 0.10 times the computed cross sections for ^{53}Cr (see the recent evaluation of ^{53}Cr by Shibata and Hetrick [SH87]). Together, $^{52,53}Cr$ account for 93.29% of natural chromium. Calculations for the minor isotopes $^{50,54}Cr$ were not performed for this work.

4.1 TOTAL CROSS SECTION

The TNG computed total cross section is compared in Fig. 2 to the measured data of Larson (LA80), which has been compared against other available data. Calculations using two different optical-model potentials are shown in the figure. The optical-model potential due to Wilmore and Hodgson was chosen for this study. However, this calculation is too large in the energy range less than 4.0 MeV. As noted earlier, the total cross section σ_t is the sum of the elastic and nonelastic cross section. The nonelastic cross section is the sum of all the individual reaction cross sections which we work hard to reproduce with TNG. For the evaluation (of which these calculations will become a part) the elastic cross section will be obtained by subtracting the nonelastic cross section from the total cross section, and the computed elastic and total cross sections are not used. Thus, it is important to use optical model parameters which reproduce the nonelastic cross section; it is less important how well the elastic and total cross sections are reproduced, as long as the elastic angular distributions are described reasonably well by the optical model parameters chosen.

4.2 NONELASTIC CROSS SECTION

Comparison of the nonelastic cross section with experiment is shown in Fig. 3. The measured elastic cross sections from Korzh et al. (KO76), Holmqvist and Wiedling (HO69), Holmqvist et al. (HO70), Sokolov et al. (SO73), and Kasakova et al. (KA65) were subtracted from the averaged total cross section of Larson (LA80) and included in the figure. Again, calculations using two different optical-model potentials are shown in the figure, with the Wilmore and Hodgson potentials giving the best fit. The agreement lends support to the optical-model parameters used for the $n + {}^{52}Cr$ channel.

4.3 ELASTIC CROSS SECTION

Measured data for the elastic cross section of ^{52}Cr and natural chromium are compared with the TNG calculations in Figs. 4-5. As for the total cross sections, the elastic cross-section calculation is too large at incident energies less than 4.0 MeV. As noted earlier, the elastic cross section is the difference between the total and nonelastic cross section and measured data are used for the total cross section in ENDF. The elastic angular distributions in ENDF/B-V for chromium are in good agreement with experimental data (PR79), and thus emphasis was placed on fitting the measured nonelastic cross section in this analysis. However, to show that the present calculations agree well with measured elastic angular distributions, see Figs. 6-9.

4.4 TOTAL INELASTIC SCATTERING CROSS SECTION

The TNG calculations of cross sections for total inelastic scattering of neutrons from ^{52}Cr and natural chromium are compared to experimental data in Figs. 10 and 11. The computed cross sections agree well with the measurements with the exception of the data from Kinney and Perey (KI74) and Fujita et al. (FU72). The data of Kinney and Perey were deduced from their neutron scattering data and are believed to be too large because they already exceed the upper limit given by the nonelastic cross section shown in Fig. 3. Fujita et al. (FU72) measured the continuum spectra of inelastically-scattered neutrons using the time-of-flight method. The total inelastic scattering cross section was deduced after

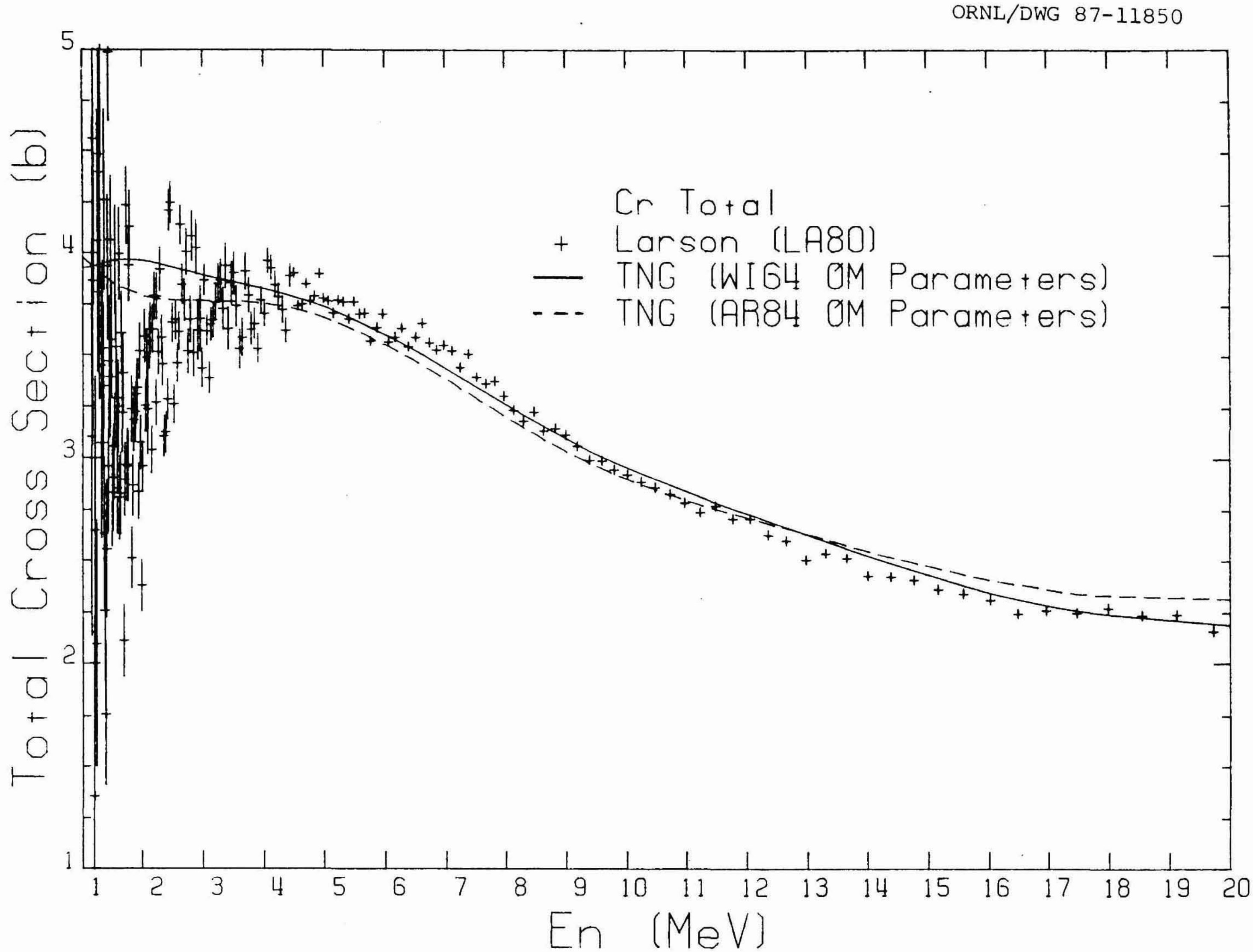

Fig. 2. Comparison of calculated and experimental total cross sections for ^{nat}Cr.

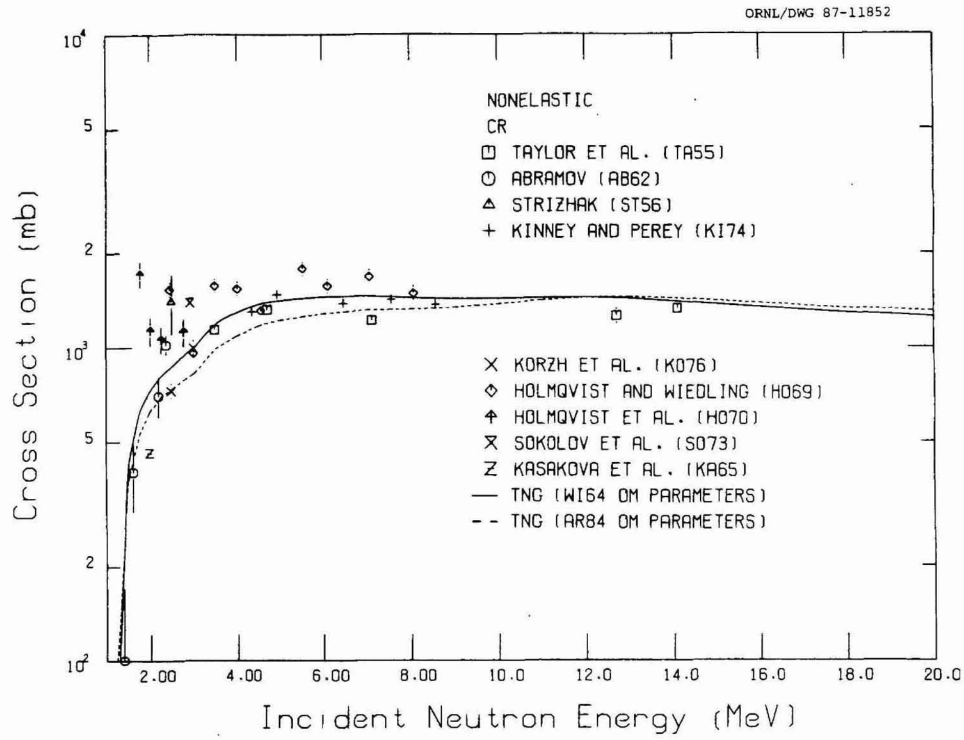

Fig. 3. Comparison of calculated and experimental nonelastic cross sections for ^{nat}Cr.

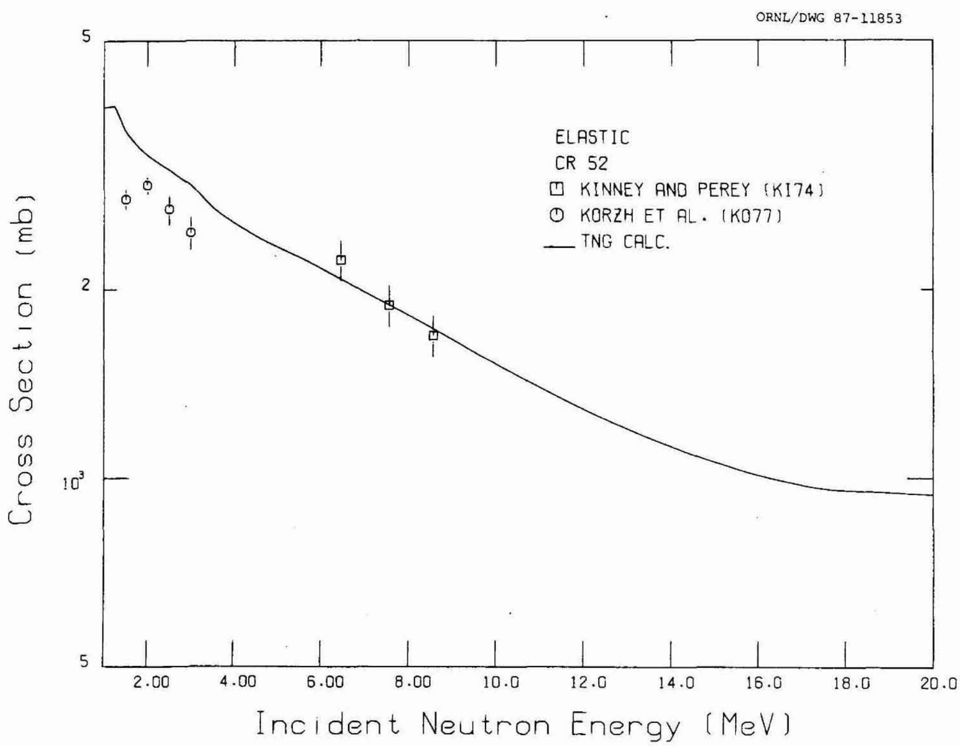

Fig. 4. Comparison of calculated and experimental elastic cross sections for ^{52}Cr.

ORNL/DWG 87-11854

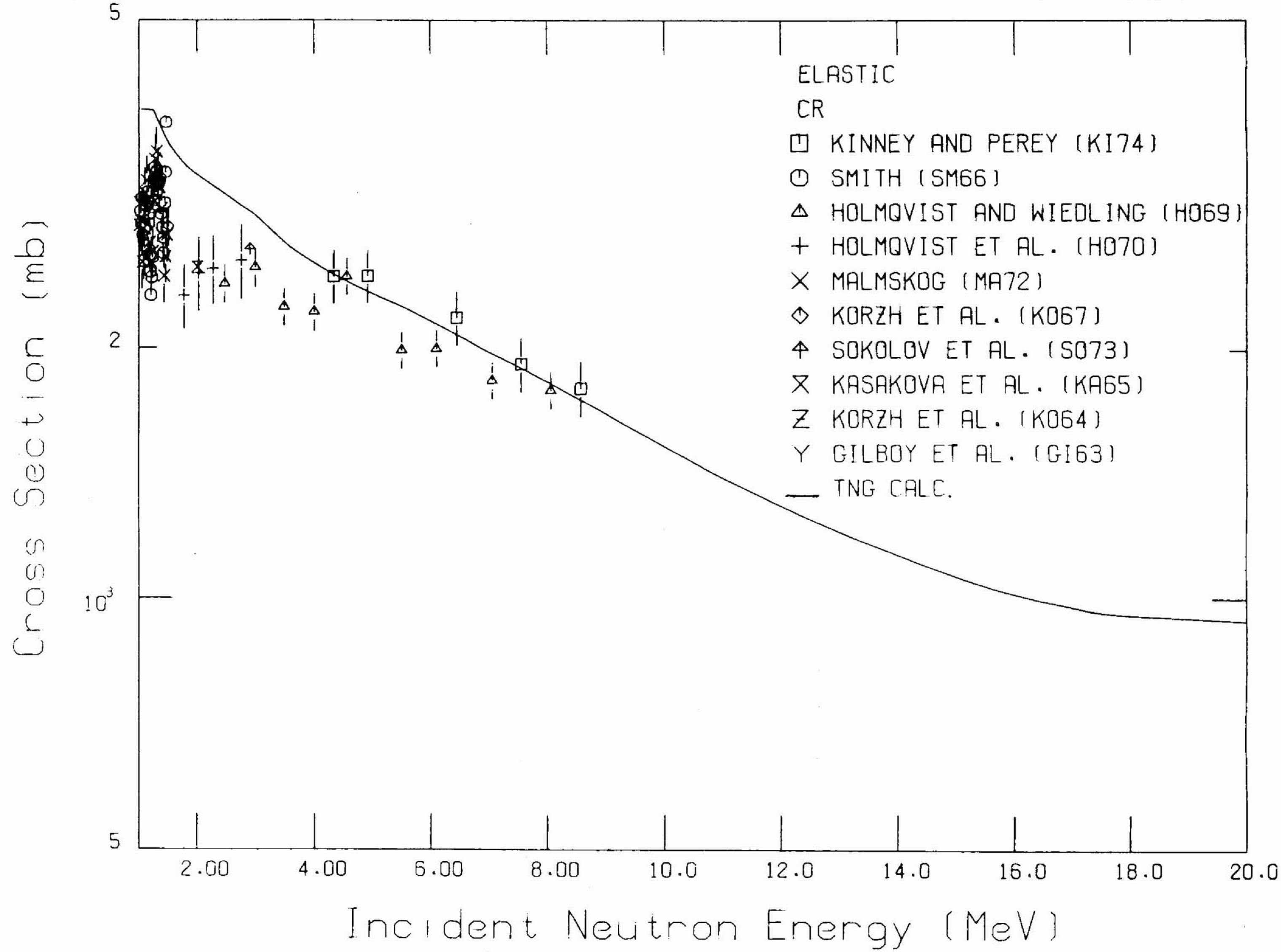

Fig. 5. Comparison of calculated and experimental elastic cross sections for ^{nat}Cr.

ORNL-DWG 87-13535

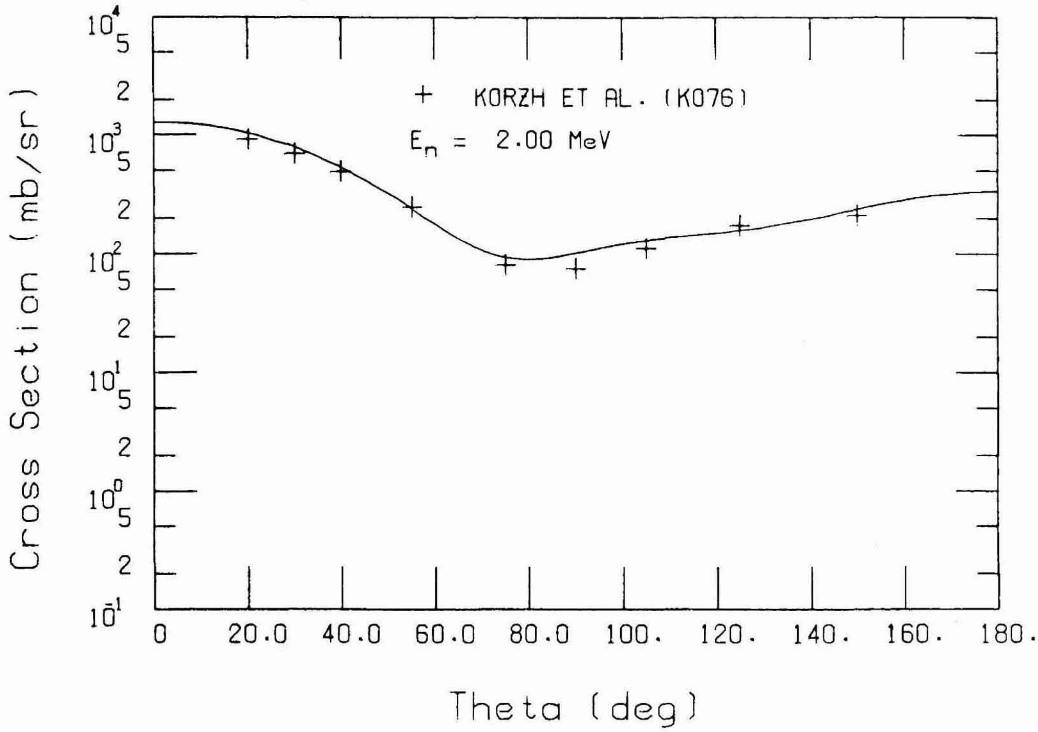

Fig. 6. Comparison of calculated and experimental differential elastic scattering cross sections for ^{52}Cr at E_n = 2.0 MeV.

ORNL-DWG 87-13636

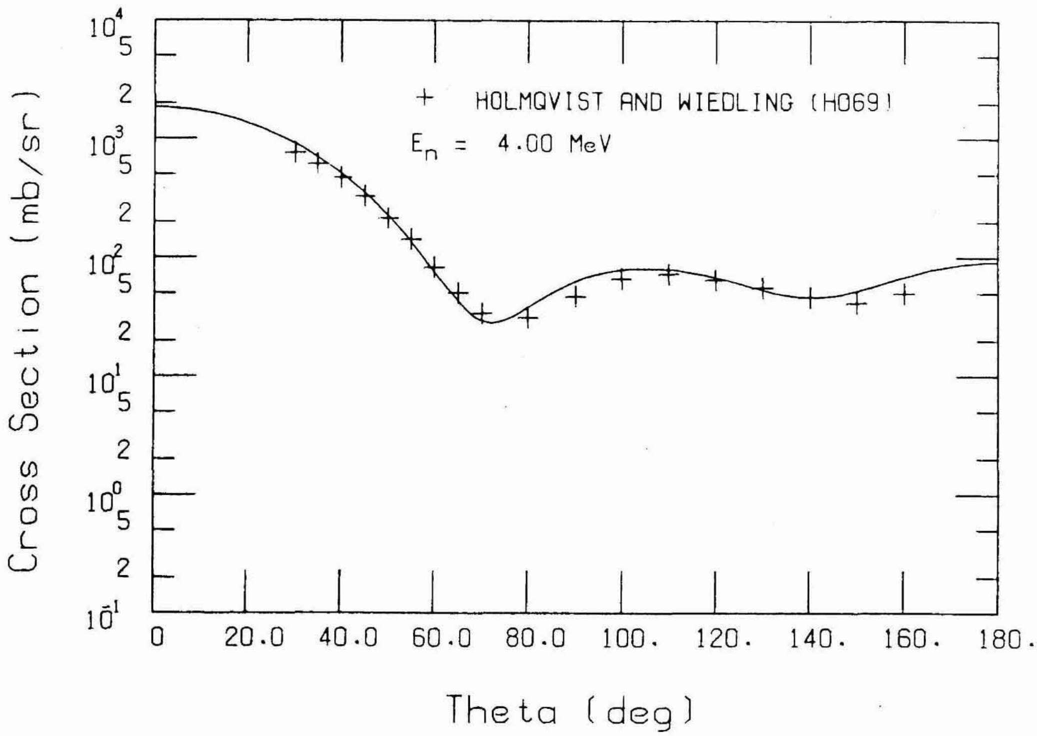

Fig. 7. Comparison of calculated (^{52}Cr) and experimental (^{nat}Cr) differential elastic scattering cross sections at E_n = 4.0 MeV.

ORNL-DWG 87-13637

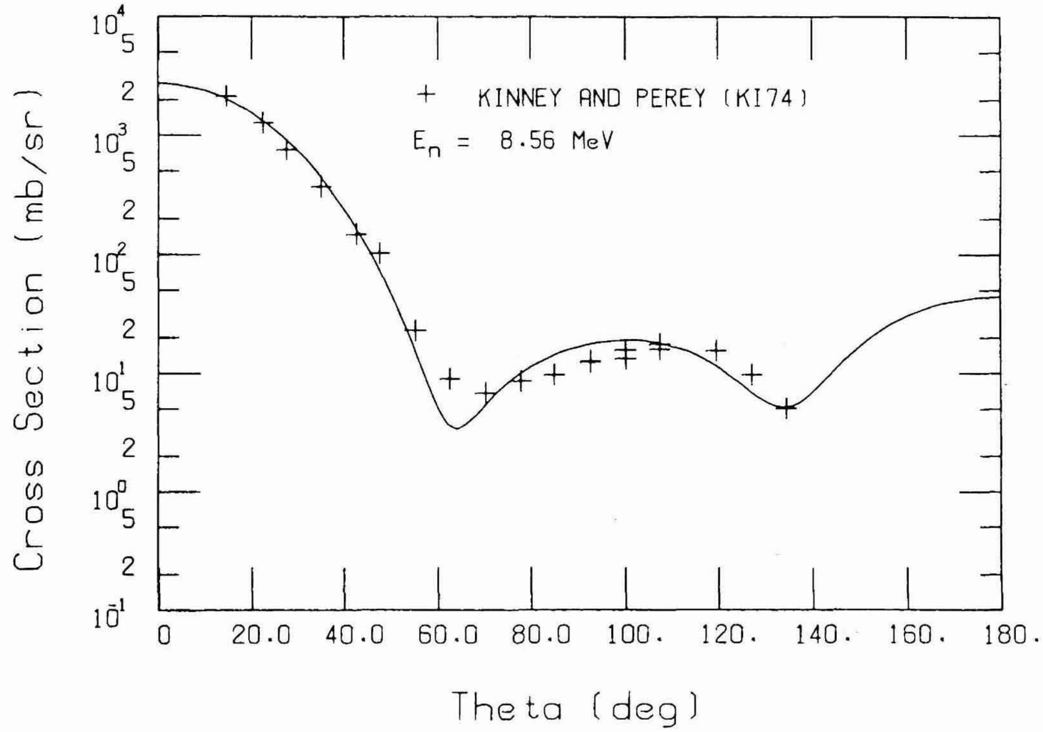

Fig. 8. Comparison of calculated and experimental differential elastic scattering cross sections for ^{52}Cr at E_n = 8.56 MeV.

ORNL-DWG 87-13638

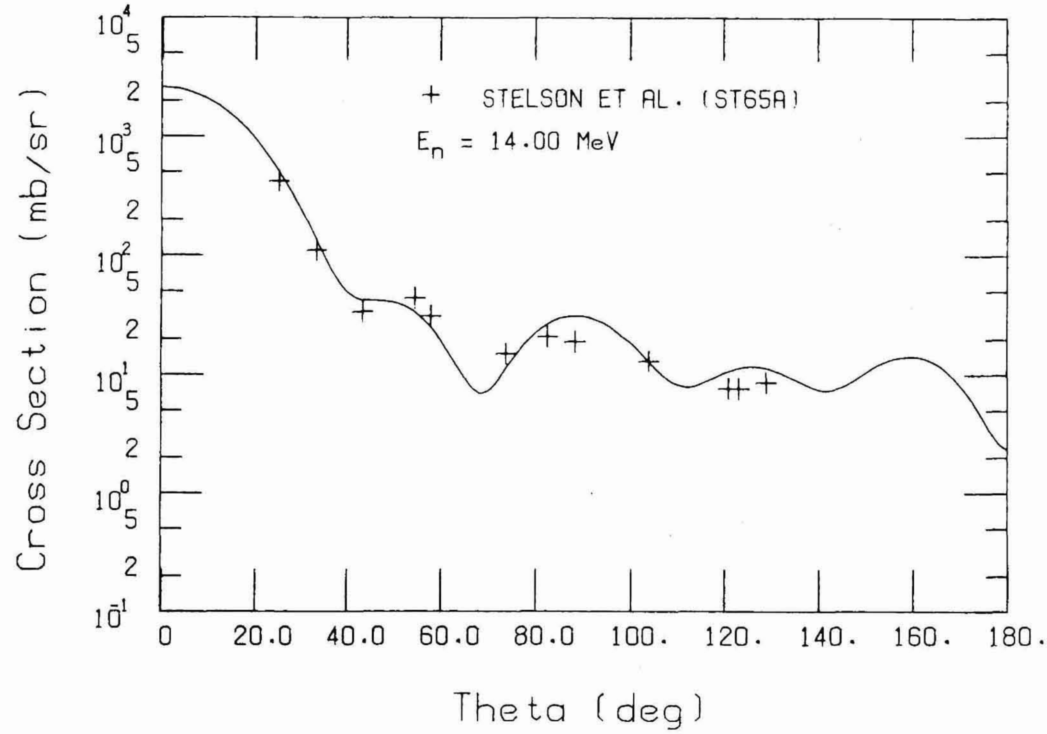

Fig. 9. Comparison of calculated (^{52}Cr) and experimental (^{nat}Cr) differential elastic scattering cross sections at E_n = 14.0 MeV.

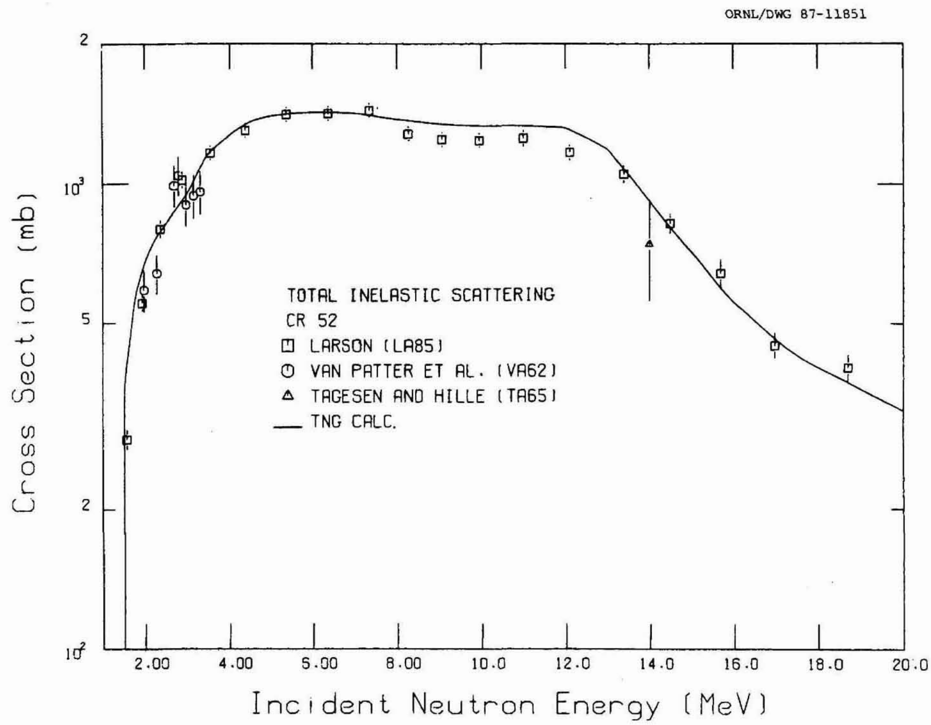

Fig. 10. Comparison of calculated and experimental total inelastic scattering cross sections for ^{52}Cr.

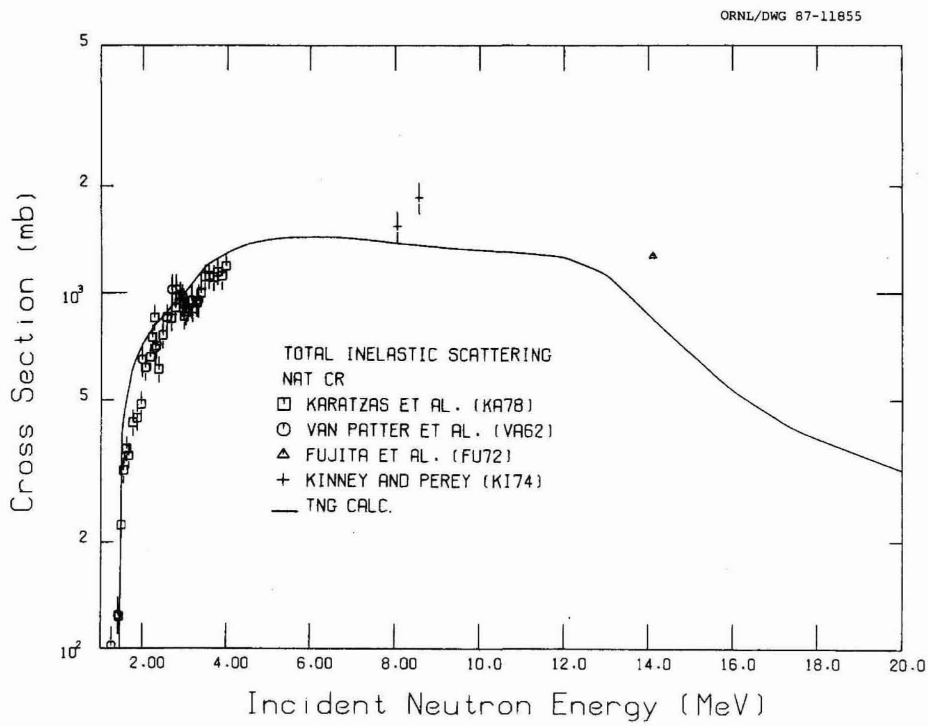

Fig. 11. Comparison of calculated and experimental total inelastic scattering cross sections for ^{nat}Cr.

allowing for contributions from (n,particle) reactions. Apparently, the (n,particle) reaction cross sections were underestimated in obtaining the unreasonably large total inelastic cross section shown in Fig. 11. The data of Larson (LA85) were obtained by summing cross sections measured for ^{52}Cr ground-state transitions of which by far the most important (i.e., largest cross section) is for the $2_1^+ \rightarrow O_{g.s.}^+$ transition.

4.5 ANGULAR DISTRIBUTIONS FOR INELASTIC SCATTERING

The calculated differential ^{52}Cr (n,n') cross sections for exciting the low-lying discrete levels are compared with measurements in Figs. 12 through 25. The DWBA calculations for inelastic scattering were combined with the TNG computations to obtain the results in these figures. Measurements of angular distributions for individual levels are presented. The need for nuclear model analyses (and preferably better data) can be seen from these figures for in some cases the measurements disagree. For example, in Fig. 13 the data of Pasechnik et al. (PA69) and Korzh et al. (KO76) disagree significantly with the calculation agreeing with Korzh et al. The calculations do agree consistently well with the data of Kinney and Perey (KI74).

4.6 INELASTIC SCATTERING TO DISCRETE LEVELS

The comparison of calculated and experimental (n,n') cross sections for individual levels for ^{52}Cr is given in Figs. 26-31. The calculated direct interaction cross sections (see Fig. 1) are included. Disagreement among measured data is quite large (e.g., see Figs. 26 and 27), and the calculation represents a good compromise in these cases. Overall, the agreement is quite good.

4.7 ANGULAR DISTRIBUTIONS OF NEUTRON PRODUCTION CROSS SECTIONS

The computed angular distributions of neutron production cross sections for chromium at an incident energy of 14.5 MeV and for secondary energies of $E_n' = 4.0\text{-}5.0$, 6.0-7.0, and 8.0-9.0 MeV are compared with experiments in Fig. 32. Again discrepancies exist between the measured data sets. The calculation agrees best with the data of Salnikov et al. (SA72), but disagrees with the measurements of Takahashi et al. (TA83) and Hermsdorf (HE75).

4.8 NEUTRON EMISSION SPECTRA

Neutron emission spectra were computed for 35 incident energies; however, measurements were available only for the incident neutron energy range from 14.1 to 14.8 MeV. Comparison of the calculated neutron spectra at incident energy of 14.5 MeV with the experimental data is shown in Fig. 33. The data of Takahashi et al. (TA83) were measured at 80°, and the other measurements (HE75, VO80, SA72) are angle integrated. The figure shows the calculated total neutron emission spectra, as well as the calculated emission spectra from the individual contributing reactions. The (n,n') continuum and discrete level computations were combined into the one curve labeled "$(n,n\gamma)$". The curve labeled "(n,np)" includes contributions from both the (n,np) and (n,pn) reactions. Likewise, the curve labeled "$(n,n\alpha)$" includes contributions from both the $(n,n\alpha)$ and $(n,\alpha n)$ reactions. The curve labeled "TNG Calculation" is the computed angle-integrated spectrum and includes the angle-integrated direct inelastic cross sections from the DWUCK code (these were input to the TNG code).

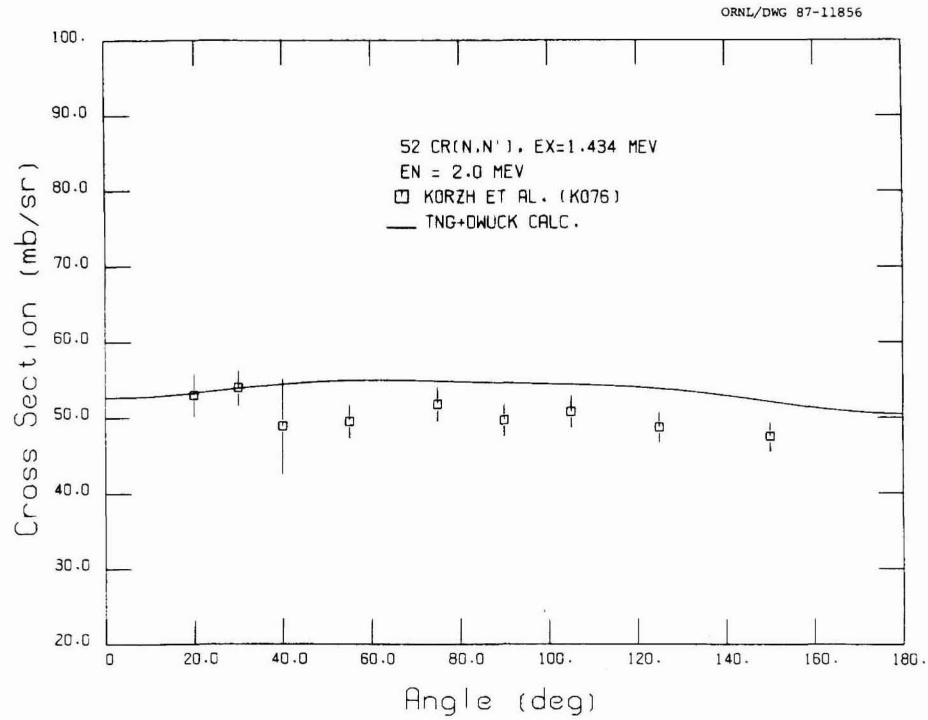

Fig. 12. Comparison of calculated and experimental differential cross sections for exciting the 1.434-MeV level at $E_n = 2.0$ MeV.

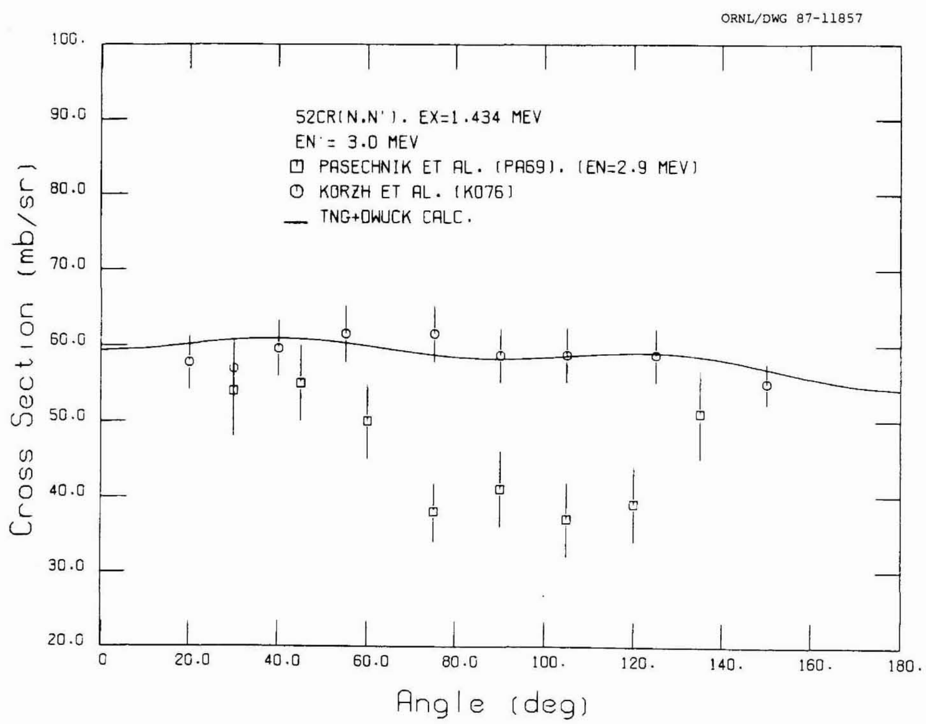

Fig. 13. Comparison of calculated and experimental differential cross sections for exciting the 1.434-MeV level at $E_n = 3.0$ MeV.

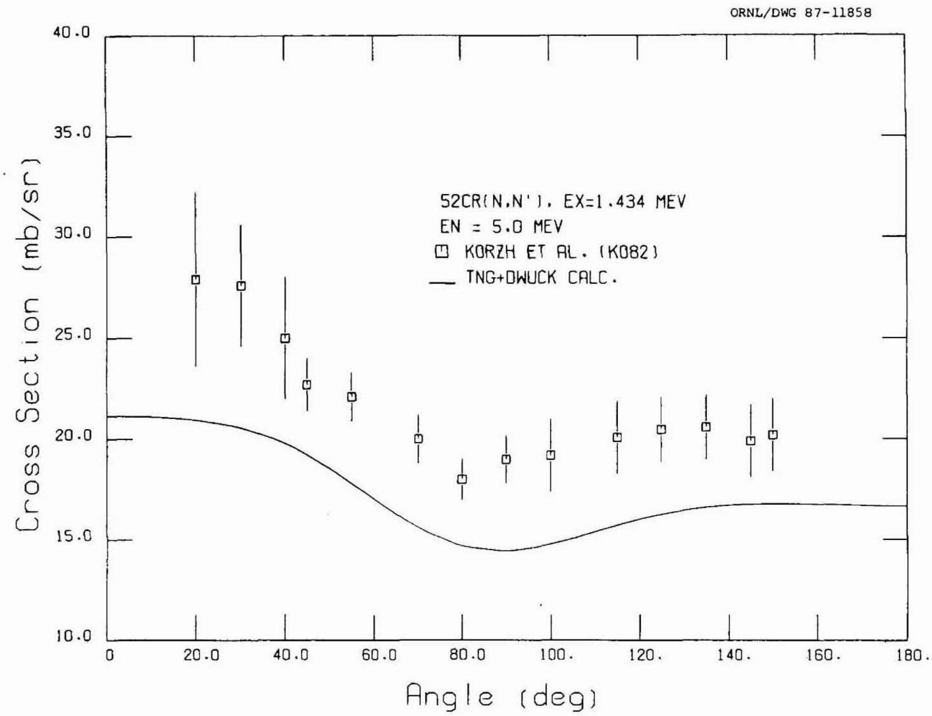

Fig. 14. Comparison of calculated and experimental differential cross sections for exciting the 1.434-MeV level at E_n = 5.0 MeV.

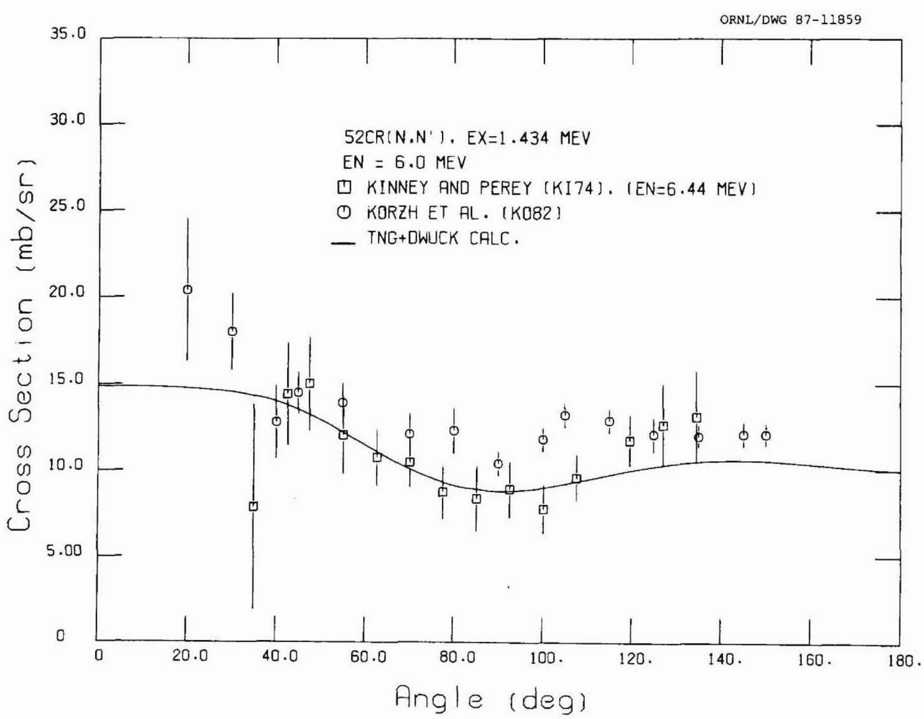

Fig. 15. Comparison of calculated and experimental differential cross sections for exciting the 1.434-MeV level at E_n = 6.0 MeV.

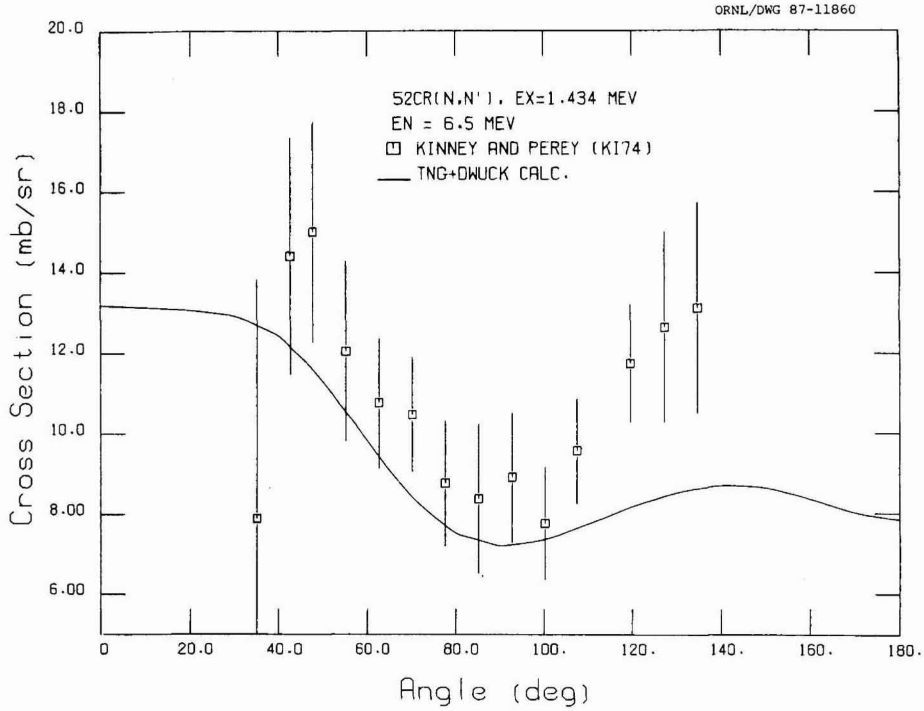

Fig. 16. Comparison of calculated and experimental differential cross sections for exciting the 1.434-MeV level at E_n = 6.5 MeV.

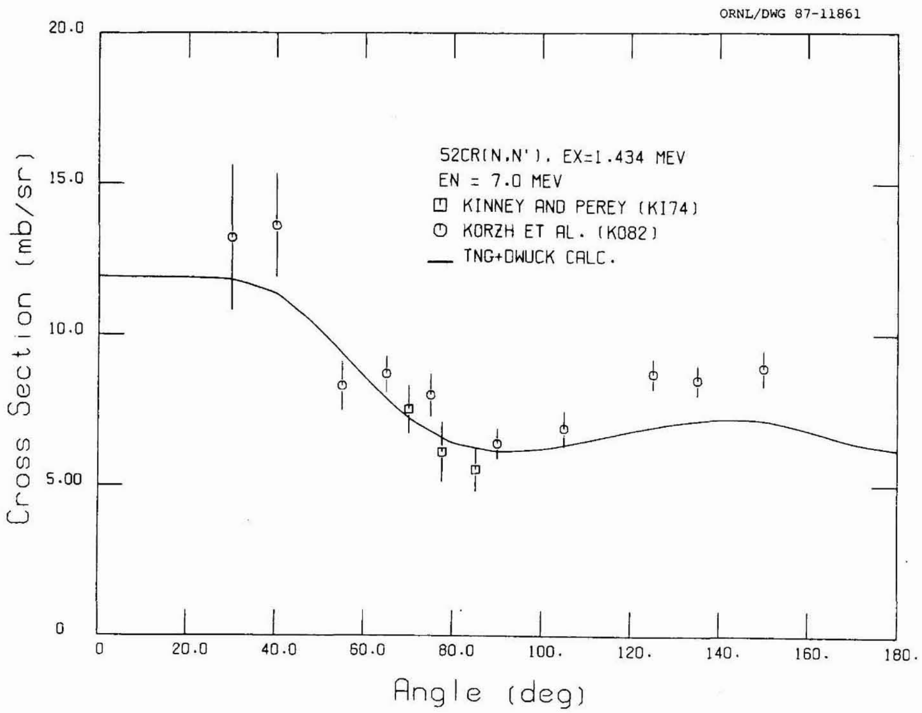

Fig. 17. Comparison of calculated and experimental differential cross sections for exciting the 1.434-MeV level at E_n = 7.0 MeV.

ORNL/DWG 87-11862

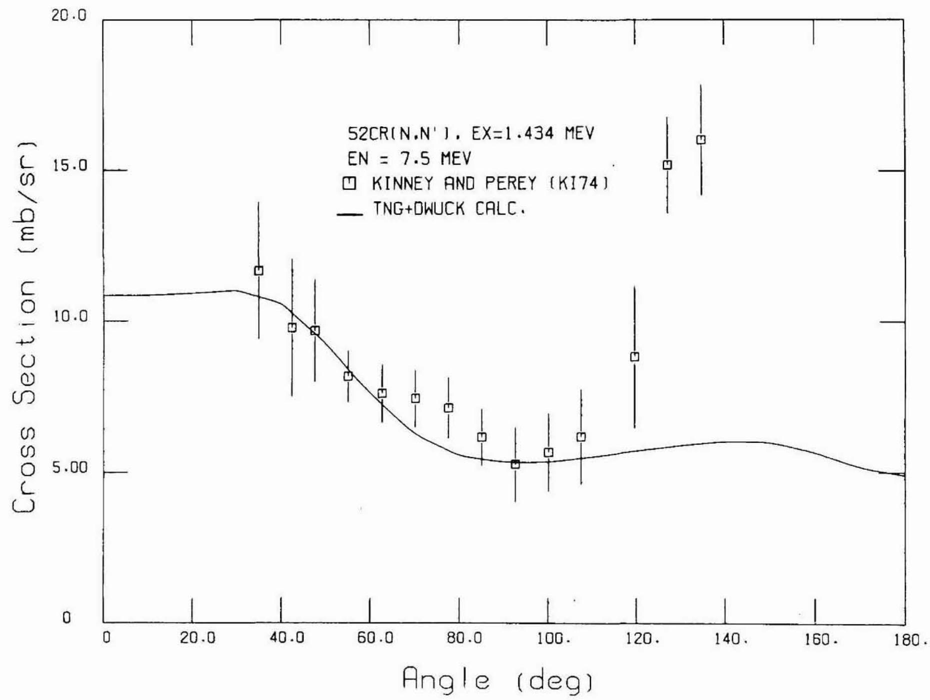

Fig. 18. Comparison of calculated and experimental differential cross sections for exciting the 1.434-MeV level at E_n = 7.5 MeV.

ORNL/DWG 87-11863

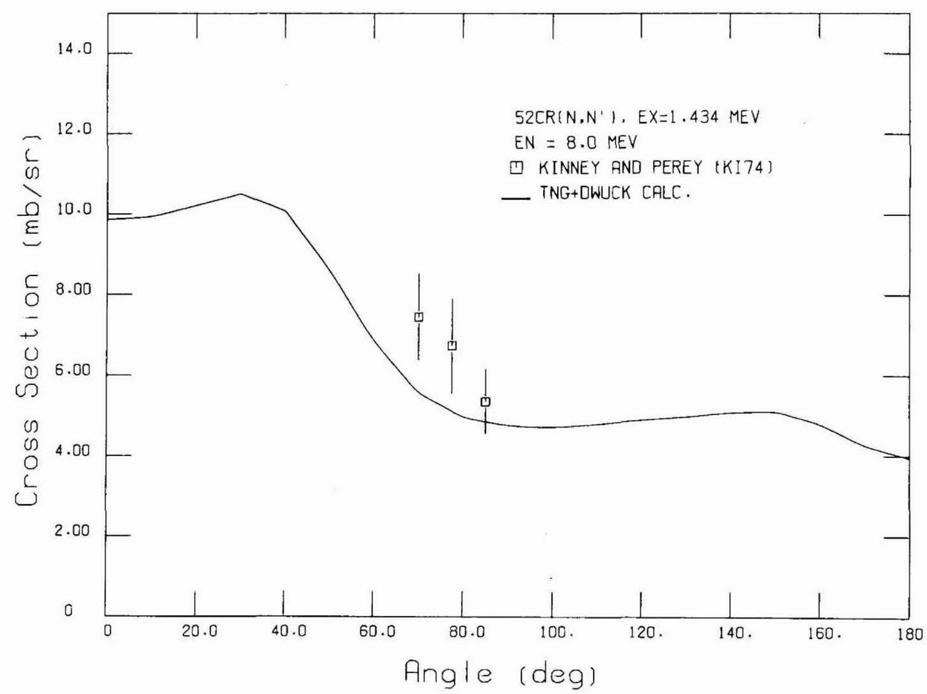

Fig. 19. Comparison of calculated and experimental differential cross sections for exciting the 1.434-MeV level at E_n = 8.0 MeV.

ORNL/DWG 87-11864

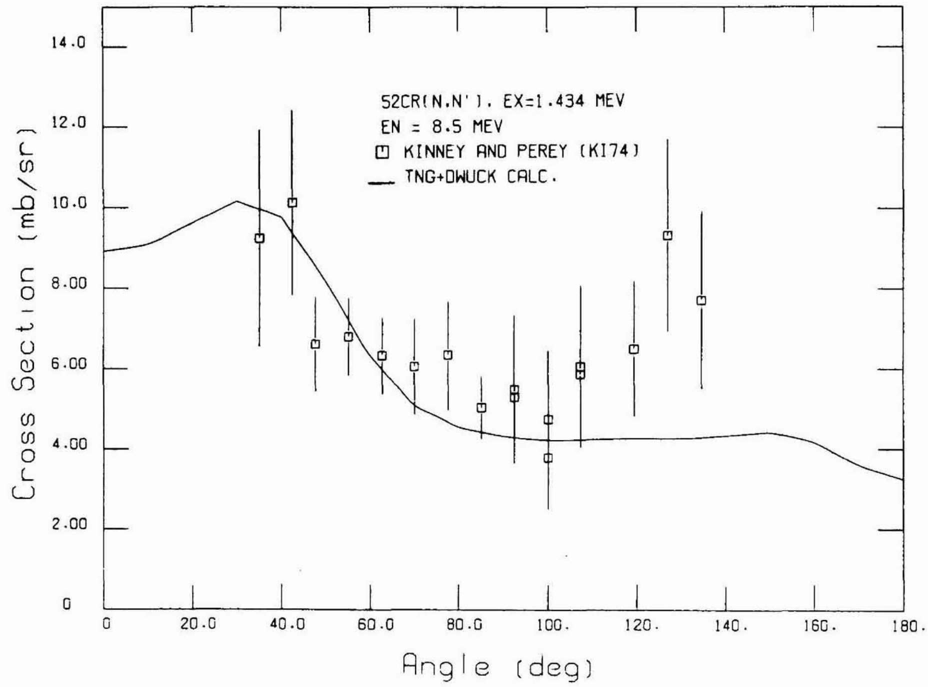

Fig. 20. Comparison of calculated and experimental differential cross sections for exciting the 1.434-MeV level at E_n = 8.5 MeV.

ORNL/DWG 87-11865

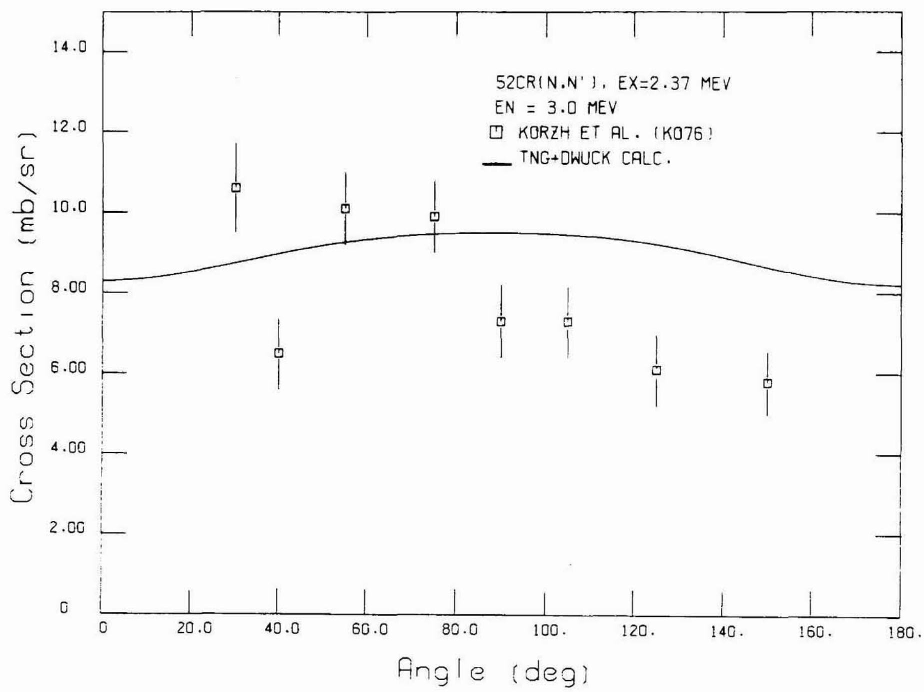

Fig. 21. Comparison of calculated and experimental differential cross sections for exciting the 2.37-MeV level at E_n = 3.0 MeV.

ORNL/DWG 87-11866

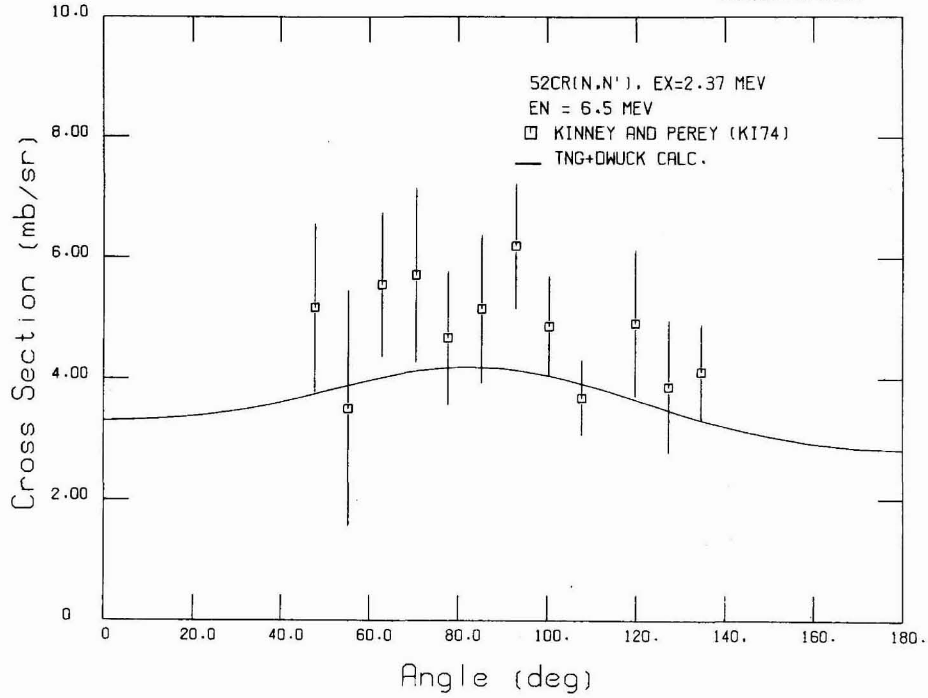

Fig. 22. Comparison of calculated and experimental differential cross sections for exciting the 2.37-MeV level at E_n = 6.5 MeV.

ORNL/DWG 87-11867

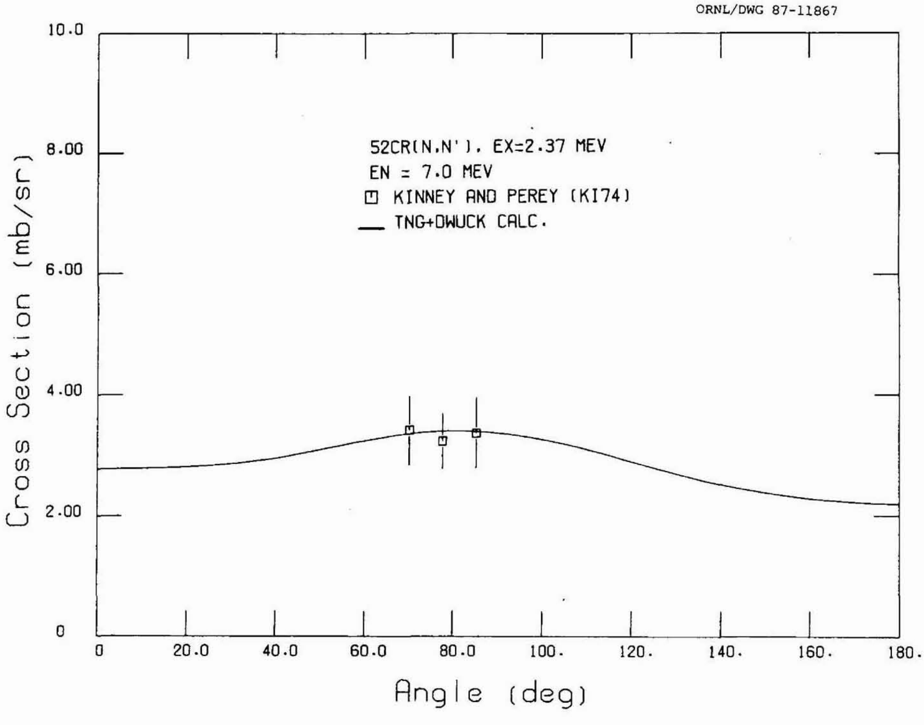

Fig. 23. Comparison of calculated and experimental differential cross sections for exciting the 2.37-MeV level at E_n = 7.0 MeV.

ORNL/DWG 87-11868

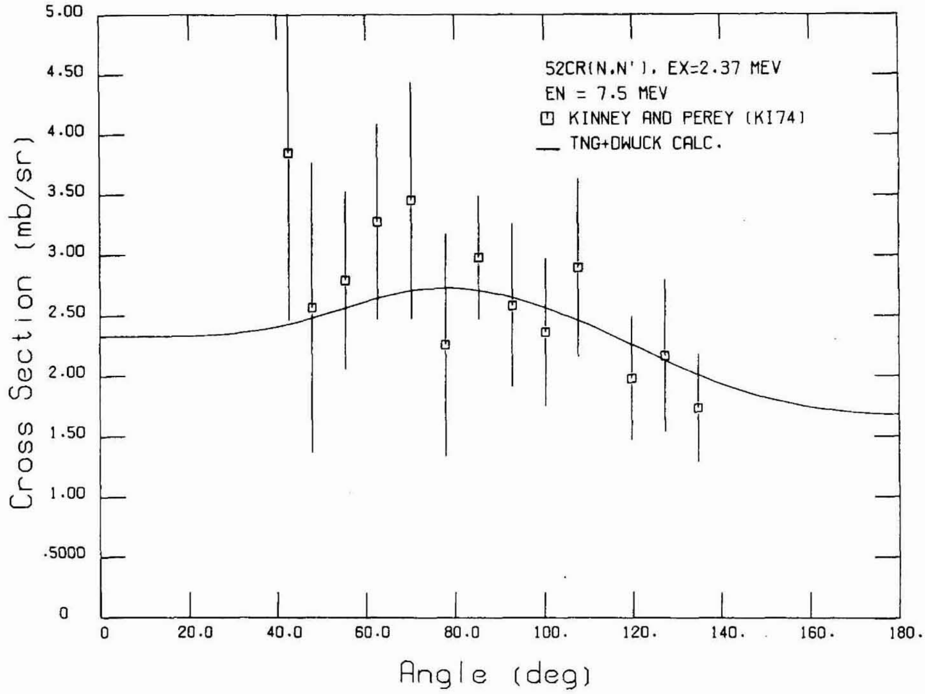

Fig. 24. Comparison of calculated and experimental differential cross sections for exciting the 2.37-MeV level at E_n = 7.5 MeV.

ORNL/DWG 87-11869

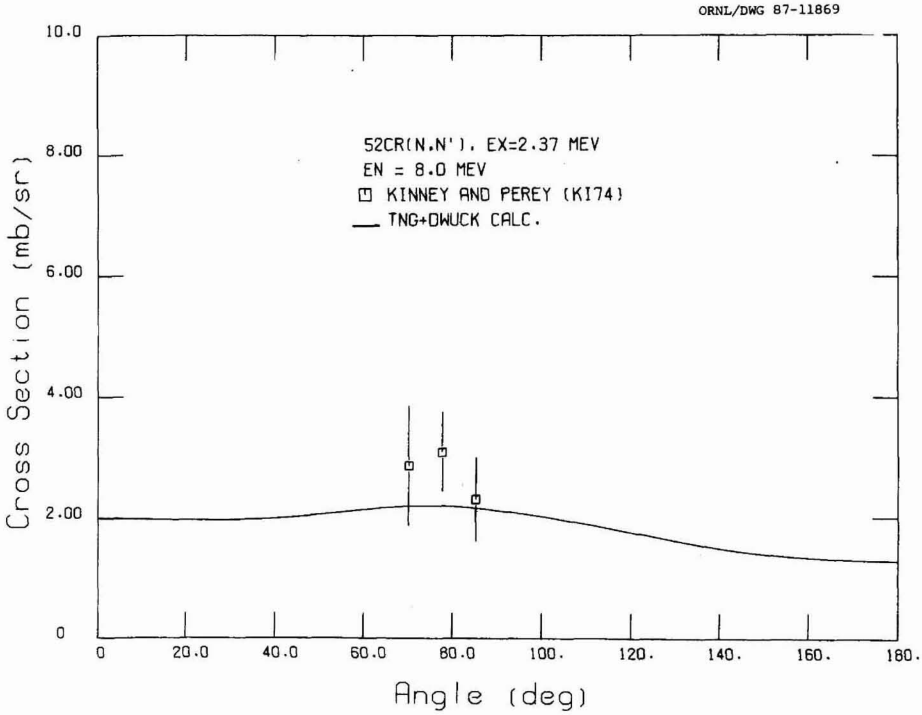

Fig. 25. Comparison of calculated and experimental differential cross sections for exciting the 2.37-MeV level at E_n = 8.0 MeV.

ORNL/DWG 87-11870

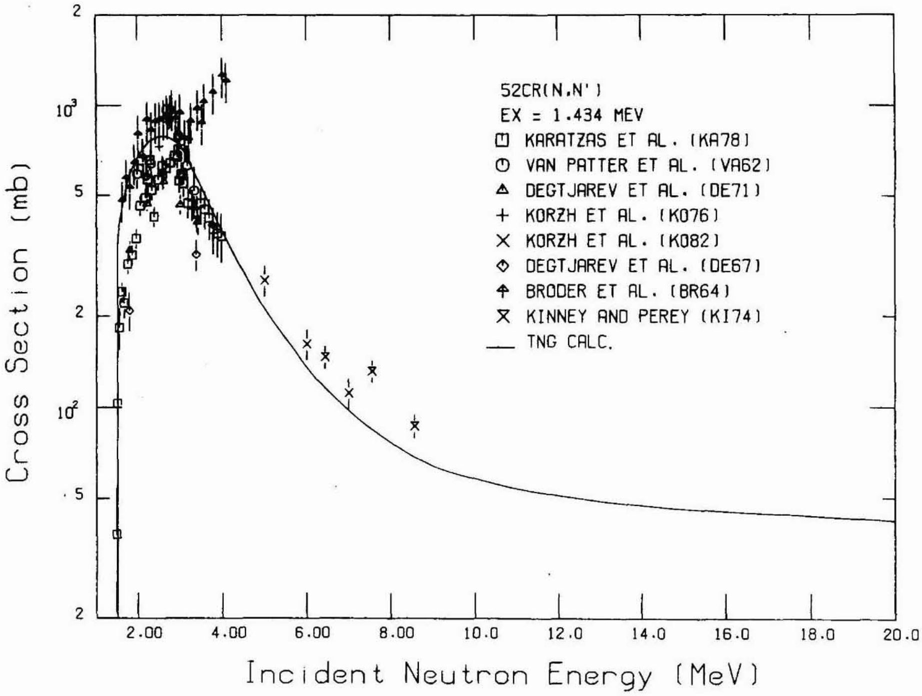

Fig. 26. Comparison of calculated and experimental $^{52}Cr(n,n')$ cross sections for exciting the 1.434-MeV level.

ORNL/DWG 87-11871

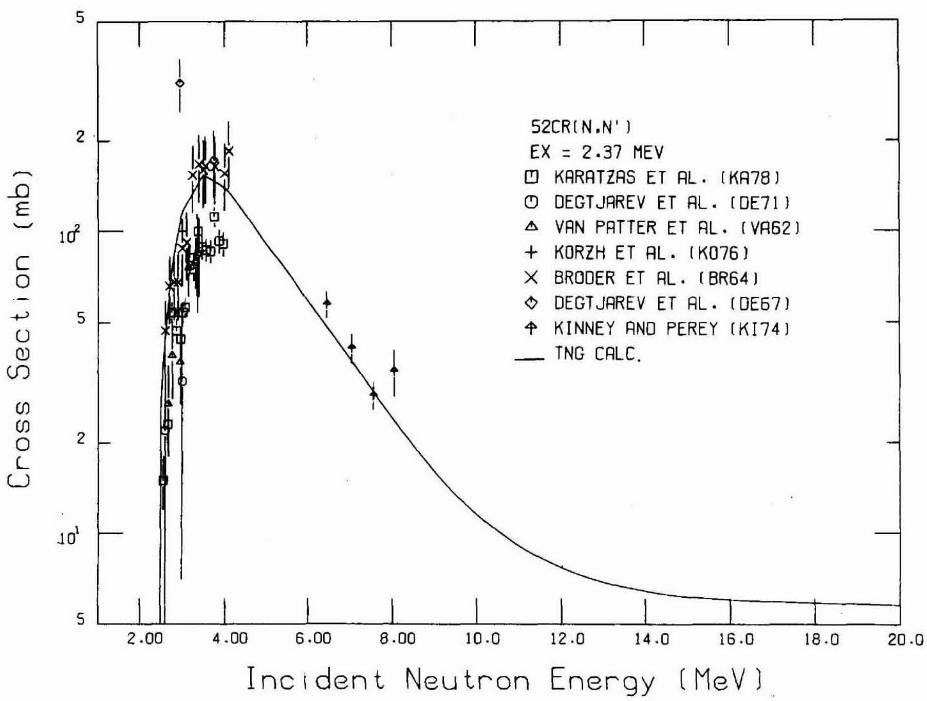

Fig. 27. Comparison of calculated and experimental $^{52}Cr(n,n')$ cross sections for exciting the 2.37-MeV level.

ORNL/DWG 87-11872

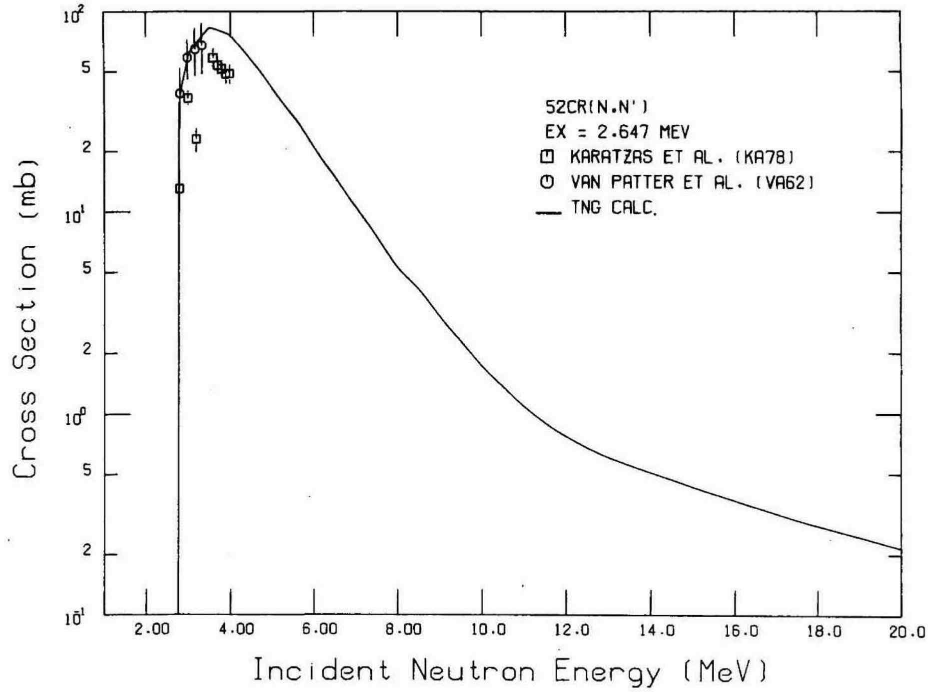

Fig. 28. Comparison of calculated and experimental ^{52}Cr(n,n') cross sections for exciting the 2.647-MeV level.

ORNL/DWG 87-11873

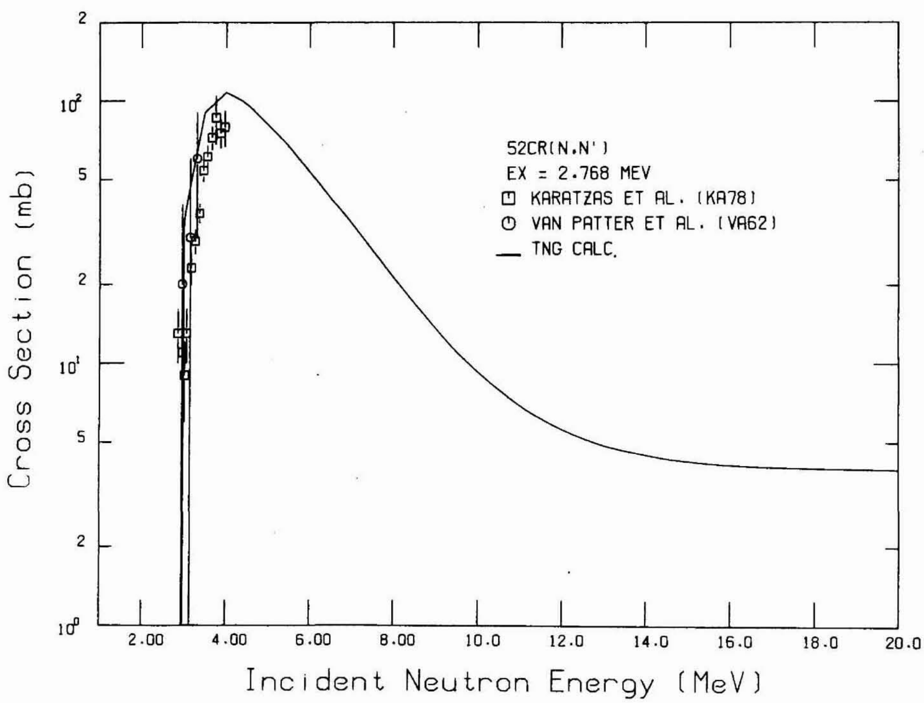

Fig. 29. Comparison of calculated and experimental ^{52}Cr(n,n') cross sections for exciting the 2.768-MeV level.

ORNL/DWG 87-11874

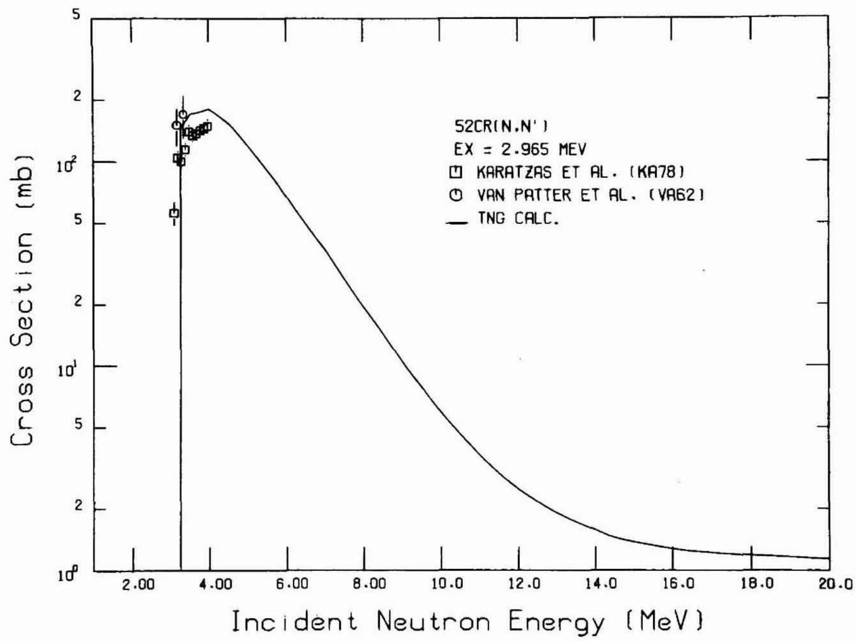

Fig. 30. Comparison of calculated and experimental ^{52}Cr(n,n') cross sections for exciting the 2.965-MeV level.

ORNL/DWG 87-11875

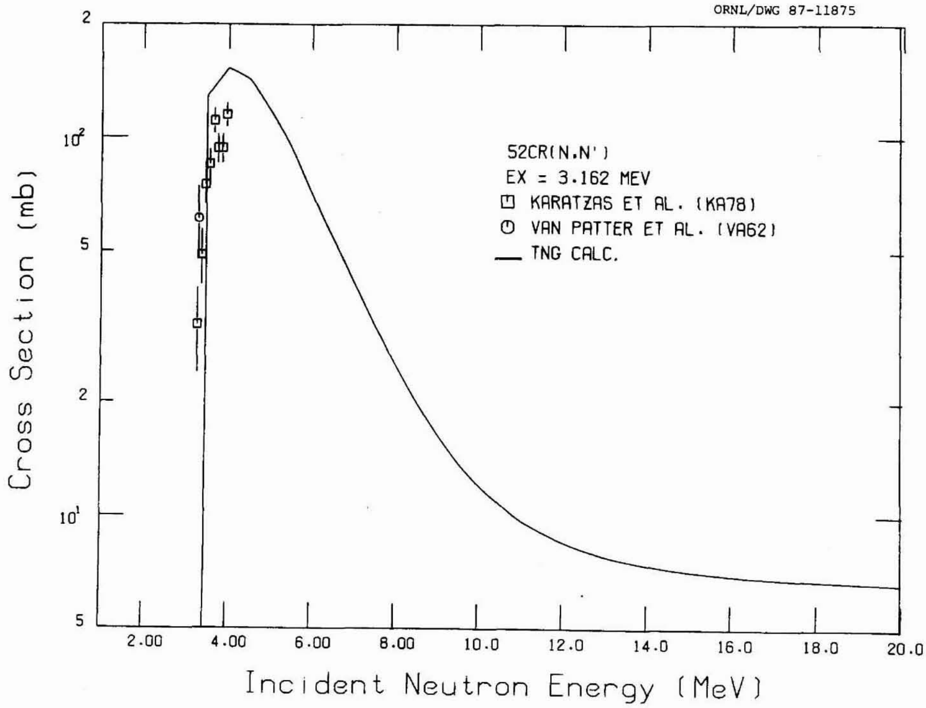

Fig. 31. Comparison of calculated and experimental ^{52}Cr(n,n') cross sections for exciting the 3.162-MeV level.

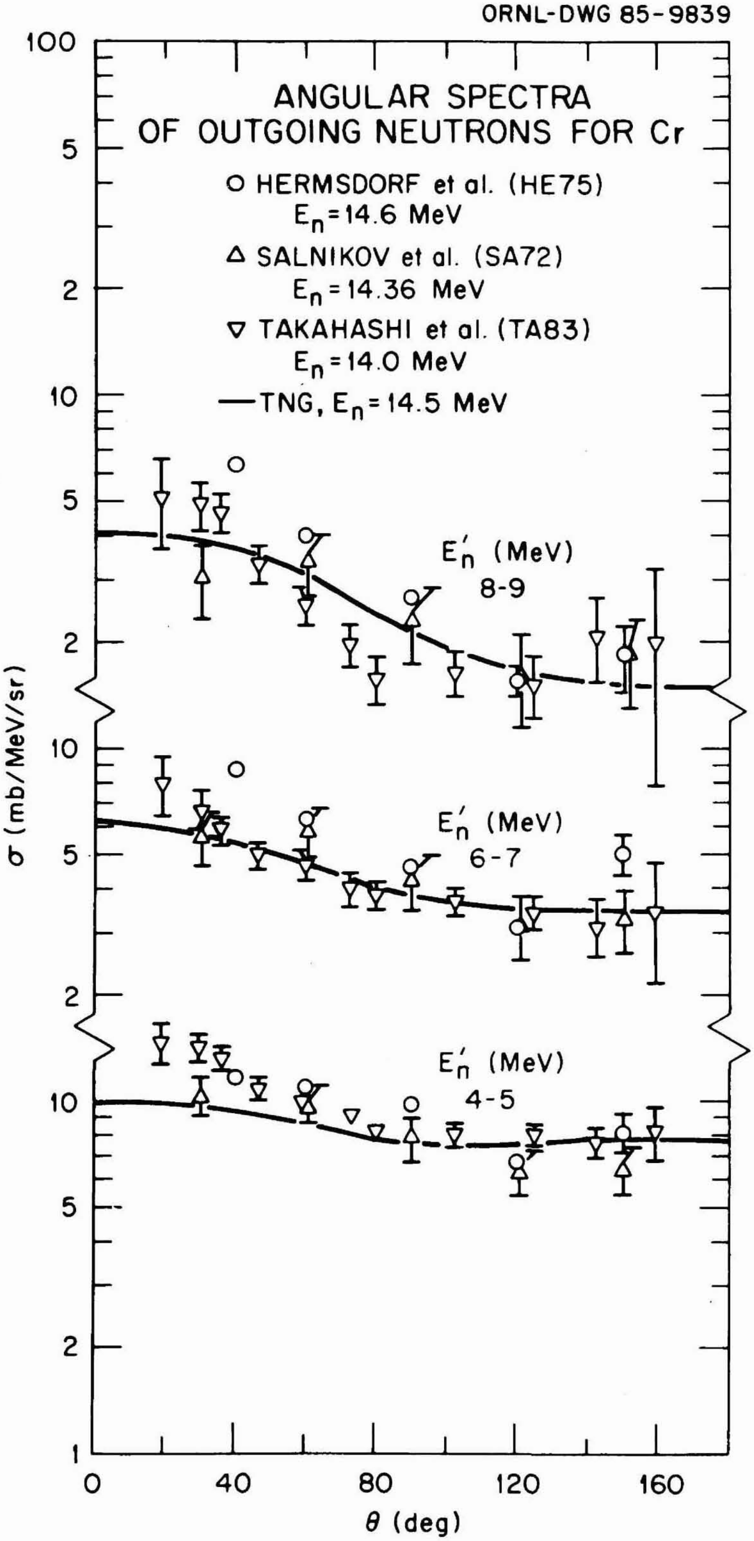

Fig. 32. Comparison of calculated and experimental neutron production cross sections.

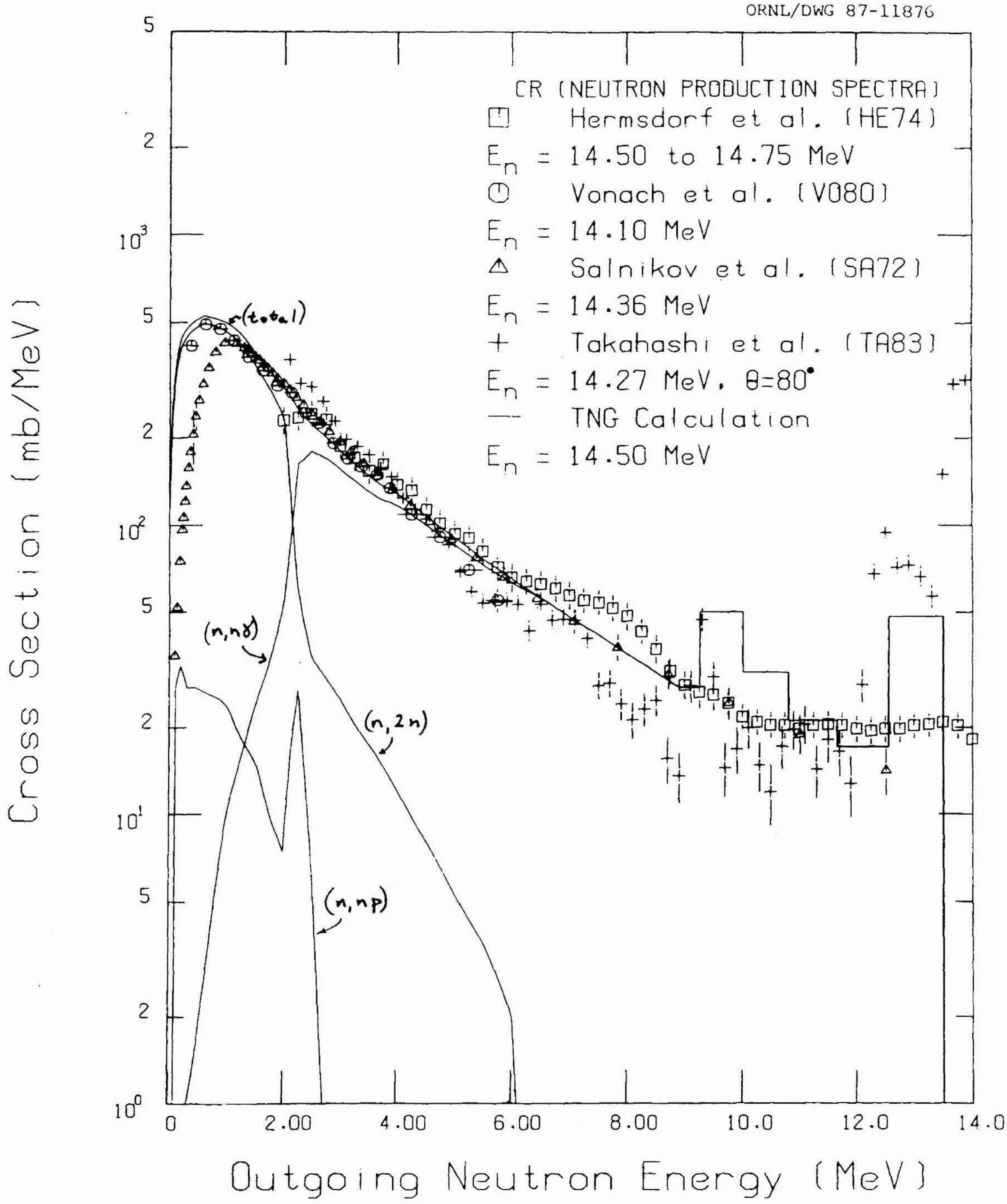

Fig. 33. Neutron emission spectra from the TNG calculation compared with experimental data. The data of Takahashi et al. (TA83) were taken at 80°, and the other measured data sets shown (HE74, VO80, and SA72) are angle integrated. Contributions from the various neutron-producing components are shown (they sum to the total). The curves labeled (*n,np*) and (*n,nα*) include the (*n,pn*) and (*n,αn*) components, respectively.

4.9 PROTON AND ALPHA-PARTICLE EMISSION SPECTRA

The calculated (n,xp) and $(n,x\alpha)$ spectra for ^{52}Cr are compared to measurements by Grimes et al. (GR79, HA77) and Colli et al. (CO62) in Figs. 34-35. The data of Colli et al. were measured at 15°; the other data are angle integrated. The (n,xp) spectra are sums of the partial spectra from the (n,p), (n,pn), and (n,np) reactions. Likewise, the $(n,x\alpha)$ spectra are sums of (n,α), $(n,\alpha n)$, and $(n,n\alpha)$. The measurements of Grimes et al. were taken at an incident energy of 14.8 MeV, and the data of Colli et al. were taken at an incident energy of 14.1 MeV. The TNG results were calculated at an incident energy of 14.5 MeV and are in good agreement with the data.

4.10 BINARY AND TERTIARY REACTION CROSS SECTIONS

The calculated binary and tertiary cross sections for ^{52}Cr are compared to available data in Figs. 36-40. Figure 36 shows the results of ^{52}Cr(n,p). The data are quite discrepant at an incident energy of 14.5 MeV, but the calculation agrees very well with the data of Holmberg et al. (HO74), Valkonen (VA76), and Dresler et al. (DR73) at this energy. The calculated total proton emission versus data for ^{52}Cr is shown in Fig. 37. The calculation agrees well with the data around an incident energy of 14 MeV, but disagrees with the data of Smith and Meadows (SM80) above an incident energy of 7 MeV.

The ^{52}Cr$(n,2n)$ data and TNG calculations are shown in Fig. 38. The calculation agrees well with the data of Sailer et al. (SA77), Wenusch and Vonach (WE62), and Borman et al. (BO68) for incident energies less than 15 MeV. The TNG calculation for ^{52}Cr$(n,2n)$ (multiplied by 0.9) is added to the calculation for ^{53}Cr$(n,2n)$ (multiplied by 0.1) and compared to available natural chromium data in Fig. 39 with very good agreement.

The total alpha-emission results from TNG for ^{52}Cr are compared to data for both ^{52}Cr and ^{nat}Cr in Fig. 40. The calculation agrees fairly well with the data of Paulsen et al. (PA81) for incident energies less than 10 MeV, but is somewhat smaller than the data around 14 MeV incident energy.

The need for nuclear model analyses can be seen from these figures for in many cases the measurements disagree and data are not available for some reactions [e.g., (n,α), (n,np), and $(n,n\alpha)$]. The TNG calculations have provided a reasonable characterization of the behavior of the binary and tertiary reaction cross sections over a wide range of incident neutron energies.

4.11 GAMMA-RAY EXCITATION FUNCTIONS

Excitation functions for 11 gamma rays of ^{52}Cr are shown in Figs. 41-51. The TNG calculations are in fairly good agreement with the data of Larson (LA85), Karatzas et al. (KA78), Breunlich et al. (BR71), and Van Patter et al. (VA62). The data of Voss et al. (VO75) are averaged in the figures and, with the exception of the excitation functions for E_γ = 0.647, 1.531, and 2.038 MeV, are consistently at least 30% smaller than the TNG calculations. The cross section measured by Burymov (BU69) is larger than the calculation (see Fig. 41). The measured data sets of Tessler et al. (TE75) and Grenier et al. (GR74) are inconsistent in their agreement/disagreement with the TNG calculations from one excitation function to the next.

4.12 INTEGRATED YIELD OF SECONDARY GAMMA RAYS

The integrated yield of secondary gamma rays with $E_\gamma \geqslant 0.5$ MeV for the TNG calculations and measurements are shown in Fig. 52. For clarity, the data of Morgan and Newman (MO76) were plotted at the midpoints of the incident neutron energy bins. The calculated yields agree very well with both the data of Morgan and Newman and the data of Drake et al. (DR78).

ORNL/DWG 87-11877

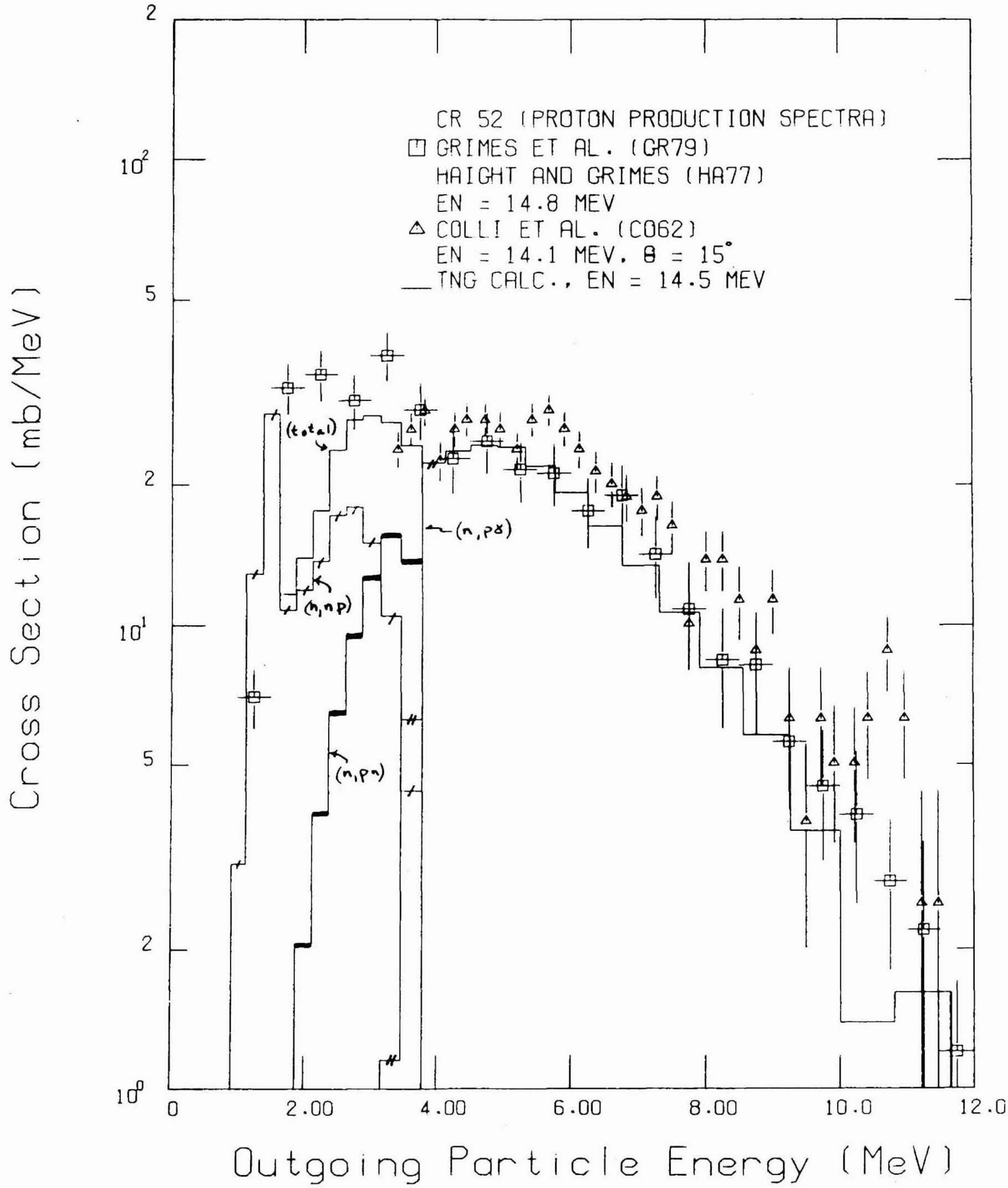

Fig. 34. Comparison of calculated experimental proton production spectra for ^{52}Cr. The measurements were taken at incident energies of 14.8 and 14.1 MeV; the TNG calculation was for E_n = 14.5 MeV. The data of Grimes et al. (GR79, HA77) are angle integrated; the data of Colli et al. (CO62) were taken at 15°.

ORNL/DWG 87-11878

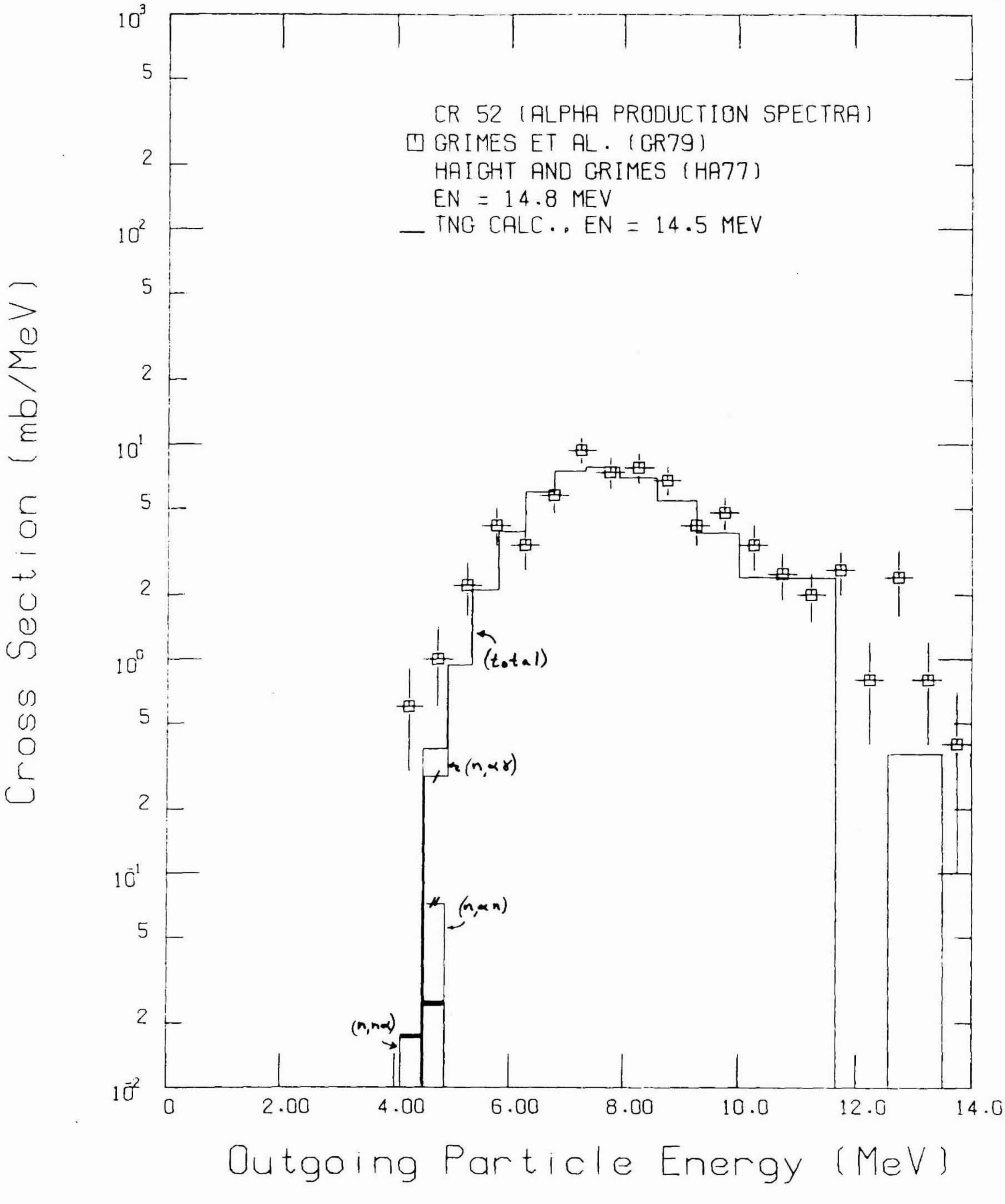

Fig. 35. Comparison of calculated and experimental alpha production spectra for ^{52}Cr. The measurement was taken at an incident energy of 14.8 MeV, the TNG calculation was for E_n = 14.5 MeV.

ORNL/DWG 87-11879

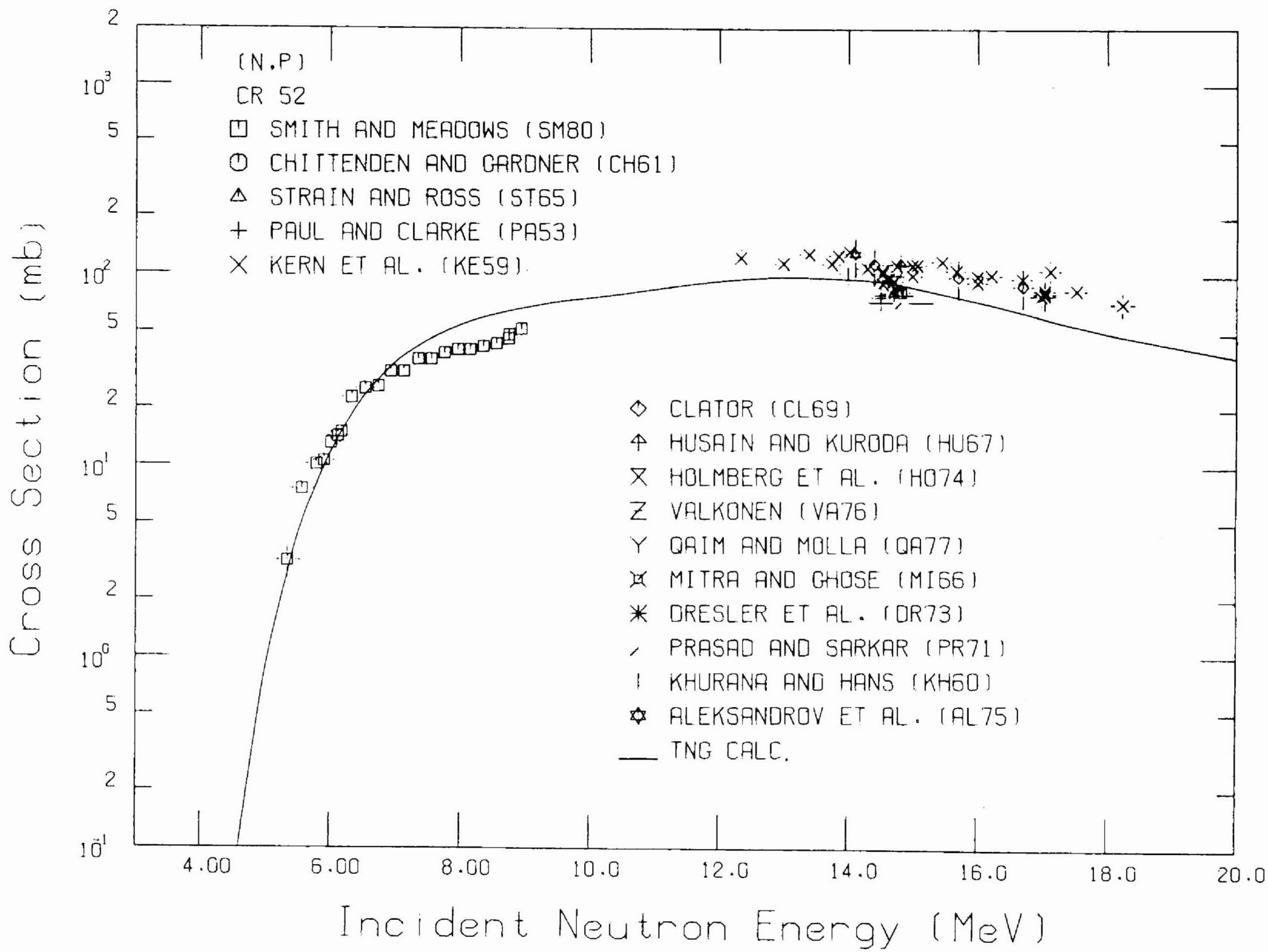

Fig. 36. Comparison of calculated and experimental $^{52}Cr(n,p)$ cross sections.

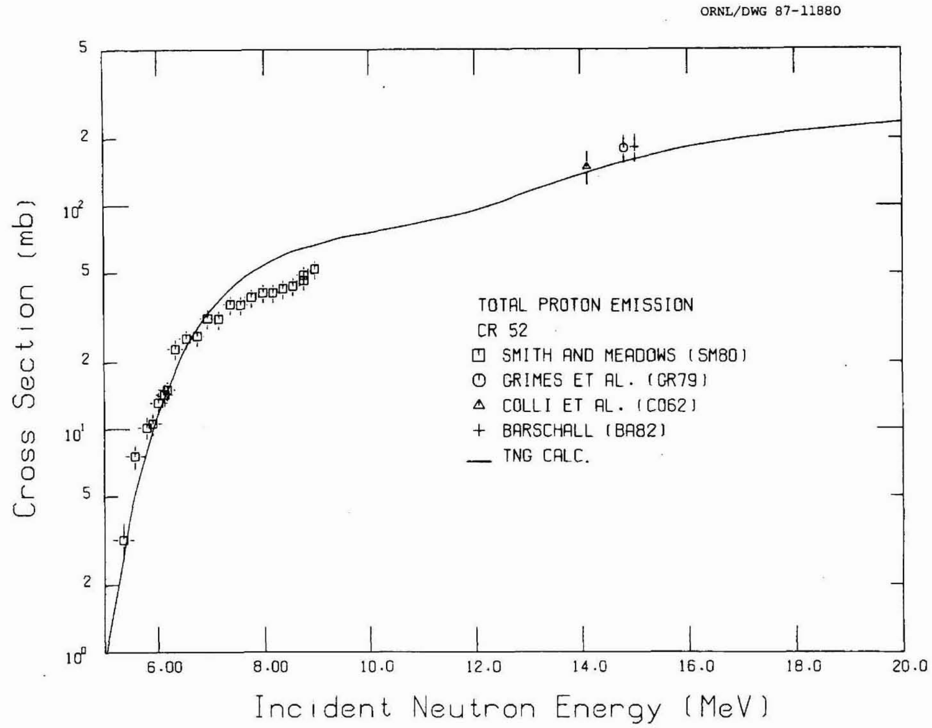

Fig. 37. Comparison of calculated and experimental cross sections for the total proton emission of ^{52}Cr.

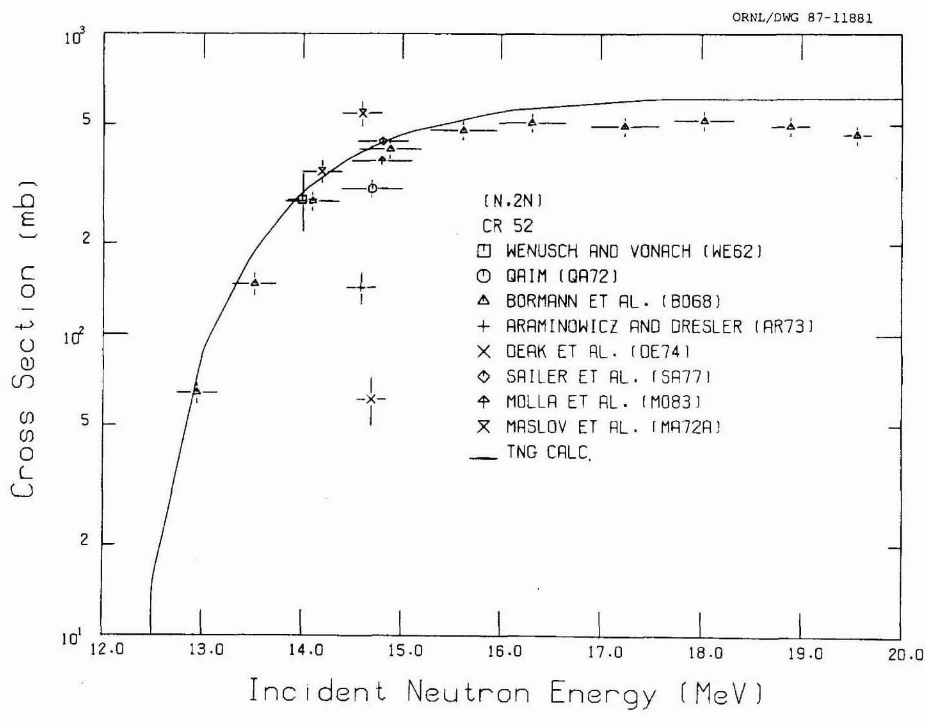

Fig. 38. Comparison of calculated and experimental ^{52}Cr(n,2n) cross sections.

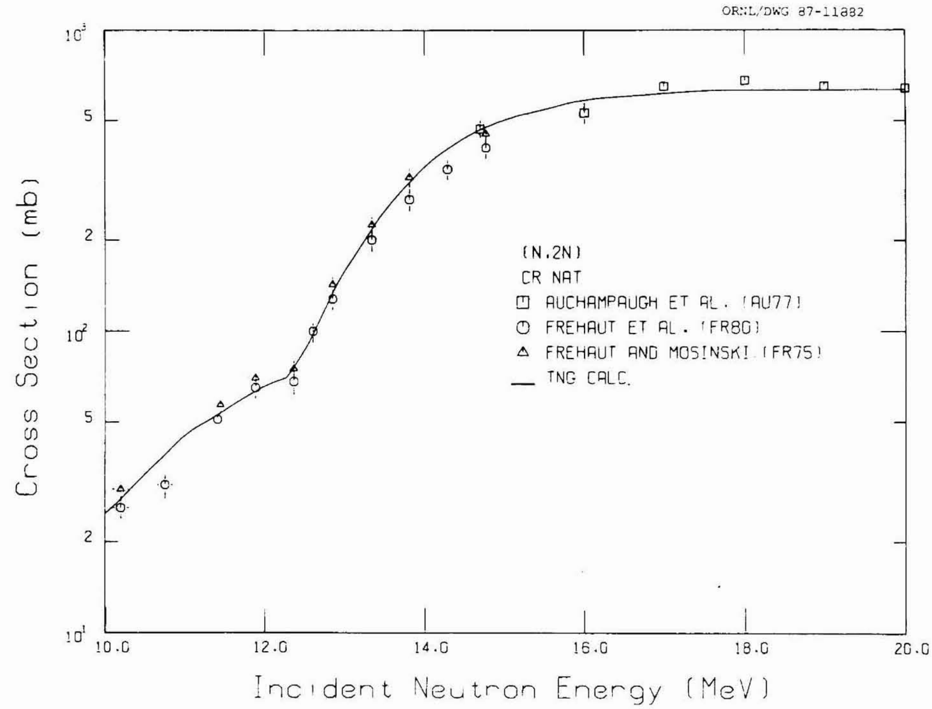

Fig. 39. Comparison of calculated and experimental $^{nat}Cr(n,2n)$ cross sections.

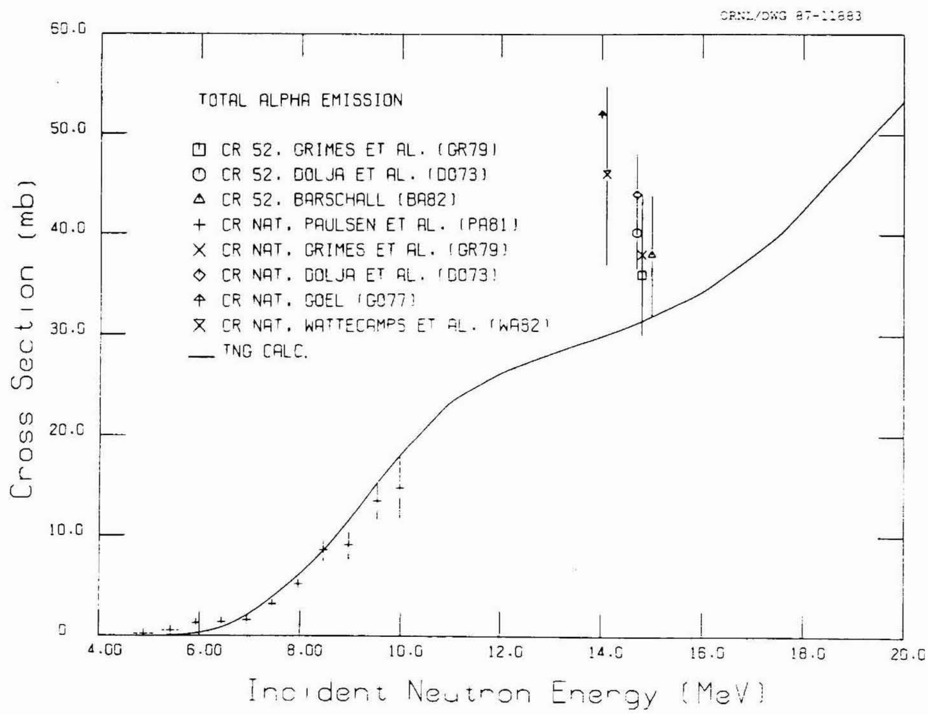

Fig. 40. Comparison of calculated (^{52}Cr) and experimental (^{52}Cr and ^{nat}Cr) cross sections for the total alpha emission.

ORNL/DWG 87-11884

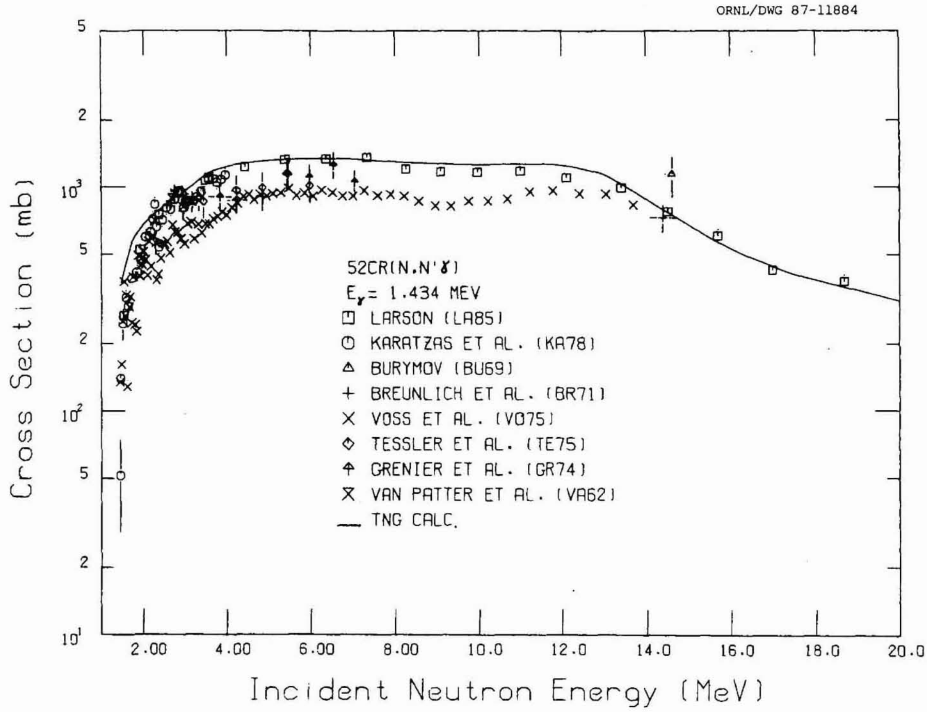

Fig. 41. Comparison of calculated and experimental data of the excitation function for the E_γ = 1.434 MeV transition following ^{52}Cr(n,$n'\gamma$).

ORNL/DWG 87-11885

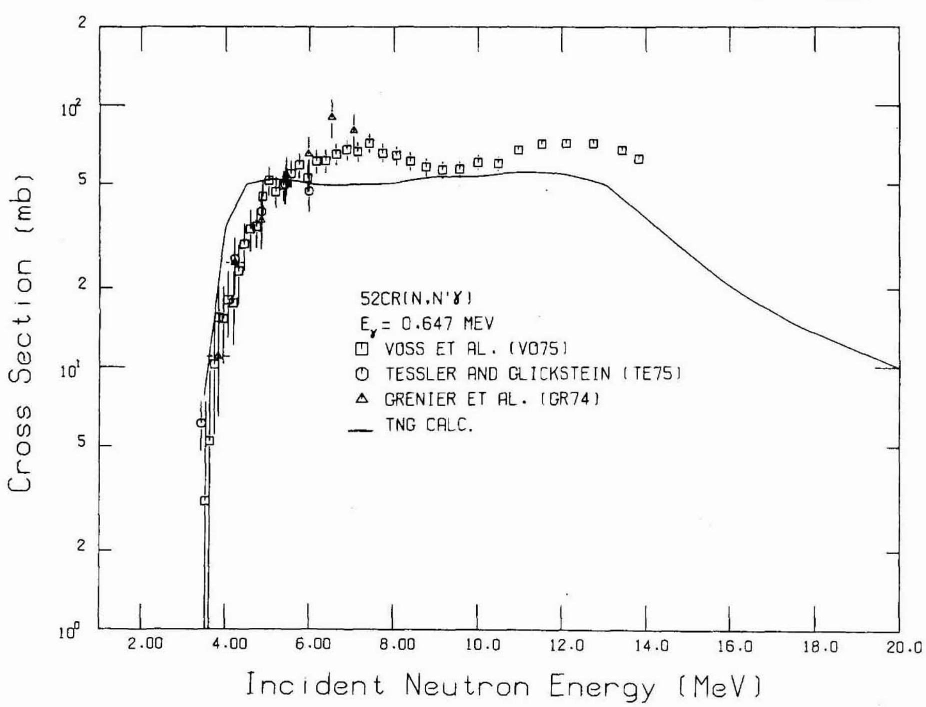

Fig. 42. Comparison of calculated and experimental data of the excitation function for the E_γ = 0.647 MeV transition following ^{52}Cr(n,$n'\gamma$).

ORNL/DWG 87-11886

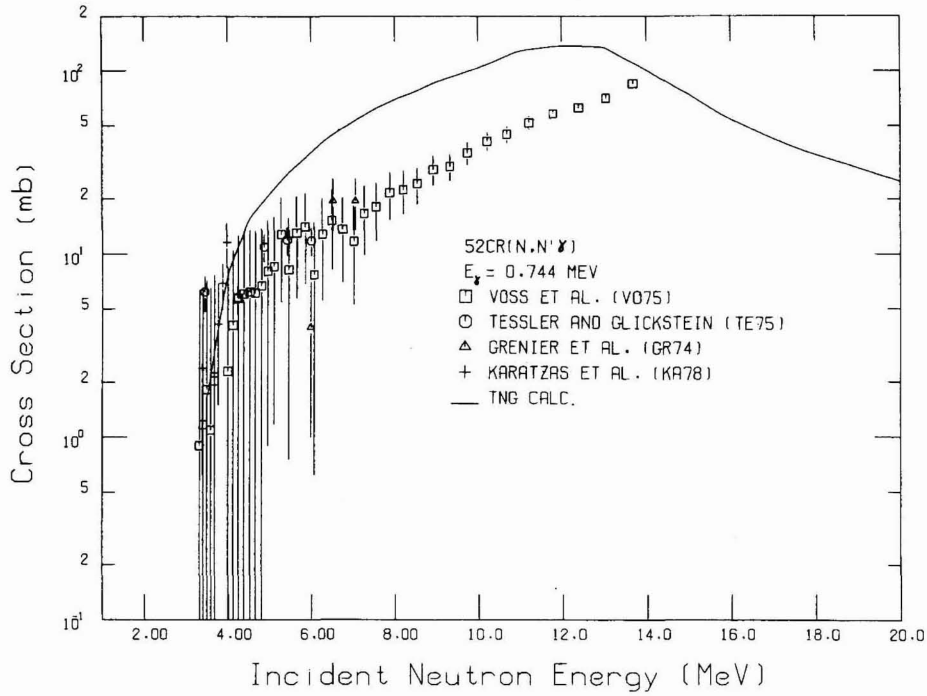

Fig. 43. Comparison of calculated and experimental data of the excitation function for the E_γ = 0.744 MeV transition following ^{52}Cr($n,n'\gamma$).

ORNL/DWG 87-11887

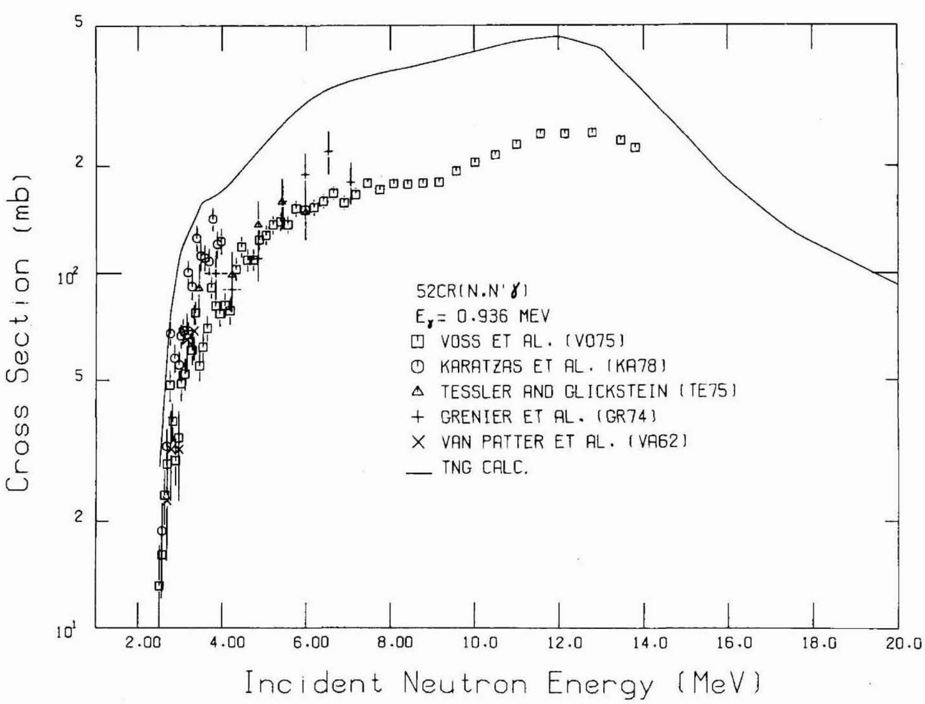

Fig. 44. Comparison of calculated and experimental data of the excitation function for the E_γ = 0.936 MeV transition following ^{52}Cr($n,n'\gamma$).

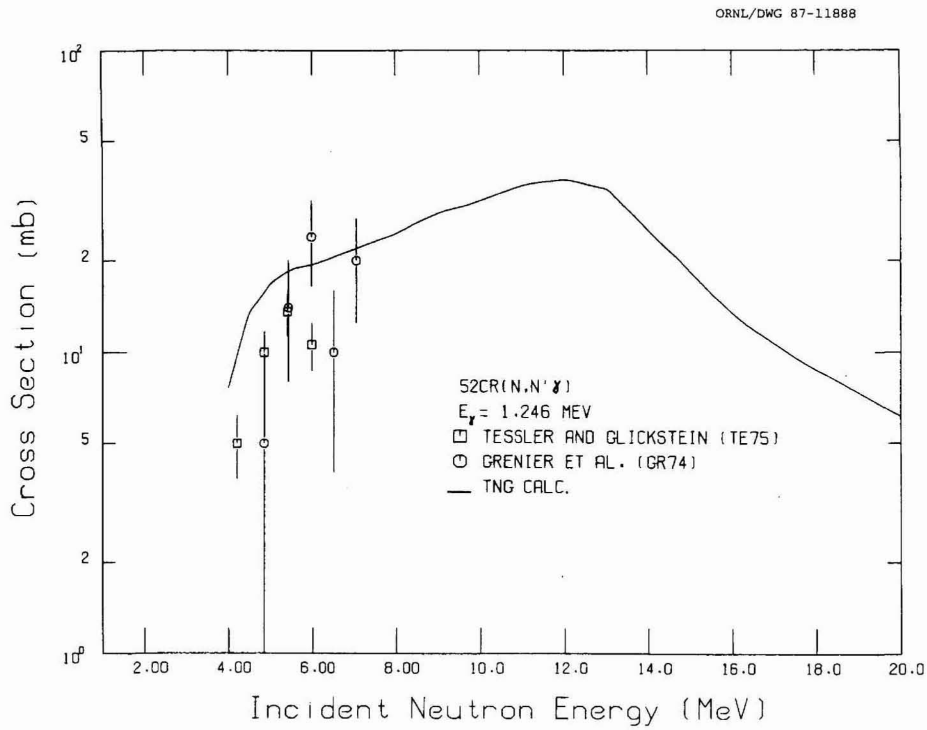

Fig. 45. Comparison of calculated and experimental data of the excitation function for the E_γ = 1.246 MeV transition following ^{52}Cr($n,n'\gamma$).

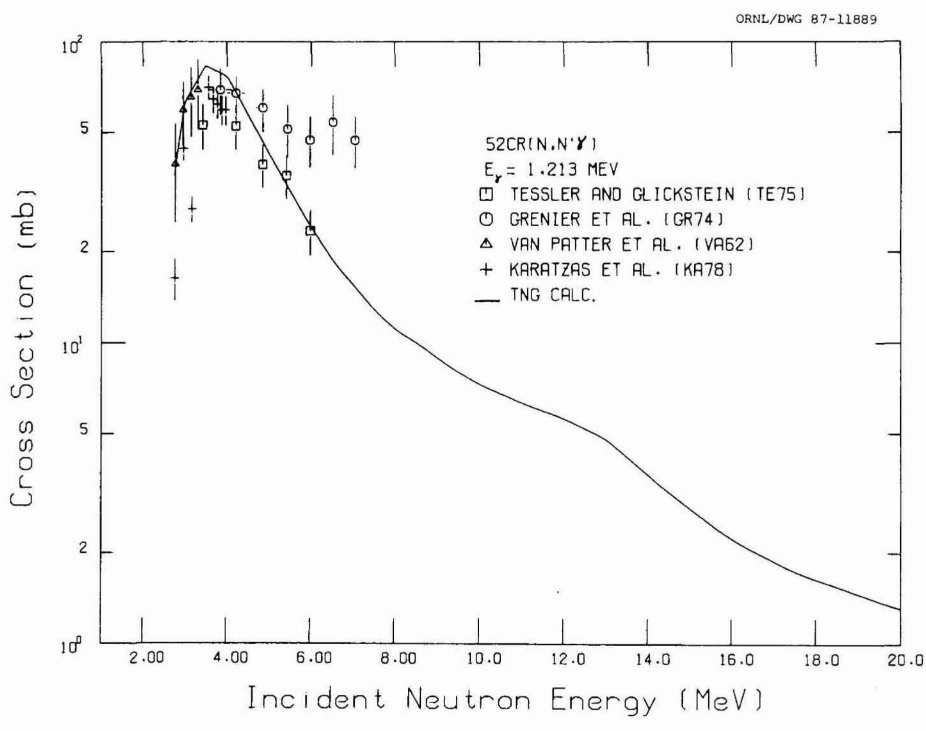

Fig. 46. Comparison of calculated and experimental data of the excitation function for the E_γ = 1.213 MeV transition following ^{52}Cr($n,n'\gamma$).

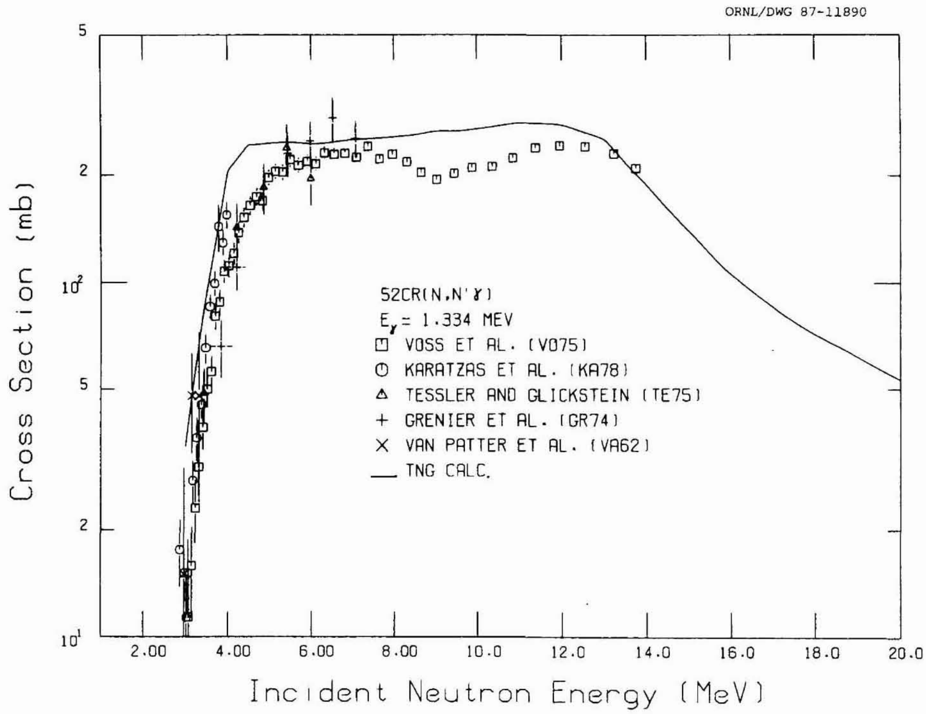

Fig. 47. Comparison of calculated and experimental data of the excitation function for the E_γ = 1.334 MeV transition following ^{52}Cr($n,n'\gamma$).

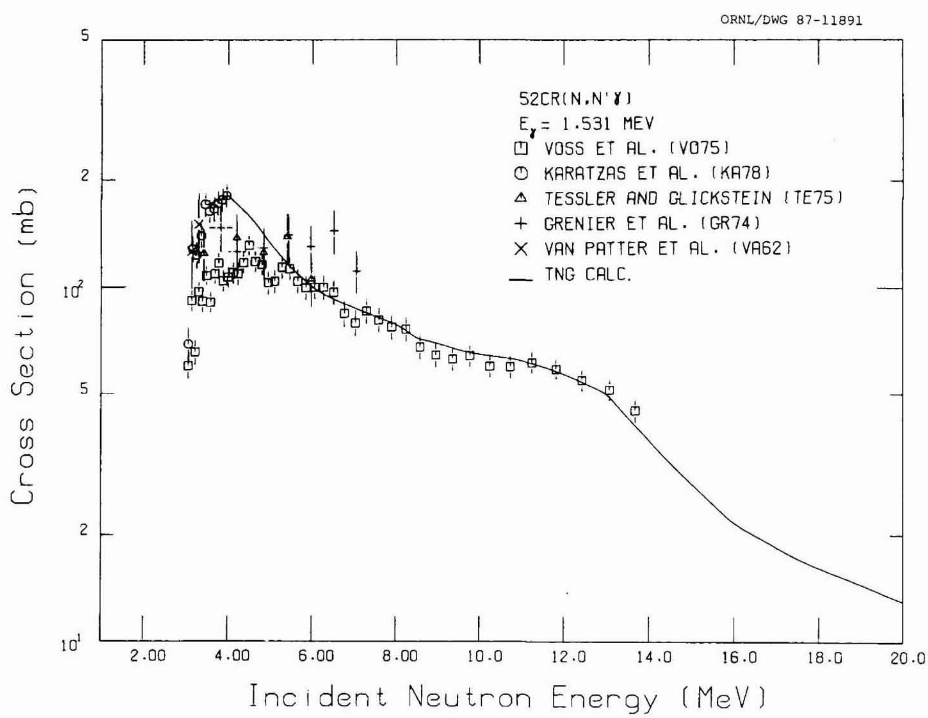

Fig. 48. Comparison of calculated and experimental data of the excitation function for the E_γ = 1.531 MeV transition following ^{52}Cr($n,n'\gamma$).

ORNL/DWG 87-11892

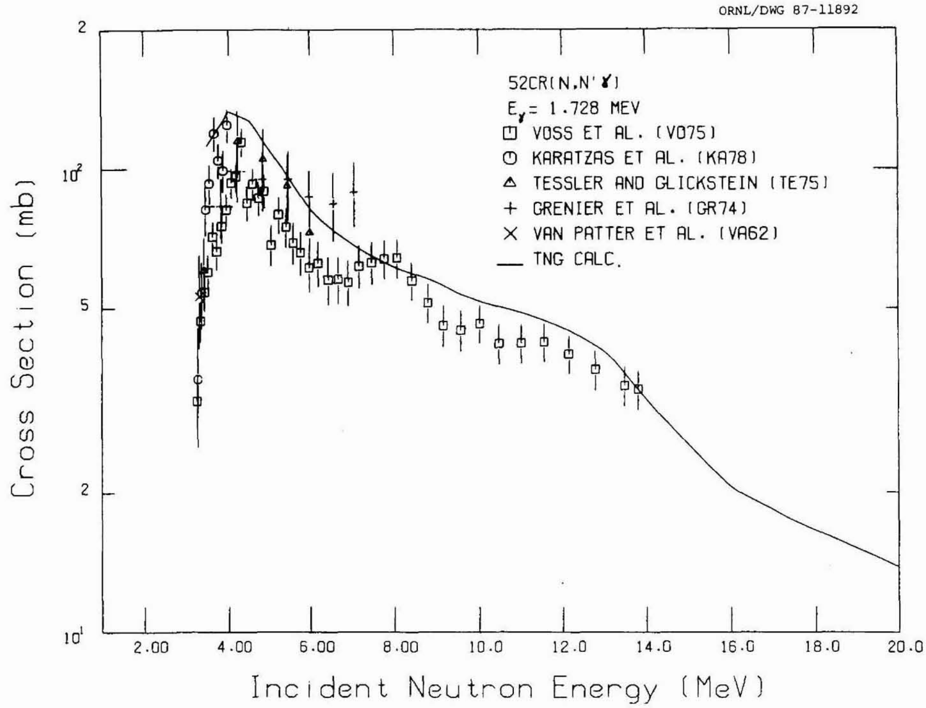

Fig. 49. Comparison of calculated and experimental data of the excitation function for the E_γ = 1.728 MeV transition following ^{52}Cr($n,n'\gamma$).

ORNL/DWG 87-11893

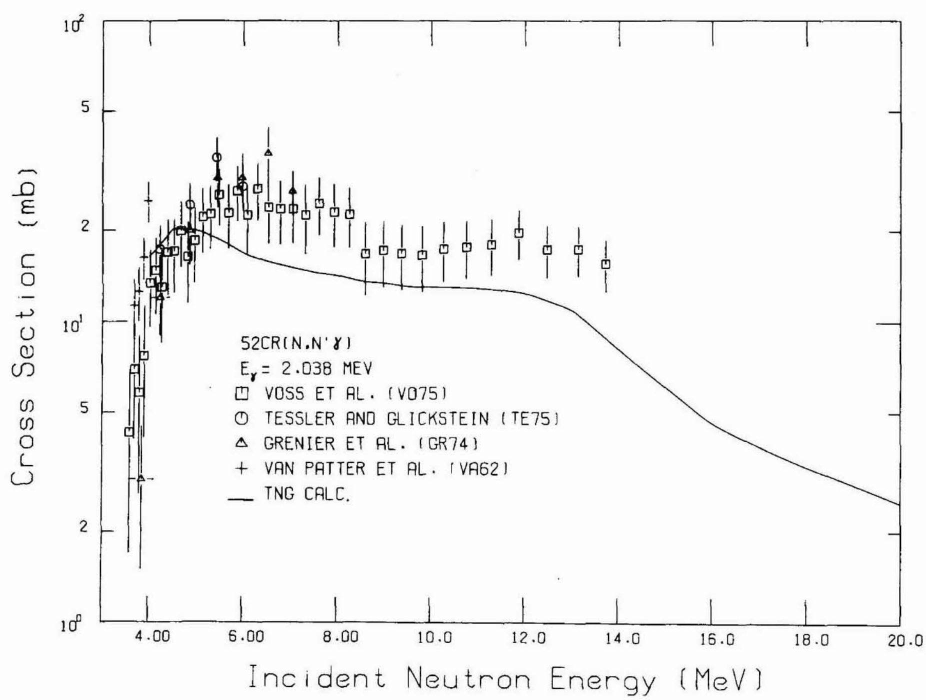

Fig. 50. Comparison of calculated and experimental data of the excitation function for the E_γ = 2.038 MeV transition following ^{52}Cr($n,n'\gamma$).

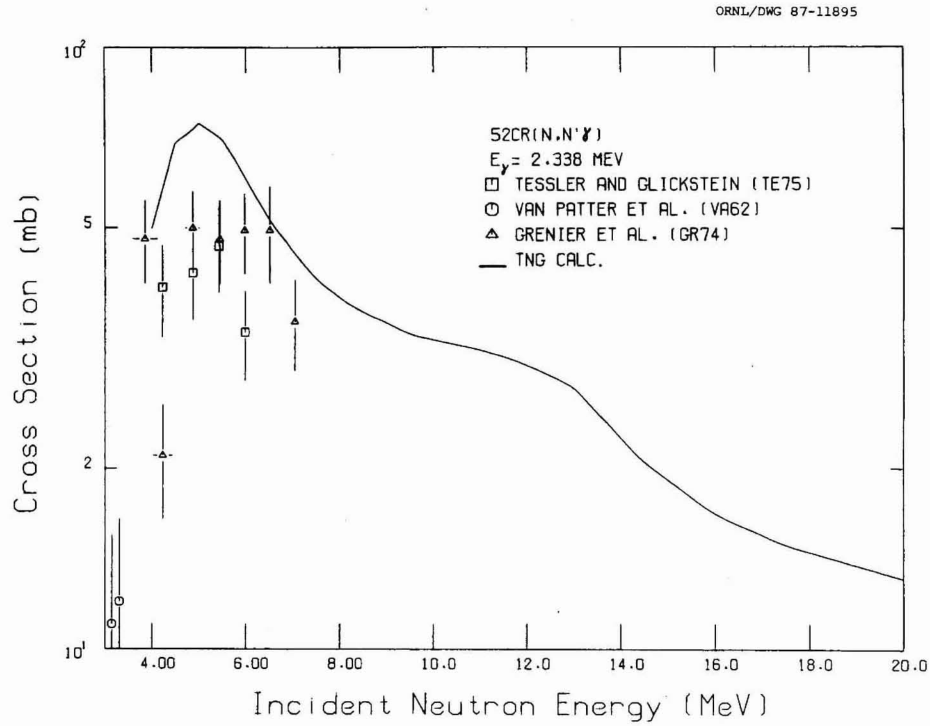

Fig. 51. Comparison of calculated and experimental data of the excitation function for the E_γ = 2.338 MeV transition following ^{52}Cr($n,n'\gamma$).

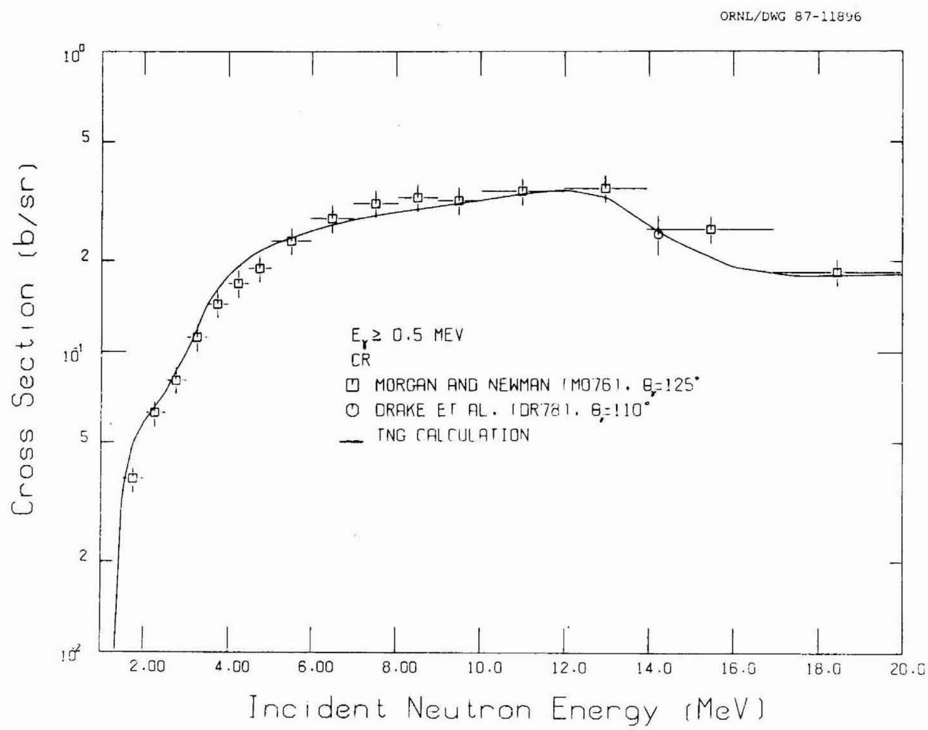

Fig. 52. Integrated yield of secondary gamma rays with $E_\gamma \geqslant$ 0.5 MeV as a function of incident neutron energy. Gamma-ray scattering angles θ_γ are given in the legend.

4.13 GAMMA-RAY PRODUCTION CROSS SECTIONS AND SPECTRAL COMPARISONS

The calculated gamma-ray production cross sections are compared to data measured by Morgan and Newman (MO76) and Drake et al. (DR78) in Figs. 53-56. Although the measurements of Morgan and Newman, as well as the calculations by TNG, were made at numerous incident energies, comparisons are shown only for energies of 5.5, 9.5, and 14.5 MeV. In each figure, the calculated secondary spectra were smeared by a Gaussian function corresponding to the resolution of the detector for the data of Morgan and Newman (MO76).

Before looking at the comparisons between the computed gamma-ray production spectra and measurements cited above, we should first discuss the energy-conservation constraint imposed in the calculation. In each reaction, the sum of the energies of the outgoing particles (including the recoiled heavy particle) and gamma rays equals the incident neutron energy plus the Q value of the reaction. Since there is good overall agreement between calculation and experiment in various partial reaction cross sections and particle-production spectra, the computed gamma-ray production spectra can be regarded as the most consistent possible with these data.

In general, the TNG calculations agree fairly well with the measurements. At 5.5-MeV incident neutron energy, the calculation does not agree well with the measurement for $E_\gamma > 2.0$ MeV, but agreement is quite good for incident energies of 9.5 and 14.5 MeV.

5. COMPARISON OF CALCULATIONS WITH ENDF/B-V

The TNG calculations are compared to a representative set of cross sections from the ENDF/B-V for chromium (MAT 1324) in Figs. 57-67. In each figure, the curves labeled "TNG Calculation" include the sum of the calculated cross sections for ^{52}Cr (multiplied by 0.9) and ^{53}Cr (multiplied by 0.10). Comparison of the total inelastic scattering cross section is given in Fig. 57. The total integrated yield of secondary neutrons as a function of incident neutron energy is shown in Fig. 58. Although the agreement appears quite reasonable in Fig. 58 for incident energies less than 13.0 MeV, a look at the neutron emission spectra for incident neutron energies of 5.5 and 9.5 in Figs. 59-60 reveals significant differences. Also, the evaluated spectrum for $E_n = 14.5$ MeV (Fig. 57) does not project enough high-energy secondary neutrons. This lack can be understood because the ENDF/B-V evaluation does not include a precompound component. It should be noted that the elastic cross section has not been included in Figs. 58-61. Comparison of the (n,p) and (n,α) cross sections are given in Figs. 62 and 63, respectively, with significant disagreement.

Differences are seen when comparing the TNG calculations for gamma rays with the ENDF/B-V values as shown in Figs. 64-67. The total integrated yields of secondary gamma rays from the calculations and from ENDF/B-V are shown in Fig. 64. The ENDF/B-V curve drops off sharply at 17.0 MeV incident neutron energy since the cross section given in the ENDF/B-V is 0.0 at 20.0 MeV incident neutron energy. The computed gamma-ray production cross sections are compared to ENDF/B-V for incident neutron energies of 5.5, 9.5, and 14.5 MeV in Figs. 65-67. In these plots, the secondary spectra were smeared by a Gaussian function; for clarity the broader resolution width due to Morgan (MO79) was used. The ENDF/B-V evaluation used the data of Morgan and Newman (MO76) that were shown in Figs. 53-55.

ORNL/DWG 87-11897

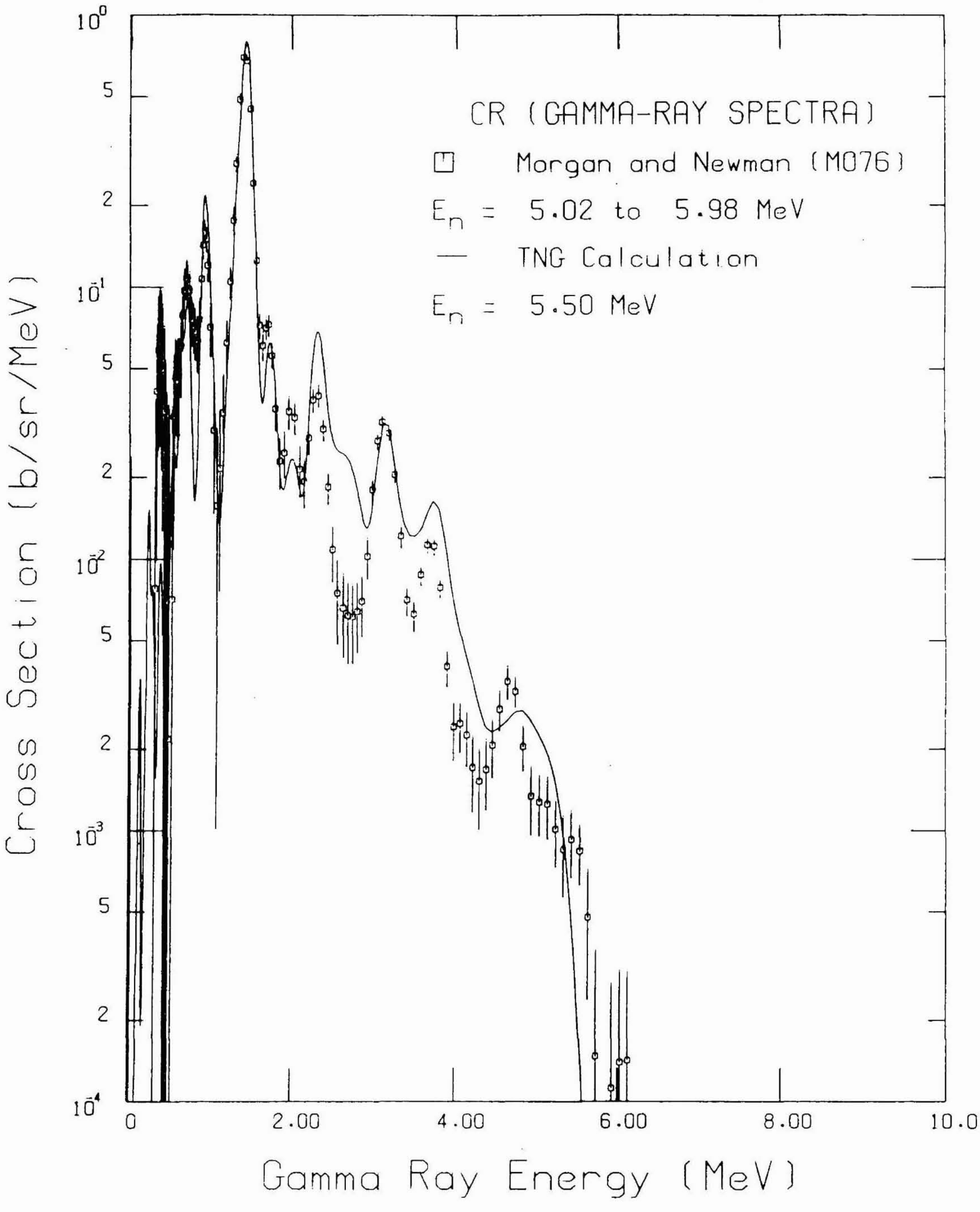

Fig. 53. Secondary gamma-ray spectra versus gamma-ray energy from the TNG calculation (incident energy E_n = 5.5 MeV) compared with the data of Morgan and Newman (MO76).

ORNL/DWG 87-11898

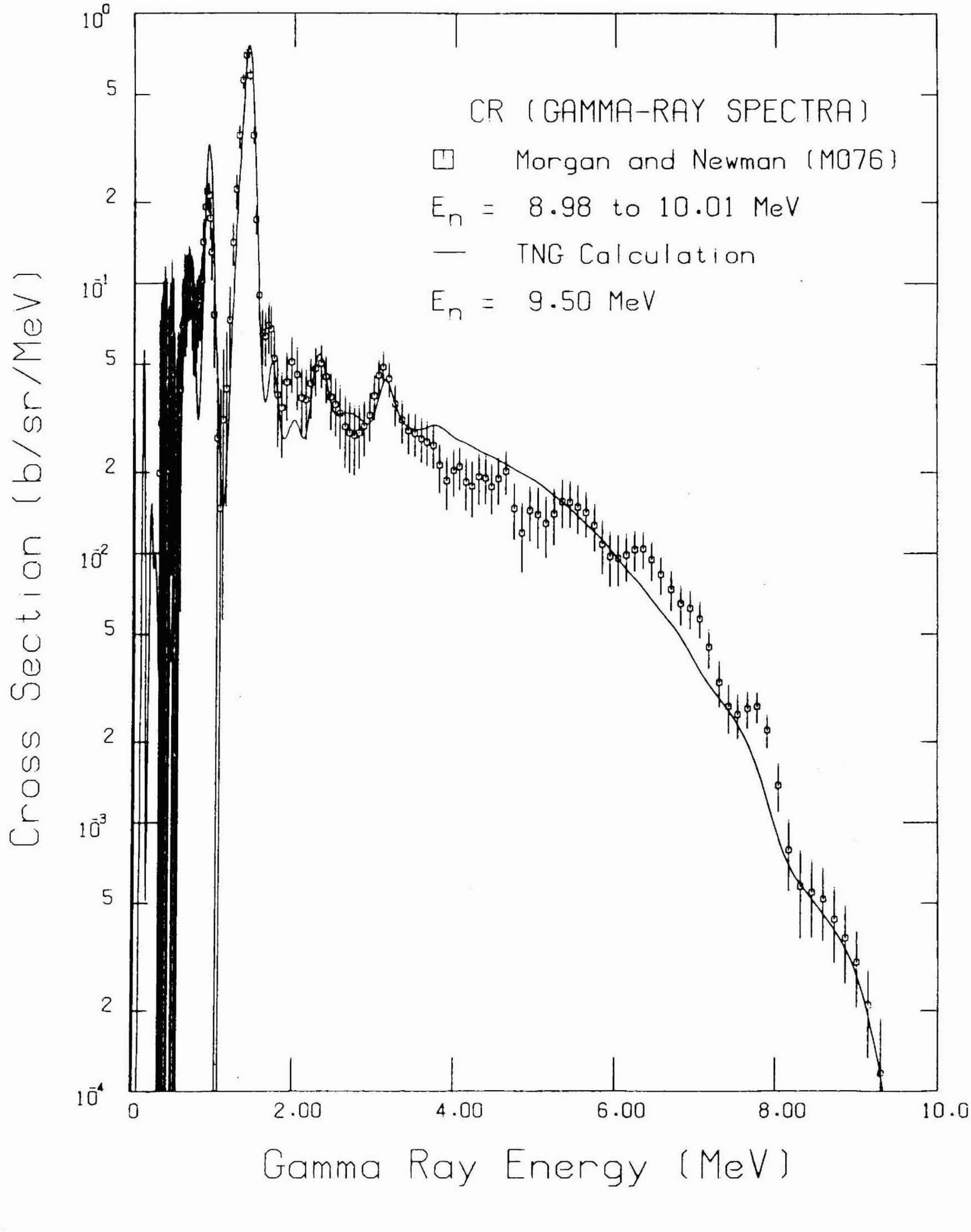

Fig. 54. Secondary gamma-ray spectra versus gamma-ray energy from the TNG calculation (incident energy E_n = 9.5 MeV) compared with the data of Morgan and Newman (MO76).

ORNL/DWG 87-11899

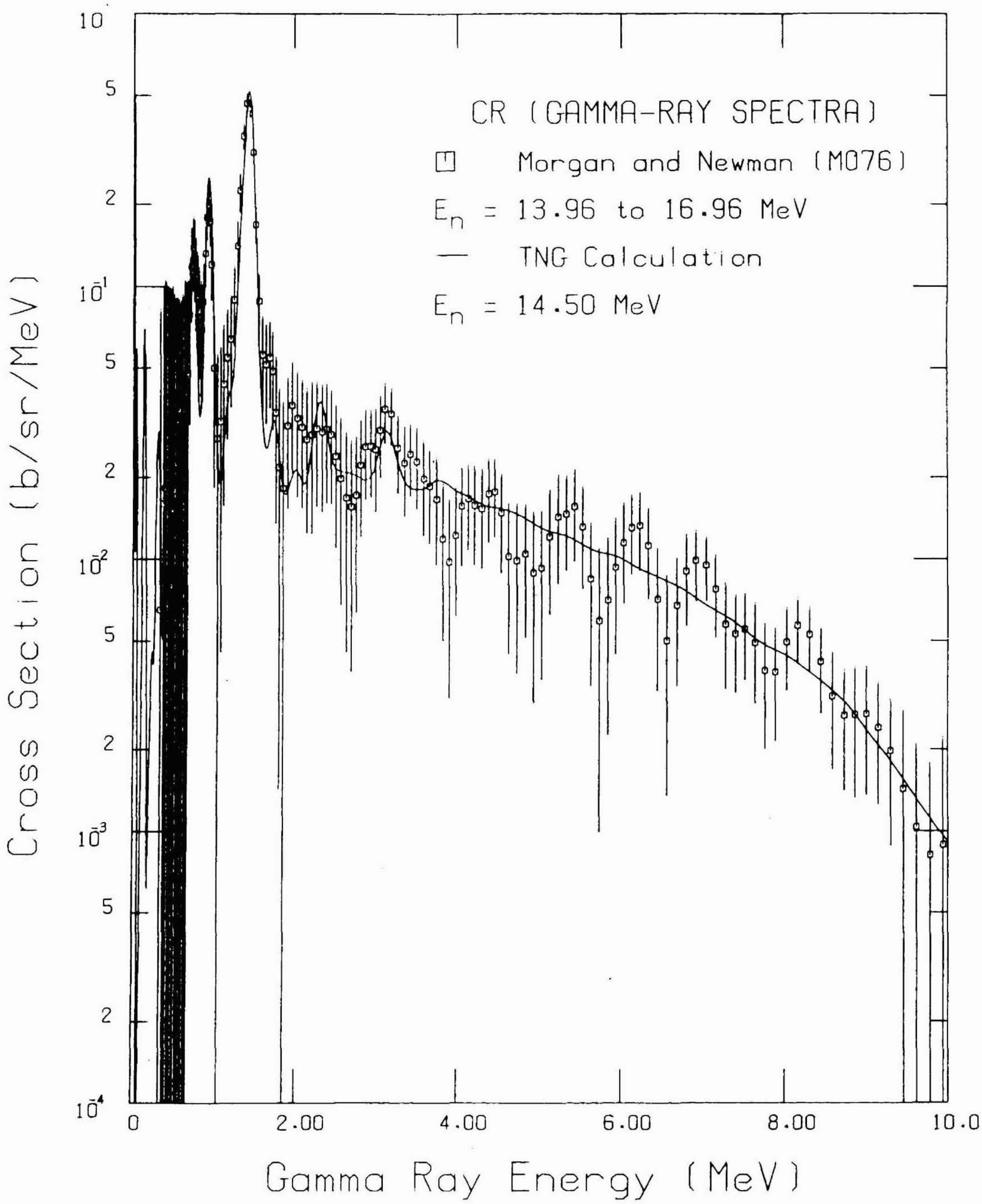

Fig. 55. Secondary gamma-ray spectra versus gamma-ray energy from the TNG calculation (incident energy E_n = 14.5 MeV) compared with the data of Morgan and Newman (MO76).

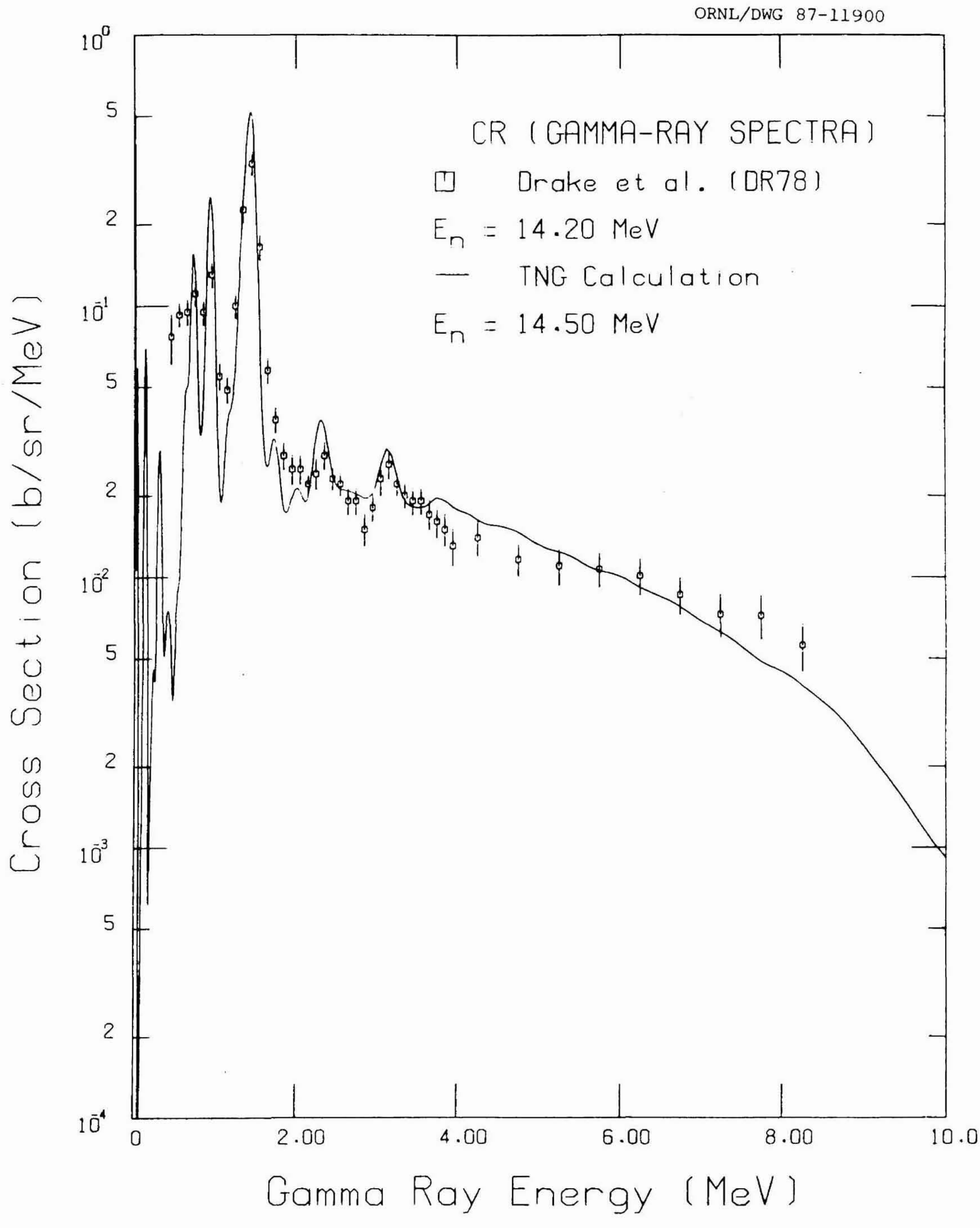

Fig. 56. Secondary gamma-ray spectra versus gamma-ray energy from the TNG calculation (incident energy E_n = 14.5 MeV) compared with the data of Drake et al. (DR78).

ORNL/DWG 87-11901

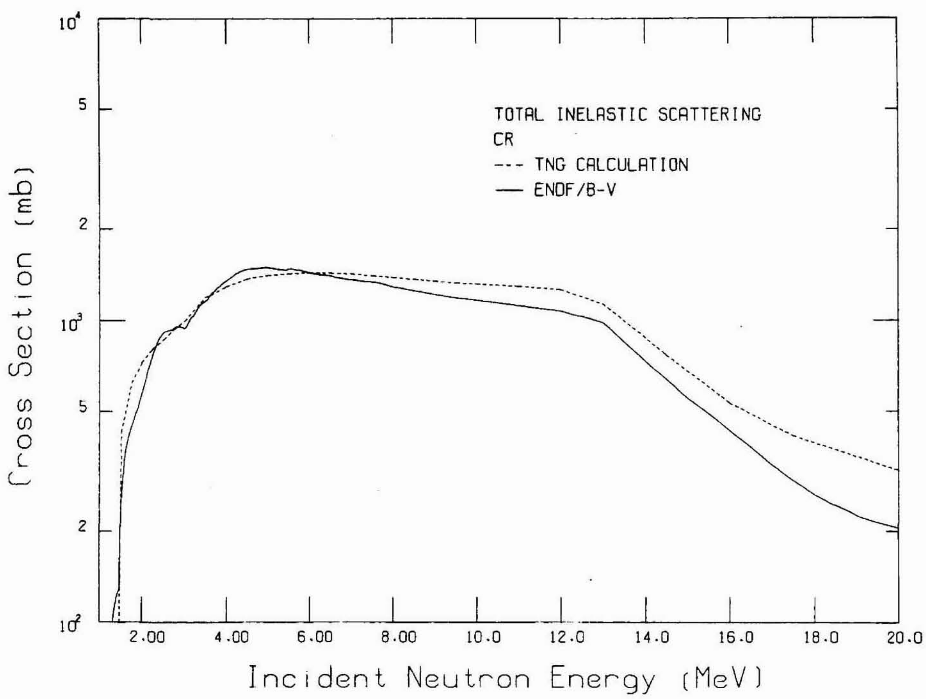

Fig. 57. Comparison of the TNG calculation with ENDF/B-V for the total inelastic scattering cross section.

ORNL/DWG 87-11902

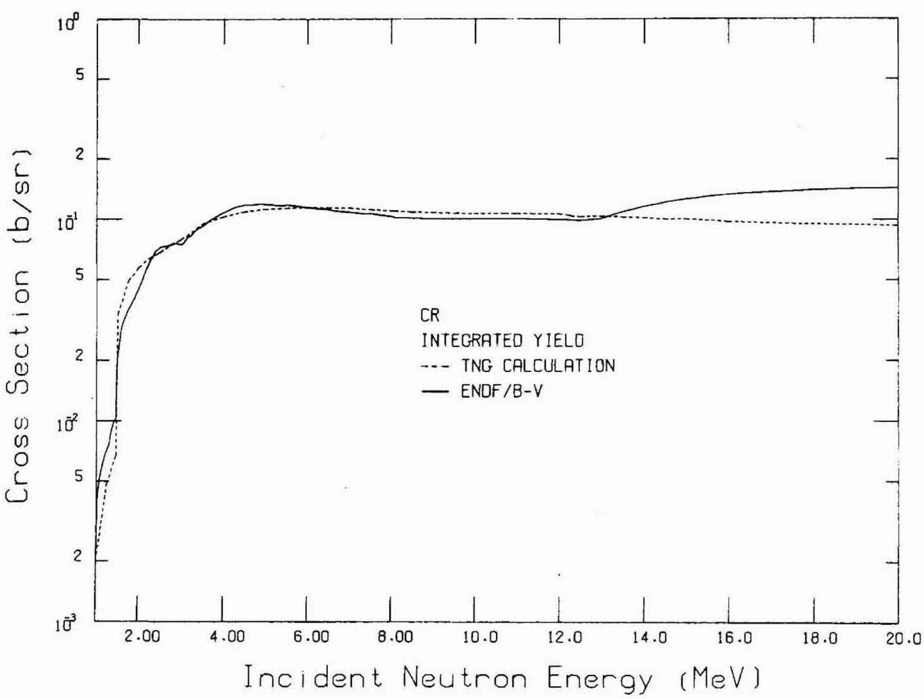

Fig. 58. Comparison of the TNG calculation with ENDF/B-V for the integrated yield of secondary neutrons as a function of incident neutron energy. The elastic contribution is not included.

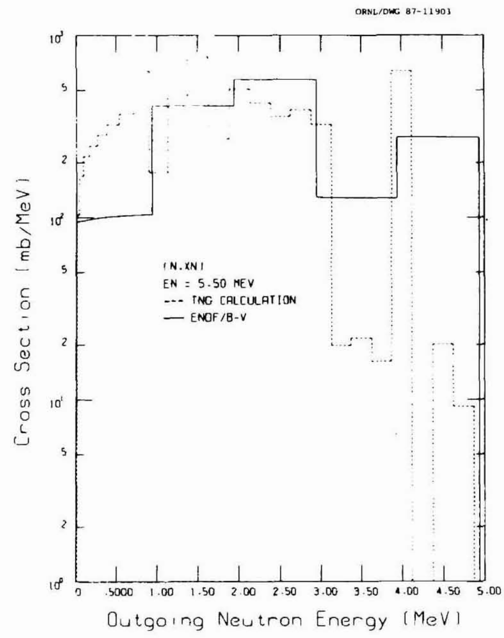

Fig. 59. Comparison of (*n,xn*) from ENDF/B-V with the TNG calculation for incident neutron energy of 5.5 MeV.

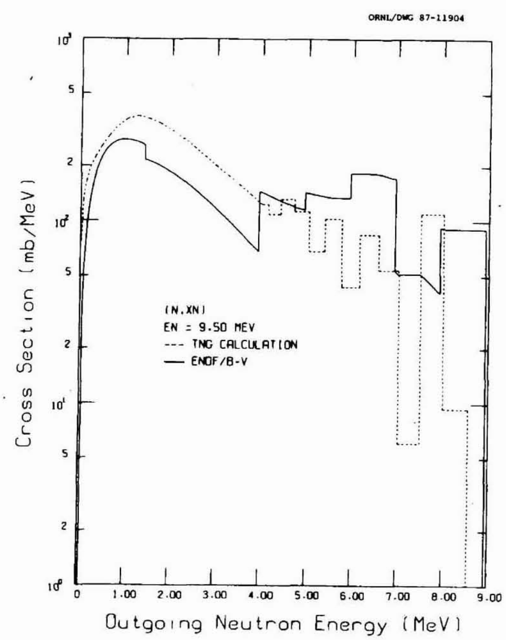

Fig. 60. Comparison of (*n,xn*) from ENDF/B-V with the TNG calculation for incident neutron energy of 9.5 MeV.

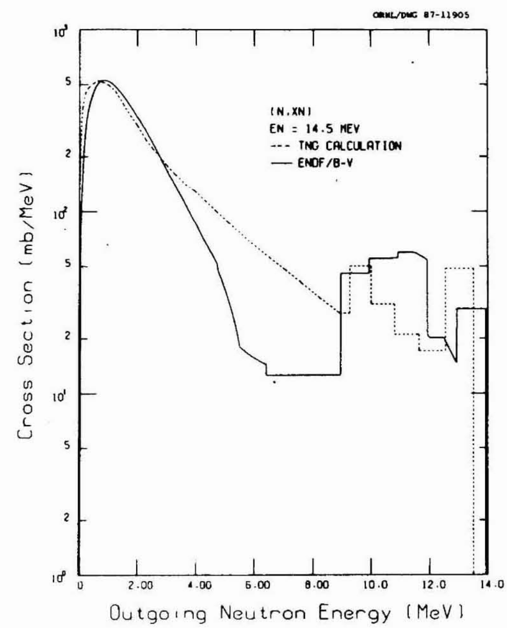

Fig. 61. Comparison of (*n,xn*) from ENDF/B-V with the TNG calculation for incident neutron energy of 14.5 MeV.

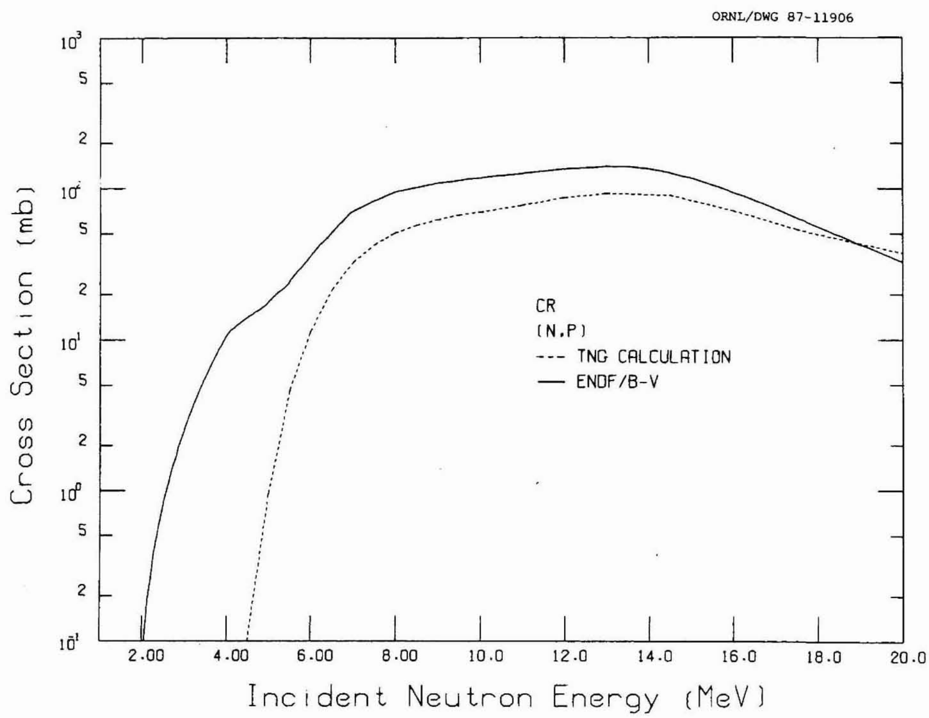

Fig. 62. Comparison of the TNG calculation with ENDF/B-V for the (*n,p*) cross section.

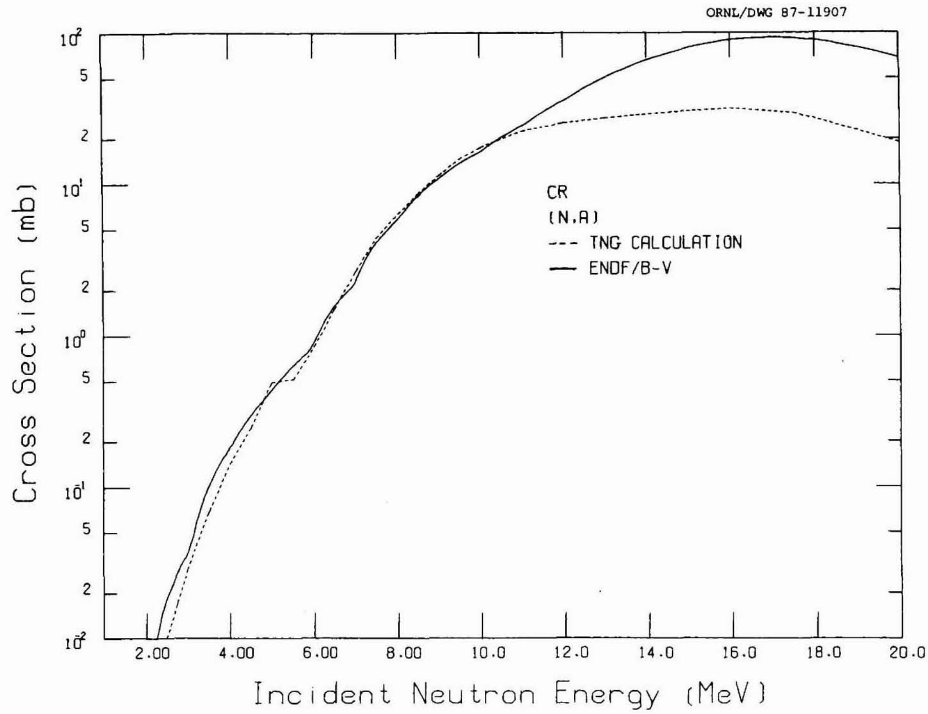

Fig. 63. Comparison of the TNG calculation with ENDF/B-V for the (*n*,*α*) cross section.

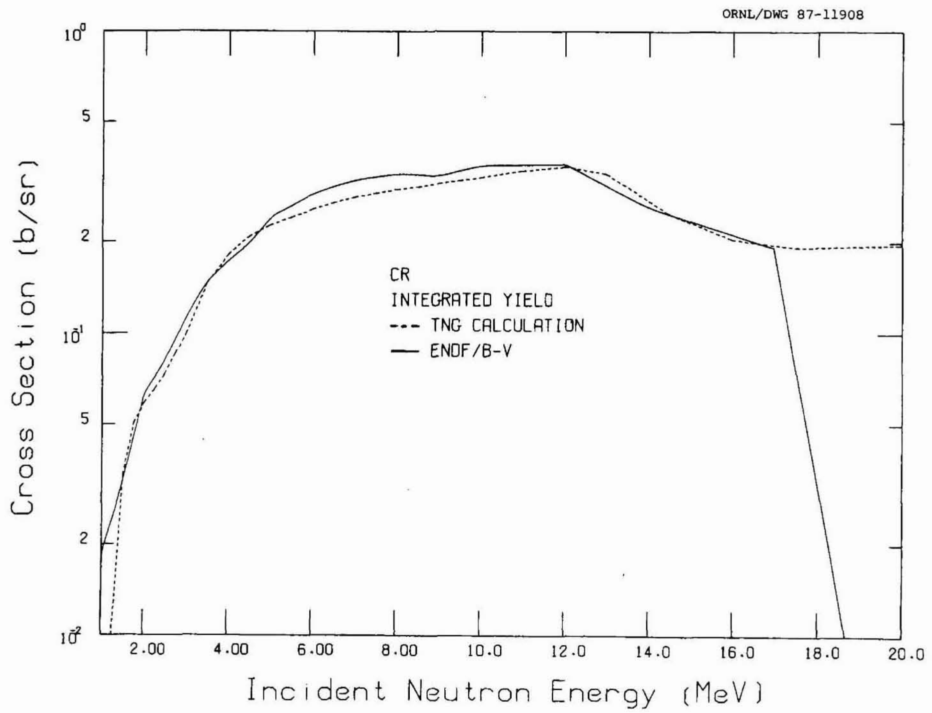

Fig. 64. Comparison of the TNG calculation with ENDF/B-V for the integrated yield of secondary gamma rays as a function of incident neutron energy.

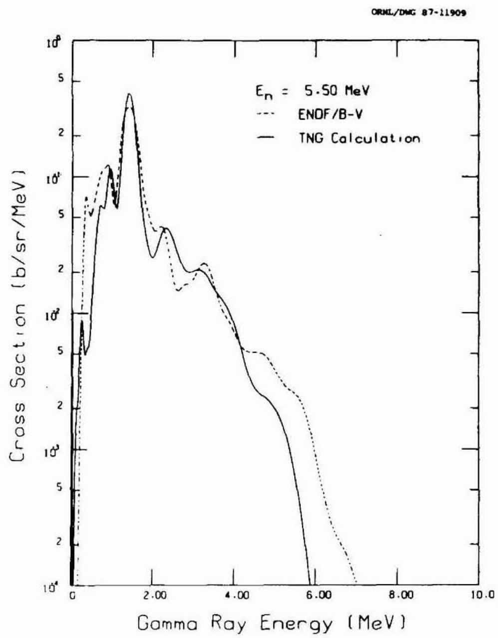

Fig. 65. Comparison of (*n,xγ*) from ENDF/B-V with the TNG calculation for incident neutron energy of 5.5 MeV.

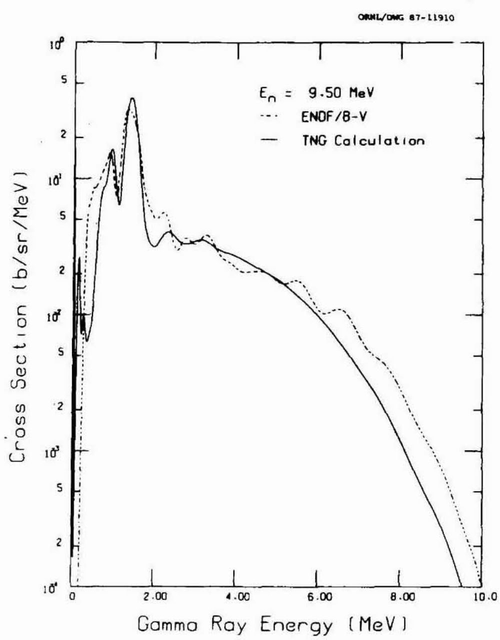

Fig. 66. Comparison of (*n,xγ*) from ENDF/B-V with the TNG calculation for incident neutron energy of 9.5 MeV.

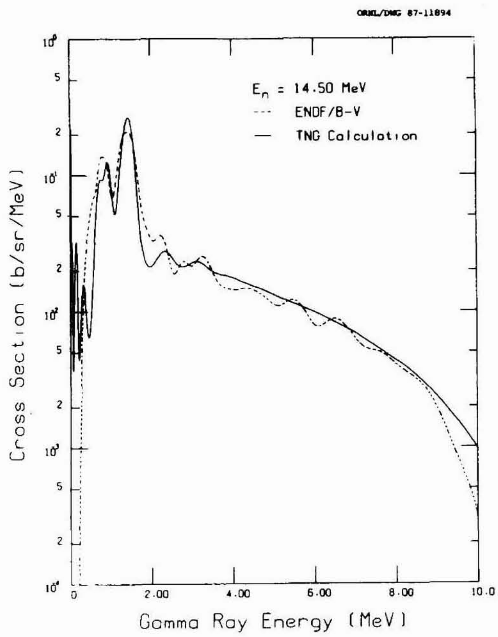

Fig. 67. Comparison of $(n,x\gamma)$ from ENDF/B-V with the TNG calculation for incident neutron energy of 14.5 MeV.

6. SUMMARY

This report has presented the nuclear models and parameters used in computing neutron-induced reactions on ^{52}Cr between 1 and 20 MeV. The calculations were made using the multistep Hauser-Feshbach/precompound model code TNG. Input parameters for TNG, including optical-model sets, discrete level information, level-density parameters, giant dipole resonance parameters, and direct reaction model parameters, were discussed. Once the input parameters were determined for TNG no other parameter adjustments were performed in the model calculations for any of the incident neutron energies for which reactions were computed. The resulting calculated cross-section sets are consistent and energy balance is ensured.

Calculated results were compared extensively to available measured data. The overall quality of the comparisons leads to the acceptance of the TNG calculations as reliable, especially for those reactions for which little or no measured data exists; for example, energy-angular distributions of the continuum neutrons for all E_n except 14.5 MeV. Also, it should be recognized from the comparisons that TNG can be used to resolve discrepancies among experimental data sets. The present work verifies that advanced nuclear-model codes can lead to internally consistent evaluations that are in good overall agreement with measured data.

The computed data were compared to cross sections from the current ENDF/B-V evaluation for chromium. The comparisons reveal serious problems in the current ENDF/B-V evaluation for natural chromium neutron-emission cross sections and spectra. These problems probably lead to difficulties with energy balance in the ENDF/B-V chromium evaluation, which can cause erroneous results for the KERMA (Kinetic Energy Release in MAterial) factor, as noted by Fu (FU80b).

These calculations, supplemented by available experimental data and resonance parameters, will be incorporated in the new isotopic evaluation of ^{52}Cr for ENDF/B-VI.

REFERENCES

AB62 A. I. Abramov, *Atomnaja Energija,* **12**, 62 (1962).

AL75 D. V. Aleksandrov, L. I. Klochkova, and B. S. Kovrigin, *Atomnaja Energija,* **39**(2), 137 (August 1978).

AR73 J. Araminowicz and J. Dresler, *Inst. Badan Jadr. (Nucl. Res.)*, Swierk and Warsaw, Rept. -1464, 14 (May 1973).

AR84 E. D. Arthur, Los Alamos National Laboratory, personal communication, 1984.

AU77 G. F. Auchampaugh, D. M. Drake, and L. R. Veeser, *Neutron Cross Section Programs in the Energy Region from 1 to 24 MeV at the LASL Van de Graaff Facilities,* BNL-NCS-50681, pp. 231-246 (May 1977).

AU78 R. L. Auble, *Nuclear Data Sheets,* **23**, 163 (1978).

BA82 H. H. Barschall, Europhys. Topical Conf. on Neutron Induced Reactions, Smolenice (June 1982); Proceedings published by Slovak Acad. Sciences as *Physics and Applications,* **10**, 279 (1982).

BE69 F. D. Becchetti and G. W. Greenlees, *Phys. Rev.,* **182**, 1190 (1969).

BE78 J. R. Beene, *Nuclear Data Sheets,* **25**(2), 235 (1978).

BE78a J. R. Beene, *Nuclear Data Sheets,* **23**(1), 1 (1978).

BO68 M. Bormann, A. Behrend, I. Riehle, and O. Vogel, *Nucl. Phys.,* **A115**, 309 (July 1968).

BR64 D. L. Broder, V. E. Kolesov, A. I. Lashuk, I. P. Sadokhin, and A. G. Dovbenko, *Atomnaja Energija,* **16**(2), 103 (February 1964).

BR71 W. Breunlich and G. Stengel, *Z. Naturforsch A,* **26**, 451 (March 1971).

BR78 E. Browne, J. M. Dairiki, R. E. Doebler, A. A. Shibab-Eldin, L. J. Jardine, J. K. Tuli, and A. B. Buyrn, *Table of Isotopes*, Seventh Edition, edited by C. M. Lederer and V. S. Shirley, John Wiley and Sons, Inc., New York (1978).

BU69 E. M. Burymov, *Yad. Fiz.,* **9**(5), 933 (1969).

CH61 D. M. Chittenden and D. G. Gardner, University of Arkansas, Report Series -61, 1 (January 1961).

CL69 I. G. Claytor, *Diss. Abstr. Int. B.,* **30**, 2850 (December 1969).

CO62 L. Colli, I. Iori, S. Micheletti, and M. Pignanelli, *Nuovo Cimento,* **21**, 966 (1962).

CS86 CSISRS Library, National Nuclear Data Center, Brookhaven National Laboratory, Upton, New York 11973.

DE67 Ju. G. Degtjarev and V. N. Protopopov, *Atomnaja Energija,* **23**(6), 568 (November 1967).

DE71 Ju. G. Degtjarev and V. N. Protopopov, *Izv. Akad. Nauk. SSSR, Ser. Fiz.,* **35**,(11), 2341 (November 1971).

DE74 F. Deak, S. Gueth, P. Kalman, and A. Kiss, *Acta Phys. Ac. Sci. Hung.,* **37**, 339 (1974).

DI87 J. K. Dickens and D. C. Larson, "Gamma-Ray Decay of Levels in ^{53}Cr," submitted to *Nuclear Physics.*

DO73 G. P. Dolja, V. P. Bozhko, V. Ja. Golovnja, A. P. Kljucharev, and A. I. Tutubalin, *Proc. Nejtronnaja Fizika,* **3**, 131 Kiev (1973).

DR73 J. Dresler, J. Araminowicz, and U. Garuska, *Inst. Badan Jadr. (Nucl. Res.),* Swierk and Warsaw, Rept. -1464, 12 (May 1973).

DR78 D. M. Drake, E. D. Arthur, and M. G. Silbert, *Nucl. Sci. Eng.*, **15**, 54 (1978).

FA68 U. Facchini and E. Saetta-Menichella, *Energia Nucleare,* **15**, 54 (1968).

FR75 J. Frehaut and G. Mosinski, 5th Int. Seminar on Interaction of Fast Neutrons with Nuclei, Gaussig, (November 1975).

FR80 J. Frehaut, A. Bertin, R. Bois, and J. Jary, *Status of (n,2n) Cross Section Measurements at Bruyeres-Li-Chatel,* BNL-NCS-51245, pp. 399-411 (May 1980).

FU72 I. Fujita, M. Sonoda, A. Katase, Y. Wakuta, H. Tawara, M. Hyakutake, and K. Iwatani, *J. Nucl. Sci. and Tech.*, **9**, 301 (1972).

FU73 E. G. Fuller, H. M. Gerstenberg, H. Vander Molen, and T. C. Dunn, "Photonuclear Reaction Data, 1973," U.S. Department of Commerce, National Bureau of Standards (March 1973).

FU76 C. Y. Fu, *Atomic Data and Nuclear Data Tables,* **17**, 127 (1976).

FU80 C. Y. Fu, "A Consistent Nuclear Model for Compound and Precompound Reactions with Conservation of Angular Momentum," p. 757 in *Proc. Int. Conf. Nuclear Cross Sections for Technology, Knoxville, TN. Oct. 22-26, 1979,* NBS-594, U.S. National Bureau of Standards. Also, ORNL/TM-7042 (1980).

FU80a C. Y. Fu, "Development and Applications of Multi-Step Hauser-Feshbach/Pre-Equilibrium Model Theory," p. 675 in *Symp. Neutron Cross Sections from 10 to 50 MeV, Upton, NY, May 12-14, 1980,* BNL-NCS-51425, Brookhaven National Laboratory.

FU80b C. Y. Fu, "Evaluation of Photon Production from Neutron-Induced Reactions," p. 753 in *Proc. of the Conference on Nuclear Data Evaluation Methods and Procedures, Upton, NY, September 22-25, 1980,* BNL-NCS-51363, Vol. II, Brookhaven National Laboratory.

GI63 W. B. Gilboy and J. H. Towle, *Nucl. Phys.*, **42**, 86 (1963).

GI65 A. Gilbert and A. G. W. Cameron, *Can. J. of Phys.*, **43**, 1446-1477 (1965).

GO77 B. Goel, *KEDAK 3,* KFK 2386/II (March 1977).

GR74 G. Grenier, B. Duchemin, and D. Paricot, Centre D'Etudes Nucleaires, Saclay, Report -4634 (November 1974).

GR79 S. M. Grimes, R. C. Haight, K. R. Alvar, H. H. Barschall, and R. R. Borchers, *Phys. Rev., C* **19**, 2127 (June 1979).

HA68 Ole Hansen, T. A. Belote, and W. E. Dorenbusch, *Nucl. Phys.*, **A118** (1968).

HA77 R. C. Haight and S. M. Grimes, Lawrence Livermore Laboratory, Report UCRL-80235 (1977).

HA78 M. L. Halbert, *Nuclear Data Sheets,* **24**, 175 (1978).

HE74 D. Hermsdorf, A. Meister, S. Sassonoff, D. Seeliger, and K. Seidel, *Kernenergie,* **17**, 176 (1974).

HE75 D. Hermsdorf, A. Meister, S. Sassonoff, D. Seeliger, K. Seidel, and F. Shahin, *Zentralinstitut fur Kernforschung Rossendorf Bei Dresden,* Zfk-277 (U) (1975).

HE79 D. M. Hetrick, D. C. Larson, and C. Y. Fu, *Status of ENDF/B-V Neutron Emission Spectra Induced by 14-MeV Neutrons*, ORNL/TM-6637, ENDF-280 (April 1979).

HO69 B. Holmqvist and T. Wiedling, *Aktiebolaget Atomenergi - 366*, Stockholm/Studsvik (June 1969).

HO70 B. Holmqvist, S. G. Johansson, G. Lodin, M. Salama, and T. Wiedling, *Aktiebolaget Atomenergi - 385*, Stockholm/Studsvik (September 1970).

HO74 P. Holmberg, R. Rieppo, J. K. Keinaenen, and M. Valkonen, *J. Inorg. Nucl. Chem.*, **36**, 715 (April 1974).

HU62 J. R. Huizenga and G. Igo, *Nucl. Phys.*, **29**, 462-473 (1962).

HU67 L. Husain and P. K. Kuroda, *J. Inorg. Nucl. Chem.*, **29**, 2665 (1967).

IS79 B. S. Ishkhanov, Yu. A. Novikov, E. S. Omarov, and I. M. Piskarev, *Sov. J. Nucl. Phys.* **30**, 610 (1979).

KA65 L. Ya Kasakova, V. F. Kolesov, V. I. Popov, O. A. Salnikov, V. M. Sluchevskaja, and V. I. Trikova, *Proc. Nucl. Structure Conf., Antwerp,* 576(200) (1965).

KA78 P. T. Karatzas, G. P. Couchell, B. K. Barnes, L. E. Beghian, P. Harihar, A. Mittler, D. Pullen, E. Sheldon, and N. B. Sullivan, *Nucl. Sci. Eng.*, **67**, 34 (1978).

KE59 B. D. Kern, W. E. Thompson, and J. M. Ferguson, *Nucl. Phys.*, **10**, 226 (May 1959).

KH60 C. S. Khurana and H. S. Hans, *Proc. Low Energy Nuclear Physics Symp.*, p. 297, Waltair, India (1960).

KI74 W. E. Kinney and F. G. Perey, *Natural Chromium and ^{52}Cr Neutron Elastic and Inelastic Scattering Cross Sections From 4.07 to 8.56 MeV*, ORNL-4806 (January 1974).

KO64 I. A. Korzh, M. T. Sklyar, and I. A. Totskiy, *Ukr. Fiz. Zh.*, **9**, 577 (1964).

KO67 I. A. Korzh, V. A. Mischenko, M. V. Pasechnik, N. M. Pravdivy, I. E. Sanzhur, and I. A. Totsky, *Ukr. Fiz. Zh.*, **12**(9), 1571 (September 1967).

KO76 I. A. Korzh, V. A. Mischenko, E. N. Mozhzhukhin, A. A. Golubova, N. M. Pravdivyj, I. E. Sanzhur, and M. V. Pasechnik, "All Union Conf. on Neutron Phys., Kiev", published in *Nejtronnaja Fizika*, **4**, 220 (May 1976).

KO82 I. A. Korzh, V. A. Mischenko, E. N. Mozhzhukhin, and N. M. Pravdivyj, *Yad. Fiz.*, **35**(5), 1097 (1982).

KU72 P. D. Kunz, "Distorted Wave Code DWUCK72," University of Colorado, unpublished (1972).

LA80 D. C. Larson, "ORELA Measurements to Meet Fusion Energy Neutron Cross Section Needs," *Proc. Symp. on Neutron Cross Sections from 10 to 50 MeV,* BNL-NCS-51245, Brookhaven National Laboratory (July 1980).

LA85 D. C. Larson, "High-Resolution Structural Material (n,xγ) Production Cross Sections for 0.2 $< E_n \leqslant 40$ MeV," p. 71 in *Proc. Conf. on Nuclear Data for Basic and Applied Science, Santa Fe, New Mexico, Vol. 1*, 1985.

MA72 S. G. Malmskog, *Aktiebolaget Atomenergi*, Stockholm, Internal Report -25 (June 1972).

MA72a G. N. Maslov, F. Nasyrov, and N. F. Pashkin, Rept. Jadernye Konstanty -9, 50 (1972).

MI66 B. Mitra and A. M. Ghose, *Nucl. Phys.*, **83**, 157 (1966).

MO76 G. L. Morgan and E. Newman, *The Cr(n,xγ) Reaction Cross Section for Incident Neutron Energies Between 0.2 and 20.0 MeV*, ORNL/TM-5098, ENDF-222 (January 1976).

MO79 G. L. Morgan, *Cross Sections for the Cu(n,xn) and Cu(n,xα) Reactions Between 1 and 20 MeV*, ORNL-5499, ENDF-273 (1979).

MO83 N. T. Molla, M. Mizanul Islam, M. Mizanur Rahman, and S. Khatun, Intern. Nucl. Data Committee Report -002, 1 (February 1983).

ND83 *Compilation of Requests for Nuclear Data*, compiled and edited by the National Nuclear Data Center for the DOE Nuclear Data Committee, BNL-NCS-51572, DOE/NDC-28/U (January 1983).

PA53 E. B. Paul and R. L. Clarke, *Can. J. Phys.*, **31**, 267 (1953).

PA69 M. V. Pasechnik, M. B. Fedorov, T. I. Jakovenko, I. E. Kashuba, and I. A. Korzh, *Ukr. Fiz. Zh.*, **14**(11), 1874 (1969).

PA81 A. Paulsen, H. Liskien, F. Arnotte, and R. Widera, *Nucl. Sci. and Eng.*, **78**, 377 (1981).

PE69 R. J. Peterson, *Ann. Phys. (N.Y)*, **53**, 40 (1969).

PE76 C. M. Perey and F. G. Perey, *Atomic Data and Nuclear Data Tables*, **17**, 1-101 (1976).

PO79 E. C. Pollacco, D. M. Parkinson, J. R. Leigh, D. C. Weisser, N. Shikazono, G. S. Foote, and D. Branford, *Nucl. Phys.*, **A330**, 173 (1979).

PR70 B. M. Preedom, C. R. Gruhn, T. Y. T. Kuo, and C. J. Maggiore, *Phys. Rev.*, **C2**, 166 (1970).

PR71 R. Prasad and D. C. Sarkar, *Nuovo Cimento A*, **3**(3), 467 (June 1971).

PR79 A. Prince and T. W. Burrows, *Evaluation of Natural Chromium Neutron Cross Sections for ENDF/B-V*, report BNL-NCS-51152, ENDF-286 (1979).

QA72 S. M. Qaim, *Nucl. Phys.*, **A185**, 614 (May 1972).

QA77 S. M. Qaim and N. I. Molla, *Nucl. Phys.*, **A283**, 269 (June 1977).

SA72 O. A. Salnikov, G. N. Lovchikova, G. V. Kotelnikova, A. M. Trufanov, and N. I. Fetisov, *Differential Cross Sections of Inelastic Scattering Neutrons on Nuclei Cr, Mn, Fe, Co, Ni, Cu, Y, Zr, Nb, W, Bi*, Report Jadernye Konstanty -7, 102 (March 1972).

SA77 K. Sailer, S. Daroczy, P. Raics, and S. Nagy, *Proc. All Union Conf. on Neutron Phys., Kiev*, **1**, 246 (April 1977).

SH86 K. Shibata and C. Y. Fu, *Recent Improvements of the TNG Statistical Model Code*, ORNL/TM-10093 (August 1986).

SH87 K. Shibata and D. M. Hetrick, *Calculated Neutron-Induced Cross Sections for ^{53}Cr from 1 to 20 MeV*, ORNL/TM-10381 (1987).

SM66 A. B. Smith, private communication (December 1966).

SM80 D. L. Smith and J. W. Meadows, *Nucl. Sci. and Eng.*, **76**, 43 (September 1980).

SO73 L. S. Sokolov, M. B. Fjodorov, E. V. Korbetskij, N. T. Surovitskaja, T. I. Jakovenko, *Ukr. Fiz. Zh.*, **18**(2), 263 (February 1973).

ST56 V. I. Strizhak, *Zh. Eksp. Teor. Fiz.*, **31**, 907 (1956).

ST65 J. E. Strain and W. J. Ross, ORNL-3672 (January 1965).

ST65a P. H. Stelson, R. L. Robinson, H. J. Kim, J. Rapaport, and G. R. Satchler, *Nucl. Phys.*, **68**, 97 (1965).

TA55 H. L. Taylor, O. Lonsjo, T. W. Bonner, *Phys. Rev.*, **100**, 174 (1955).

TA65 S. Tagesen and P. Hille, *Oesterr. Akad. Wiss., Math. Naturwiss. Kl., Sitz. Abt. 2*, **174**, 85 (March 1965).

TA83 A. Takahashi, J. Yamamoto, T. Murakami, K. Oshima, H. Oda, K. Fujimoto, M. Ueda, M. Fukazawa, Y. Yanagi, J. Miyaguchi, and K. Sumita, Oktavian Report A-83-01, Osaka University, Japan (June 1983).

TE75 G. Tessler and S. Glickstein, *Proc. Conf. on Nuclear Cross Sections and Technology, Washington, D.C., Vol. 2*, 934 (March 1975).

VA62 D. M. Van Patter, N. Nath, S. M. Shafroth, S. S. Malik, and M. A. Rothman, *Phys. Rev.*, **128**, 1246 (1962).

VA76 M. Valkonen, Univ. of Jyvaeskylae, Dept. of Physics, Report -1/1976 (1976).

VO75 F. Voss, S. Cierjacks, D. Erbe, and G. Scmalz, *Proc. Conf. on Nuclear Cross Sections and Technology, Washington, D.C.*, Vol. 2, 916 (March 1975).

VO80 H. Vonach, A. Chalupka, F. Wenninger, and G. Staffel, "Measurement of the Angle-Integrated Secondary Neutron Spectra from Interaction of 14 MeV Neutrons with Medium and Heavy Nuclei," *Proc. Symp. on Neutron Cross-Sections from 10 to 50 MeV*, BNL-NCS-51245, Brookhaven National Laboratory (July 1980).

WA82 E. Wattecamps, H. Liskien, and F. Arnotte, *Proc. Int. Conf. on Nucl. Data for Sci. and Tech.*, 156 (1982).

WE62 R. Wenusch and H. Vonach, *Anz. Oesterr. Akad. Wiss, Math - Naturwiss. Kl.*, **99**, 1 (January 1962).

WI64 D. Wilmore and P. E. Hodgson, *Nucl. Phys.*, **55**, 673 (1964).

ORNL/TM-10417
ENDF-346

INTERNAL DISTRIBUTION

1. R. G. Alsmiller, Jr.
2. H. P. Carter/G. E. Whitesides/ CS X-10 library
3. J. K. Dickens
4-8. C. Y. Fu
9. T. A. Gabriel
10-14. D. M. Hetrick
15. J. T. Holdeman
16-20. D. C. Larson
21. N. M. Larson
22. F. C. Maienschein
23. B. F. Maskewitz
24. B. D. Murphy
25. M. R. Patterson
26. R. W. Peelle
27. F. G. Perey
28. R. W. Roussin
29. R. T. Santoro
30. R. R. Spencer
31. A. Zucker
32. P. W. Dickson, Jr. (consultant)
33. G. H. Golub (consultant)
34. R. M. Haralick (consultant)
35. D. Steiner (consultant)
36. Central Research Library
37. Document Reference Section
38. K-25 Plant Library
39. Laboratory Records
40. Laboratory Records - RC
41. ORNL Patent Section
42. EPMD Reports Office

EXTERNAL DISTRIBUTION

43. E. D. Arthur, T-2, MS-243, Los Alamos National Laboratory, P. O. Box 1663, Los Alamos, NM 87545.

44. S. E. Berk, G234, Division of Development and Technology, Office of Fusion Energy, U.S. Department of Energy, Washington, DC 20545

45. P. Rose, Building 197D, National Nuclear Data Center, Brookhaven National Laboratory, Upton, NY 11973.

46. Chief, Mathematics and Geoscience Branch, U.S. Department of Energy, Washington, DC 20545.

47. Herbert Goldstein, 211 Mudd Columbia University, 520 West 120th St., New York, NY 10027.

48. Robert MacFarlane, T-2, MS-243, Los Alamos National Laboratory, P. O. Box 1663, Los Alamos, NM 87545.

49. F. M. Mann, W/A-4, Westinghouse Hanford, P. O. Box 1970, Richland, WA 99352.

50. G. L. Morgan, Los Alamos National Laboratory, P. O. Box 1663, Group P-15, MS D406, Los Alamos, NM 87545.

51. J. N. Rogers, Division 8324, Sandia Laboratories, Livermore, CA 94550.

52. R. E. Schenter, Westinghouse Hanford, P. O. Box 1970, Richland, WA 99352.

53. D. L. Smith, Building 314, Applied Physics Division, Argonne National Laboratory, 9700 South Cass Avenue, Argonne, IL 60439.

54. S. L. Whetstone, Division of Nuclear Sciences, Office of Basic Energy Sciences, U.S. Department of Energy, Washington, DC 20545.

55. P. G. Young, T-2, MS-243, Los Alamos National Laboratory, P. O. Box 1663, Los Alamos, NM 87545.

56. Office of Assistant Manager for Energy Research and Development, U.S. Department of Energy, Oak Ridge Operations, Oak Ridge, TN 37831.

57-181. Charles Dunford, National Nuclear Data Center, ENDF, Bldg. 197D, Brookhaven National Laboratory, Upton, NY 11973.

182-212. Technical Information Center, Oak Ridge, TN 37831.